AQUEOUS COORDINATION CHEMISTRY OF ALUMINUM AND GALLIUM WITH 3-HYDROXY-4-PYRIDINONE LIGANDS

by

WILLIAM OTTO NELSON

B.Sc., University of Wisconsin-Superior, 1984

A THESIS SUBMITTED IN PARTIAL FULFILLMENT OF

THE REQUIREMENTS FOR THE DEGREE OF

DOCTOR OF PHILOSOPHY

in

THE FACULTY OF GRADUATE STUDIES

(Department of Chemistry)

We accept this thesis as conforming

to the required standard

THE UNIVERSITY OF BRITISH COLUMBIA

December 1988

In presenting this thesis in partial fulfilment of the requirements for an advanced degree at the University of British Columbia, I agree that the Library shall make it freely available for reference and study. I further agree that permission for extensive copying of this thesis for scholarly purposes may be granted by the head of my department or by his or her representatives. It is understood that copying or publication of this thesis for financial gain shall not be allowed without my written permission.

Department of Chemistry

The University of British Columbia
Vancouver, Canada

Date Dec. 3, 1988

ABSTRACT

Aluminum(III) and gallium(III) complexes with the following ligands were synthesized: 3-hydroxy-2-methyl-4(1H)-pyridinone (Hmpp), the 1-methyl (Hdpp), 1-ethyl (Hmepp), and 1-hexyl (Hmhpp) derivatives of Hmpp, and β-[N-(3-hydroxy-4-pyridinone)]-α-aminopropionic acid (mimosine). The 3-hydroxy-4-pyridinone ligands employed in this study (except mimosine) were prepared by the conversion of an oxygen heterocycle, 3-hydroxy-2-methyl-4-pyrone, to the corresponding nitrogen heterocycle by reaction with a primary amine. These bidentate ligands contain an α-hydroxyketone moiety and their conjugate bases form neutral complexes with trivalent metals. The ligands and the metal complexes were fully characterized by mass spectrometry and infrared, proton NMR, and ultraviolet spectroscopy.

The structures of several ligands and metal complexes were determined by X-ray diffraction. Hmpp, Hdpp, and Hmepp crystallize as centrosymmetric O-H···O=C hydrogen bonded dimeric units. The *facial* geometric isomers of Al- and Ga(dpp)$_3$ crystallize as the dodecahydrate in which the water molecules are associated in hexagonal rings similar in structure to that of ice I_h. The oxygen atoms of the metal complexes are hydrogen bonded to bridging waters so that the water rings and metal complexes are interconnected in a three-dimensional array. An analogous water network is found in the structures of Al- and Ga(mepp)$_3$.

The proton NMR spectra in CD_3OD and D_2O indicate the metal complexes are fluxional above -30 °C. Variable-temperature proton NMR experiments identified the exchange process as *facial* to *meridional* geometric isomerization. Ligand exchange experiments using proton NMR indicated the isomerization follows an intermolecular rather than intramolecular pathway in CD_3OD. Variable-pH ^{27}Al NMR experiments show the tris-ligand aluminum complexes to be resistant to hydrolysis from pH 4-9. The formation

constants of the metal-ligand complexes were determined by potentiometric titrations, and this study indicates the gallium complexes have a similar pH region of hydrolytic stability. The overall formation constants for the tris-ligand aluminum and gallium complexes were all greater than 10^{30}, indicating that these ligands could compete for aluminum and gallium in blood plasma models. Water solubilities and octanol/water partition coefficients of the ligands and metal complexes were measured and they indicate the suitability of these complexes for ^{67}Ga animal biodistribution experiments. The results of the biodistribution study show that under conditions of ligand excess ^{67}Ga is redirected from transferrin; however, the ^{67}Ga-ligand complexes do not localize in any organs. It appears the ligands greatly enhance the removal of the radionuclide from the body.

TABLE OF CONTENTS

LIST OF TABLES

LIST OF FIGURES

LIST OF ABBREVIATIONS

Abbreviation	Meaning
acac	acetylacetonate
α-RT	α-substituted tropolonate
Al_{13}	$[AlO_4Al_{12}(OH)_{24}(H_2O)_{12}]^{7+}$
$Al(dpp)_3$	tris(3-hydroxy-1,2-dimethyl-4-pyridinonato)aluminum(III)
$Al(ma)_3$	tris(maltolato)aluminum(III)
$Al(mepp)_3$	tris(3-hydroxy-2-methyl-1-ethyl-4-pyridinonato)aluminum(III)
$Al(mhpp)_3$	tris(3-hydroxy-2-methyl-1-hexyl-4-pyridinonato)aluminum(III)
$Al(mimo)_3$	tris(mimosinato)aluminum(III)
$Al(mpp)_3$	tris(3-hydroxy-2-methyl-4-pyridinonato)aluminum(III)
β_n	overall formation constant
B-band	benzenoid ultraviolet absorbance band
BBB	blood-brain barrier
Bzma	3-benzyloxy-2-methyl-4-pyrone
Bzmpp	3-benzyloxy-2-methyl-4(1H)-pyridinone
Catechol	1,2-dihydroxybenzene
Chlorokojic acid	5-hydroxy-2-(chloromethyl)-4-pyrone
C/IR	charge to ionic radius ratio
$\Delta\nu$	frequency shift in Hertz between peaks in absence of exchange
$\Delta\nu_e$	experimentally observed frequency shift
δ_{x-y}	vibrational in-plane bending mode
ε	molar absorptivity
EDTA	ethylenediaminetetraacetic acid
FAAS	flame atomic absorption spectroscopy

fac	facial geometric isomer
$Ga(ma)_3$	tris(maltolato)gallium(III)
$Ga(dpp)_3$	tris(3-hydroxy-1,2-dimethyl-4-pyridinonato)gallium(III)
$Ga(mepp)_3$	tris(3-hydroxy-2-methyl-1-ethyl-4-pyridinonato)gallium(III)
$Ga(mhpp)_3$	tris(3–hydroxy–2–methyl–1–hexyl–4–pyridinonato)gallium(III)
$Ga(mimo)_3$	tris(mimosinato)gallium(III)
$Ga(mpp)_3$	tris(3-hydroxy-2-methyl-4-pyridinonato)gallium(III)
η	absolute hardness
H-bond	hydrogen bond
Hdpp	3-hydroxy-1,2-dimethyl-4-pyridinone
H_2exn	1,6–di(3–hydroxy–2–methyl–4–pyridinone)hexane
Hmepp	3-hydroxy-2-methyl-1-ethyl-4-pyridinone
Hmhpp	3-hydroxy-2-methyl-1-hexyl-4-pyridinone
Hmpp	3-hydroxy-2-methyl-4(1H)-pyridinone
IR	infrared
K_n	stepwise formation constant
Kojic acid	5-hydroxy-2-(hydroxymethyl)-4-pyrone
λ_{max}	wavelength of maximum absorbance
L-dopa	L-3,4-dihydroxyphenylalanine
Maltol	3-hydroxy-2-methyl-4-pyrone
mer	meridional geometric isomer
mCi	milliCurrie; equals 3.7×10^7 disintegrations/second
Mimosine	β-[N-(3-hydroxy-4-pyridinone)]-α-aminopropionic acid
NMR	nuclear magnetic resonance
ν_{x-y}	vibrational stretching mode
P	*n*-octanol/water partition coefficient

π_{x-y}	vibrational out-of-plane bending mode
pyromeconic acid	3-hydroxy-4(1H)-pyridinone
tfac	trifluroacetylacetonate
T_c	coalescence temperature
T_1	spin-lattice (longitudinal) relaxation
T_2	spin-spin (transverse) relaxation
T_Q	nuclear quadrupole relaxation
τ_c	correlation time
UV	ultraviolet
$W_{1/2}$	peak width at half height

ACKNOWLEDGEMENTS

I would like to thank the technical staff of the Mass Spectroscopy lab and the Chemistry Department support staff for all their help. I would especially like to thank Dr. S.O. Chan and Marietta Austria of the NMR lab for their help with the ^{27}Al NMR, and Steve the elder and Steve the younger in the glassblowing shop. Many thanks to Randy for the lengthy conversations about DNMR3 and to Ove for listening to my organic ramblings.

The financial assistance in the form of a University Graduate Fellowship and a Teaching Assistantship is gratefully acknowledged, as is a research grant received from Sigma Xi.

Those whose work appears in this thesis are deserving of special mention. Therefore I would like to thank Steve Rettig to whom I owe a great debt, Peter Borda for his prompt determination of the elemental analyses, Dave for all his hard work and copious quantities of speciation diagrams, Tim K. and Carey for their synthetic endeavors, Tami for having to smell as much octanol as I did, and Don, Terri and Gordon for all their work at the hot lab.

This would not be complete without acknowledging the support and encouragement of all the members of the "Orvig Team" past and present. A special thank you is extended to Alexis for changing Orvig's student into Orvig's students, and of course to Chris himself for being willing to take on a graduate student who, according to F. Aubke, was not only older than his research director but also had more hair!

Finally, to Marian who would make my life a misery if I didn't thank her, and to Sir Isaac Newt wherever he might be, "thank's for making those lonely nights in the lab less lonely."

To Marian, and to my parents, Bud and Doris,who always
wanted a doctor in the family.

I leave my colleagues on the Orvig team with the immortal words
of Yogi Berra in the seventh game of the 1960 World Series:

"It ain't over 'til it's over."

Chapter I General Introduction

Aluminum is the most abundant metal and the third most common element in the earth's crust. It is bound as oxides, primarily alumina, and complex aluminosilicates. Surface water concentrations have remained minimal due to the low solubility of the natural Al minerals; however, acidification due to acid precipitation has facilitated the transport of Al from soil to surface waters.[1] Elevated concentrations of Al have been reported for lakes and rivers in regions throughout the northern temperate zone that receive high inputs of acidic substances, including eastern Canada[2] and the northeastern United States.[3]

The increasing concentrations of Al in surface waters can be considered an unforeseen consequence of human activity. By design, municipal water supplies can have high levels of Al (up to 1 mg/L) because $Al_2(SO_4)_3$ is commonly used as a flocculant during water purification.[4] Al is also found in relatively high concentrations in a number of products used for human consumption[5] including drugs (e.g., 10-15 mg per tablet of buffered aspirin), processed foods (cheese can be up to 0.7% Al), and baking powder (about 5% Al). In spite of this exposure, Al is largely excluded from the body because of low gastrointestinal absorption and efficient renal excretion. On average, Al is ingested in the range of 20-50 mg/day and the total body burden in normal persons is about 30 mg.[2]

As recently as 1974 Al was regarded as a generally benign element,[6] but over the last twenty years a large body of evidence has accumulated to link Al with several neurological dysfunctions that appear to have an environmental etiology.[4,7,8] Dialysis encephalopathy (DE) and amyotrophic lateral sclerosis (ALS) are especially interesting because of their association with Al in drinking water. Patients on long term dialysis are

the victims of DE and a correlation has been established between the levels of Al in the dialysis solutions and this often fatal syndrome.[9] Natives of the island of Guam have an inordinately high incidence of ALS (commonly referred to as Lou Gehrig's disease) and it has been hypothesized that this could be related to the high levels of Al found in the soils and surface waters of the regions where the disease is endemic.[10]

The association of Al with Alzheimer's disease was first recognized through animal experiments where it was found that aluminum-induced encephalopathy had a clinical course and histopathology similar but not identical to that found in Alzheimer's disease.[11,12] It has since been established that victims of Alzheimer's have elevated Al levels (10 to 30 times above normal) in the nuclei of the affected brain cells.[13] Although it has not been proven that Al is the cause of Alzheimer's or any other human neurological disorder, the circumstantial evidence is compelling when coupled with the well established neurotoxicity of Al (first documented[14] in 1886). The case against Al is strong enough that several studies have been undertaken to assess chelating agents for the removal of this "benign" element from the body.[4,8,15] It was in the context of the potentially deleterious consequences of the increasing environmental exposure to aluminum that we first became interested in the aqueous coordination chemistry of this group 13 metal.

Our interest in gallium is due to its utilization as a radiopharmaceutical imaging agent. Ga has two isotopes that lend themselves to the detection methods of nuclear medicine: ^{67}Ga ($t_{1/2}$ = 78.1 h; γ = 93.3, 185, 300 KeV; accelerator product) and ^{68}Ga ($t_{1/2}$ = 68.3 m; γ = 511 KeV from β^+ annihilation; generator product). The discovery in the 1960's that ^{67}Ga (administered as the citrate) localized in soft tissue tumors[16] engendered considerable clinical research and the citrate (the only commercially available radiopharmaceutical of ^{67}Ga) is now widely used in oncological nuclear medicine.[17-19] Despite its availability and easy detection, the use of ^{67}Ga has been limited to the detection of tumors and inflammatory lesions.[20,21]

The aqueous coordination chemistry of Ga with multidentate ligands incorporating hydroxy, amino, carboxylate, and catechol moieties has been explored with nuclear medicine in mind;[22-24] however, there has not been much work on the aqueous chemistry of this trivalent metal with simple bidentate ligands. One reason for this is the hydrolytic instability of the group 13 metals; Al and Ga undergo extensive and complex hydrolysis that is pH, concentration, and time dependent.[7,25] Figure 1.1 is a diagram showing the pH dependent speciation of Ga^{3+} (the speciation diagram for Al^{3+} is very similar). The diagram is simplified as no polymeric species are included and it illustrates the amphoteric nature of the Ga-hydroxide complexes. Al and Ga form insoluble neutral hydroxides in the pH 4-8 region and the logarithm of the overall formation constants for the Al- and $Ga(OH)_3$ gelatinous precipitates are 12.7 and 23.2, respectively (based on data from ref. 25). To chelate these metals in an aqueous environment, a ligand must be able to compete with the hydroxide ion.

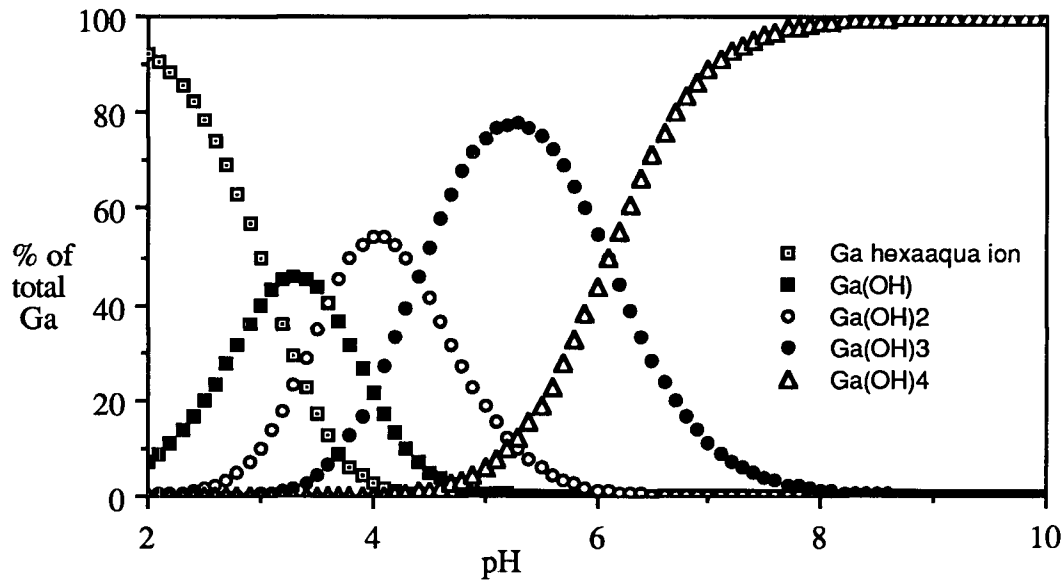

Figure 1.1. Speciation diagram for 1mM Ga^{3+} at 25 °C (based on data from ref. 25).

We are interested in ligands and metal-ligand complexes that are "biologically relevant". For the purposes of our research, biologically relevant compounds would have the following properties: molecular weight (MW) < 600, water solubility, enough lipophilicity to cross cell membranes, neutral charge at physiological pH (7.4), and (for the metal-ligand complexes) significant thermodynamic stability. In addition, the ligands need to be reasonably nontoxic as they are to be used in animal biodistribution studies with ^{67}Ga. This is of use both to determine the efficacy of the ligands as in vivo directors of this radionuclide and to gain some idea of the biodistribution of the Al complexes as there are no Al isotopes suitable for this type of study.

In ^{67}Ga imaging experiments, water solubility at the μM level (or lower) is sufficient; for facile spectral characterization of the metal-ligand complexes, solubility > 1 mM is desirable. The constraints on size, lipophilicity, and charge are necessary because of our interest in ligands and metal-ligand complexes that could conceivably enter the brain. The brain is separated from the circulatory system by the most selective barrier in the body, the blood-brain barrier (BBB). It has been shown that the permeability of the BBB is directly related to the size and lipophilicity (and therefore charge) of a substance.[26] The upper limit on size has yet to be determined, but it is thought that penetration of the BBB is not inhibited by size for compounds of MW < 500.[27]

For in vivo experiments, the need for thermodynamic stability is dictated primarily by the affinity of the blood serum protein transferrin for trivalent metal ions.[28] Transferrin is an iron transport protein that has two binding sites for metal ions similar in size to Fe^{3+}. (The ionic radii and transferrin binding constants (K_1 and K_2) for Al, Ga, In, and Fe are listed in Table 1.1.) The large binding constants and the high concentration of vacant transferrin binding sites in human blood (~50 μM[29]) make transferrin a powerful scavenger of trivalent metal ions. The size specificity of transferrin binding is shown by the large difference in the stability of the Al and In complexes. When ^{67}Ga-citrate is used for

imaging, the observed biodistribution is that of ^{67}Ga-transferrin as citrate cannot compete for the metal ion. A ligand must be able to maintain the radionuclide when confronted with the high levels of transferrin in the circulatory system even to be considered as a ^{67}Ga imaging agent.

Table 1.1. Effective ionic radii (six coordinate)[a] and transferrin binding constants.[b]

	Al	Ga	In	Fe
Ionic Radius (Å)	0.535	0.620	0.800	0.645
Log K_1	12.9	20.3	30.5	22.7
Log K_2	12.3	19.3	25.5	22.1

[a] From ref. 30.

[b] In from ref. 28, Al and Fe from ref. 29, and Ga from ref. 31.

The group 13 metals have an affinity for oxygen containing compounds and the research in our laboratory has concentrated on bidentate ligands with dihydroxy or α-hydroxyketone binding groups. My initial project was the synthesis of Al and Ga complexes with several 1,2-dihydroxybenzene derivatives (catechols). Various catechols have been used as ligands for a number of metals,[32] including aluminum[33] and gallium.[34] In addition, the catecholamines (dopamine, noradrenaline, and adrenaline) are adrenal medullary hormones responsible for the coordination of the sympathetic nervous system and the adrenal medulla. The catechol ligand of greatest interest to us was L-3,4-dihydroxyphenylalanine (L-dopa). L-Dopa is not a neurotransmitter, but it is a biological precursor that is converted to dopamine by L-dopa decarboxylase.[35] L-Dopa can cross the BBB and it is the principal therapeutic for the treatment of Parkinson's disease, another neurological disorder considered to have an environmental etiology.[36]

The ability of L-dopa to localize in the brain made it a good starting point for our research. However, it has two properties that are liabilities within the framework of this study: the tris-ligand metal complexes are trianionic and free (and complexed) L-dopa is readily oxidized in water. The first property makes it more difficult for the metal-ligand complexes to cross cell membranes. The second property is one shared by all catechols as they can be oxidized to the free radical *o*-semiquinone and to *o*-benzoquinone (Fig. 1.2). The redox sensitivity of the catechol ligands complicated the synthesis of the tris(catecholato) Al and Ga complexes, and we were unable to develop this ligand system with these metals.

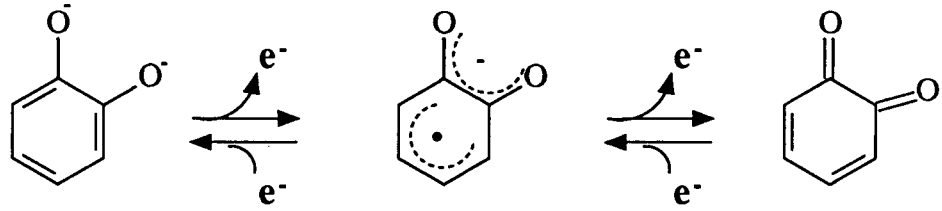

Figure 1.2. The catechol to *o*-semiquinone to *o*-benzoquinone redox cycle.

Our research group enjoyed greater success with two classes of heterocyclic ligands containing the α-hydroxyketone moiety. The binding group is the same as that in *o*-semiquinone (Fig. 1.3) and a number of transition metal complexes with *o*-semiquinone ligands have been isolated.[32] These heterocyclic ligands do not have the facile redox properties of the catechols and their tris-ligand metal complexes are neutral at physiological pH. Contemporaneous with my catechol research, other members of our group were synthesizing Al and Ga complexes with several 3-hydroxy-4-pyrones.[37] The ligand that proved the most interesting was 3-hydroxy-2-methyl-4-pyrone (maltol), a naturally occurring compound that is used as a food additive. In animal studies conducted by our collaborators, tris(maltolato)aluminum(III) ($Al(ma)_3$) was found to be 20 times as

neurotoxic as Al-lactate, the agent commonly used to induce aluminum encephalopathy.[38] The work in our laboratory established the affinity of the α-hydroxyketone binding group for Al and Ga; however, maltol was not able to redirect ^{67}Ga from transferrin in preliminary imaging experiments.

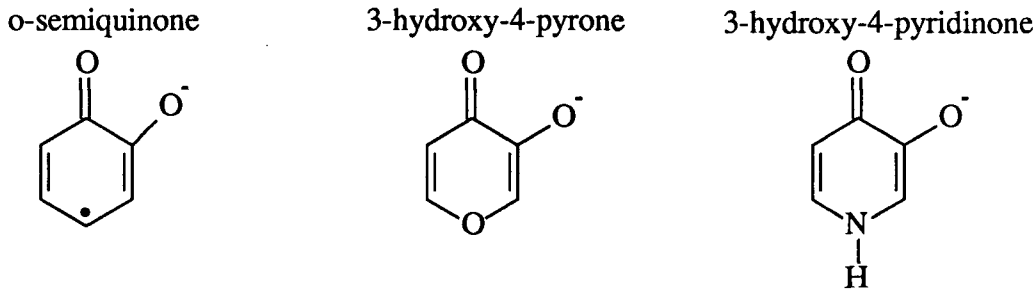

Figure 1.3. Heterocyclic ligands comparable to *o*-semiquinone.

The 3-hydroxy-4-pyridinone* nitrogen heterocycles offered several advantages over the 3-hydroxy-4-pyrones. The primary advantage was synthetic versatility: the cyclic ether in 4-pyrone is essentially inert whereas a variety of substituents can be attached to the ring nitrogen in 4-pyridinone. The 3-hydroxy-4-pyridinones are also stronger bases (as indicated by the pK_a of the 3-hydroxyl group) and this should result in tris-ligand metal complexes that are more stable than those formed by the 3-hydroxy-4-pyrones. Therefore, my research was diverted from the catechols and was directed toward the synthesis of tris(3-hydroxy-4-pyridinonato) Al and Ga complexes. One of the 3-hydroxy-4-pyridinone ligands employed in this study has been used in clinical trials as a therapeutic chelator for iron overload diseases.[39,40] The ligand was shown to be nontoxic which indicates this class of nitrogen heterocycles would be suitable for animal biodistribution studies. It was

* These compounds are also commonly referred to as 4-pyridones or 3,4-dihydroxypyridines.

felt the 3-hydroxy-4-pyridinones were similar enough to maltol to retain the positive attributes (sufficient water solubility and lipophilicity) of the Al- and $Ga(ma)_3$ complexes while having the potential to form tris-ligand metal complexes of greater stability and variability.

My project involved the synthesis of a homologous series of N-alkyl substituted-3-hydroxy-4-pyridinones. This was done to provide bidentate ligands of increasing lipophilicity that could possibly have different biodistributions. A potentially tetradentate ligand was also synthesized by linking together two 4-pyridinones via the ring nitrogens. Once isolated, the ligands were used to synthesize tris(3-hydroxy-4-pyridinonato) Al and Ga complexes that (by design) were all near the upper size limit for unhindered passage into the brain.* The ligands and metal-ligand complexes were fully characterized by elemental analysis, mass spectrometry, and infrared, proton NMR, and ultraviolet spectroscopy. Several studies were then undertaken to determine how well these compounds fit our criteria for biological relevance. The water solubility was measured and, to indicate the degree of lipophilicity, the octanol-water partition coefficients were determined. The hydrolytic stability of the Al complexes was examined by ^{27}Al NMR and potentiometric titrations were used to determine the thermodynamic stability of the Al and Ga complexes.

The proton NMR spectra of the metal complexes indicated an exchange process was occurring and this process was identified by a variable-temperature NMR study. Single crystals of several ligands and metal complexes were grown and the solid state structures were determined by X-ray diffraction. A concerted effort was made to correlate the solid state structures to the aqueous solution behavior of these compounds. Particular emphasis

---

* See Table A.1 in the Appendix for a listing of molecular weights.

was placed on examining the hydrogen bonding interactions that were a dominant force in the solid state and were also found to persist in solution for both the free ligands and the tris-ligand metal complexes.

Based on the results of this research project, several of the ligands were used in a ^{67}Ga biodistribution study. This study is still underway and the preliminary findings are briefly discussed in Chapter VI. Under conditions of ligand excess, the 3-hydroxy-4-pyridinones can redirect ^{67}Ga from transferrin; however, the resulting biodistribution is not significantly different from that of Ga-citrate and it is doubtful these ligands would have any applicability as radiopharmaceutical imaging agents. Because the transferrin binding constants for Ga are seven orders of magnitude greater than those for Al, a ligand that can compete for ^{67}Ga has the potential to form stable Al complexes in vivo. The ^{67}Ga biodistribution study does indicate the 3-hydroxy-4-pyridinone ligands have potential as therapeutic Al chelators and this application may be pursued in the future.

This research project had another goal separate from the examination of the coordination chemistry of group 13 metals and the appraisal of the biological utility of a class of ligands. This goal was the development of a methodology that would be generally applicable for future projects undertaken in this laboratory. We especially wanted to identify and assess the techniques that would be the most useful in determining the biological potential of a ligand prior to the transition from in vitro to in vivo studies.

Chapter II Synthesis and Characterization

A. 3-Hydroxy-4-Pyridinone Ligands

2.1 Introduction

The first synthesis[41] of a 4-pyridinone was reported in 1884 and since then a considerable literature has accumulated on these nitrogen heterocycles.[42-44] The methods for their synthesis can be grouped into three categories: ring closure of acyclic compounds, conversion of other heterocyclic ring systems, and substitution and displacement on pyridine or its derivatives. A review of the literature indicated that ring conversion was the simplest method for the synthesis of 3-hydroxy-4-pyridinones.

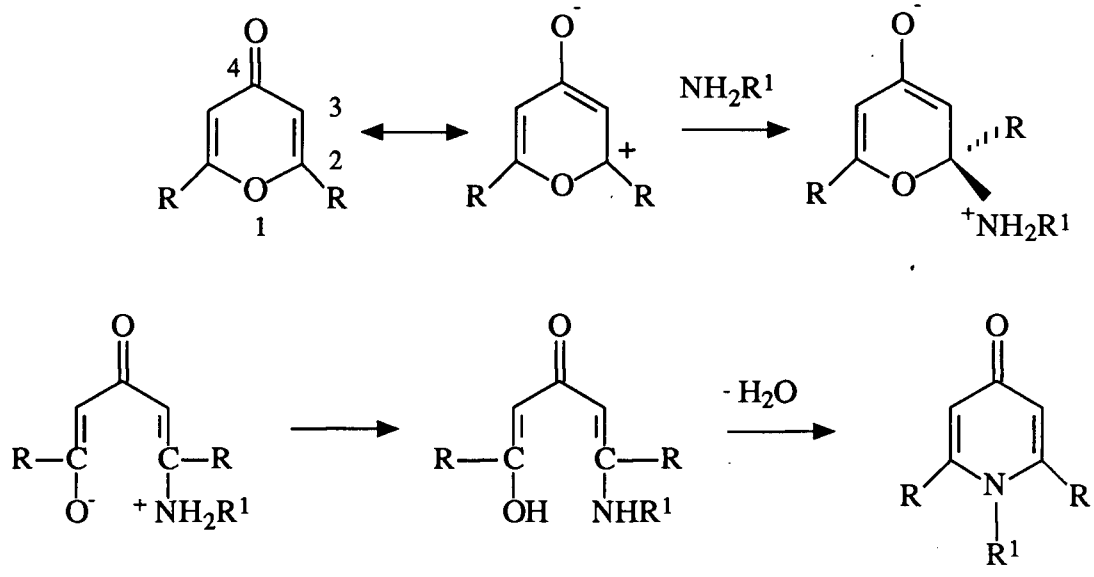

Figure 2.1. Mechanism for the conversion of a 4-pyrone to a 4-pyridinone.

One of the oldest ring conversions involves the ammonolysis and aminolysis of the cyclic ether 4-pyrone. The accepted mechanism (Fig. 2.1) is nucleophilic attack by a primary amine, followed by ring opening, loss of water, and ring closure to give the corresponding 4-pyridinone.[45] There is no direct proof offered for this mechanism, but molecular orbital calculations predict an enhanced probability of nucleophilic attack occurring at position 2.[46] Further indirect evidence is the effect ring substituents have on the conversion reaction: by induction (when in the 2 position) and resonance interaction, electron-withdrawing groups enhance reactivity while electron-donating groups have the opposite effect.[44]

Although the electron-donating hydroxyl substituent can reduce the effectiveness of the reaction, there are many examples of the conversion of 3-hydroxy-4-pyrones to the corresponding 3-hydroxy-4-pyridinones. The 3-hydroxy-4-pyrones that were considered as possible synthetic precursors in this study are listed below.

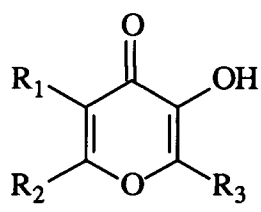

R_1,R_2, R_3 = H	Pyromeconic acid
R_1 = H; R_2, R_3 = CO_2H	Meconic acid
R_1, R_3 = H; R_2 = CH_2OH_3	Kojic acid
R_1, R_2 = H; R_3 = CH_3	Maltol

Figure 2.2. Precursor 3-hydroxy-4-pyrones.

The conversion reaction was first used for the structural determination of naturally occurring compounds. The structures of maltol[47] (in 1906) and kojic acid[48] (in 1924) were confirmed by their reactivity with primary amines; conversely, the structures of 4-pyridinones were also verified with the conversion reaction. Meconic acid and its

pyrolysis product pyromeconic acid were employed in the structure elucidation of 3-hydroxy-1-alanine-4-pyridinone (mimosine*); this was a difficult problem that provoked some controversy prior to its definitive resolution in 1947.[49,50] The synthetic utilization of the conversion reaction followed from its investigative role: kojic acid and maltol were used in the attempted synthesis of 4-piperidinols,[51] pyromeconic acid was the starting material in the first total synthesis of mimosine,[52] and a series of N-alkyl substituted-4-pyridinones was made from pyromeconic and meconic acid.[53]

The conversion reaction with the 3-hydroxy-4-pyrones, however, was seen to be somewhat inconsistent. For example, meconic acid gave the expected 4-pyridinone with methyl-, ethyl-, and propylamine but not with n-butylamine or α-phenylethylamine.[53] The reported yields were further evidence of inconsistency: a 40% yield with methylamine and a 15% yield with ethylamine. The enhanced reactivity imparted by carboxyl groups was shown by the even lower yield (10%) for the reaction of pyromeconic acid with methylamine. An extensive study on the conversion reaction concluded that the more basic and less hindered amines would give the greatest yields of 4-pyridinones.[54] However, even the results with ammonia were subject to variation: Heyns and Vogelsang found a 30% yield for the ammonolysis of kojic acid but others found this reaction to be unproductive.[43]

It is possible to improve the reactivity of the 3-hydroxy-4-pyrones by blocking the hydroxyl group. The utility of including a blocking step has long been recognized: in 1906 it was found that maltol and pyromeconic acid would not undergo ammonolysis but the 3-methoxy derivatives would react to give the expected 4-pyridinones.[47] A typical

---

* Earlier authors refer to this compound as leucaenol or leucaenine, a natural product isolated from the seeds of Leucaena glauca in 1937. It was subsequently shown to be identical to mimosine, first isolated in 1936 from the sap of the tropical shrub Mimosa pudica; since mimosine was coined first, proof of identity made the other names redundant.

blocking-deblocking sequence used dimethyl sulfate to form the methoxy derivative with deblocking by acid hydrolysis in HI or HBr. The blocking reaction was reasonably facile, but the rigorous conditions for deblocking could be a major experimental impediment.

Spenser and Notation attributed the poor yield and irreproducibility of the first mimosine synthesis to the six hours of refluxing in aqueous HI required to remove the methyl blocking group. His mimosine synthesis (from pyromeconic acid) used a benzyl blocking group because it could be removed under less strenuous conditions.[55] A continued interest in mimosine* led Harris to attempt the improvement of its synthesis; ancillary to this goal, he reported a preparation for the ammonolysis of maltol at ambient conditions that also employed the benzyl blocking group.[56] His preparation provided the starting point for our synthesis of N-alkyl substituted-3-hydroxy-4-pyridinones.

Maltol was chosen as the synthetic precursor despite the electron-donating methyl group in the 2 position. By induction the methyl substituent reduces the efficacy of the conversion reaction, but by the ortho effect[57] it reduces the acidity of the hydroxyl proton (pK_a of 8.36 for maltol vs. 7.69 for pyromeconic acid and 7.66 for kojic acid[58]). Maltol is therefore a stronger base and a better ligand for Lewis acid metal ions. Recently it was found that maltol formed Al complexes of greater stability than did kojic acid.[59] Results from our laboratory had shown maltol to be a good ligand for group 13 metals and most importantly, the metal complexes had the desired degree of water solubility and lipophilicity.[37] We felt the 2-methyl substituent would play a similar positive role in the chemistry of the 3-hydroxy-4-pyridinones synthesized from maltol thereby compensating for the reduced effectiveness of the conversion reaction.

---

* Animals fed the seeds or leaves of Leucaena glauca suffered from hair loss, and mimosine was found to be the active ingredient responsible for this. This depilitory activity was the reason for the renewed interest in its synthesis as it was thought to show promise as a chemical de-fleecing agent to improve wool harvesting.

3-Hydroxy-2-methyl-4-pyridinone ligands were synthesized from maltol and the following primary amines: methyl-, ethyl- and *n*-hexylamine; ammonia and 1,6-diaminohexane. The diamine was used to synthesize a bispyridinone that would be a potentially tetradentate ligand. The monopyridinone ligands were named from the first letters of the substituents, e.g., 3-**H**ydroxy-2-**m**ethyl-1-**h**exyl-4(**p**ara)-**p**yridinone became Hmhpp. The substituents were ordered to emphasize the acidic proton so that the conjugate base of the ligand could be readily identified, e.g., mhpp$^-$. The bispyridinone H_2exn was named from its hexane progenitor again stressing the protons. The structures of the ligands synthesized in this study are in Figure 2.3.

3-Hydroxy-2-methyl-4-pyridinone

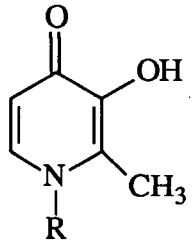

R = H	Hmpp
CH_3	Hdpp
CH_2CH_3	Hmepp
$(CH_2)_5CH_3$	Hmhpp

1,6-Di(3-hydroxy-2-methyl-4-pyridinone)hexane H_2exn

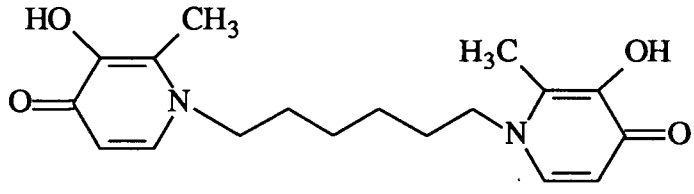

Figure 2.3. Ligand structures and abbreviations.

2.2 Materials and Methods

Of the preparations in Method A, that of Hmpp was according to Harris;[56] the others were reported previously by us, with ours being the first synthesis of H_2exn.[60] Hmpp has been synthesized by other methods.[61] The synthesis of Hdpp from maltol[62,63] and of Hmhpp from maltol D-glucoside[64] had been reported prior to our work. Further experimentation was undertaken to simplify Method A by eliminating the blocking step and the results are reported as Method B. The precedents and rationale for this additional synthetic effort will be presented in Section 2.3.

All chemicals were reagent grade or better and were used without further purification. The progress of the reactions was monitored by thin layer chromatography (TLC) on silica gel plates with 5% methanol in CH_2Cl_2 as the eluting solvent. The starting material 3-benzyloxy-2-methyl-4-pyrone (Bzma) was made from the commercially available maltol (Aldrich) by the method of Harris (> 95% yield).[56] Bzma is a viscous yellow liguid that was used without further purification (TLC pure) The melting points were measured with a Mel-Temp apparatus and are uncorrected. Unless stated otherwise, the quoted yields were for purified compound and they were calculated from maltol. The characterization data, including the elemental analyses, are found in Section 2.4.

Method A

2.2.1 3-Benzyloxy-2-methyl-4(1H)-pyridinone, Bzmpp. This intermediate was prepared by the treatment of Bzma with a solution of ammonia in ethanol according to the method of Harris.[56] Crystallization from hot ethanol gave 4.70 g (60% yield) of pale yellow crystals. Mp 166 °C.

2.2.2 3-Hydroxy-2-methyl-4(1H)-pyridinone, Hmpp. Bzmpp was deblocked by acid hydrolysis with 40% HBr in acetic acid.[56] The crude product was redissolved in water and NH_4OH was added to adjust to pH 8. The solution was cooled overnight at 10 °C and gave 2.63 g (47% yield) of pink crystals. Mp 265 °C dec.

2.2.3 3-Hydroxy-1,2-dimethyl-4-pyridinone, Hdpp. A solution of Bzma (10.0 g, 46.0 mmol) in 50 mL ethanol and 100 mL 40% methylamine in water (130 mmol) was placed in a sealed flask at 20 °C for 72 hours. The excess amine was removed in vacuo and the oily residue taken up in 100 mL water. The organic phase was extracted into CH_2Cl_2 (2 x 100 mL) and evaporation gave a yellow oil. The benzyl ether (Bzdpp) was dissolved in 50 mL THF and hydrogenated under ambient conditions over 5% Pd/C catalyst (1 g) until hydrogen uptake ceased. The solution was filtered and the solid extracted with boiling water (3 x 100 mL). The aqueous solution was concentrated until crystallization commenced and then chilled at 10 °C overnight. Recrystallization from hot methanol gave 3.46 g (52% yield) of white crystals. Mp 260 °C dec.

2.2.4 3-Hydroxy-2-methyl-1-hexyl-4-pyridinone, Hmhpp. Bzma (7.10 g, 32.8 mmol) and hexylamine (16.6 g, 164 mmol) were dissolved in 100 mL methanol and placed in a sealed flask at 20 °C for 72 hours. The solution was concentrated in vacuo and 100 mL 12M HCl was added to the oily residue. After heating on a steambath for 1 hour, the excess acid was removed in vacuo. To the residue was added 100 mL water and the pH adjusted to 8 with 2 M NaOH at which time a precipitate formed. Sublimation of this beige solid gave 3.40 g (48% yield) of a yellow powder. Mp 123 °C.

2.2.5 1,6–Di(3–hydroxy–2–methyl–4–pyridinone)hexane, H_2exn. Bzma (3.0 g, 14.0 mmol) and 1,6-diaminohexane (8.0 g, 69.0 mmol) were stirred in 25 mL methanol for 72 hours at 20 °C. Concentration in vacuo gave an oil that was treated with 50 mL concentrated HCl and heated for 30 minutes on a steambath. The acid was removed in

vacuo and the residue was dissolved in 50 mL water. The pH was adjusted to 8 with 2 M KOH and the resulting precipitate was collected. The filtrate was extracted with $CHCl_3$; evaporation left a solid residue that was added to the earlier precipitate to give 0.43 g (18% yield) of a yellow powder. Sublimation gave analytically pure sample. Mp 295 °C dec.

Method B

The reactions were done under positive N_2 pressure. The flasks were fitted with condensing columns but the reactions were only heated to 50 °C. Before extraction or aqueous recrystallization, the pH was adjusted to take advantage of the difference in acidity between the 3-hydroxy-4-pyridinones and maltol (pK_a of ~9.8 and 8.4, respectively). Purification at pH 8 ensured disproportionately greater ionization of the unreacted starting material thus aiding in the removal of the primary contaminant in these reactions. The solution pH was measured with a Fisher Accumet model 805 pH meter.

2.2.6 3-Hydroxy-2-methyl-4-(1H)pyridinone, Hmpp. To a chilled solution of maltol (2.53 g, 20.1 mmol) in 30 mL of water was added 4 mL concentrated NH_4OH (60 mmol) followed by the slow addition of 5 mL 6 N HCl. The pH was adjusted to 9.3 and the solution was heated for 36 hours. Concentration in vacuo and cooling at 10 °C for 24 hours gave 1.42 g of crystalline product. Recrystallization from hot methanol gave 1.20 g (48% yield).

2.2.7 3-Hydroxy-1,2-dimethyl-4-pyridinone, Hdpp. Maltol (5.05 g, 40.3 mmol) in 75 mL water was placed in a 3-necked flask to which was connected an addition funnel with 15 mL 40% methylamine in water (193 mmol) and 50 mL water. The solution was heated for 12 hours with the amine being slowly added during the first 4 hours. The solution was concentrated in vacuo and cooling at 10 °C overnight gave 2.80 g of a yellow microcrystalline solid. The filtrate was extracted with 150 mL CH_2Cl_2 for 12 hours in a liquid-liquid extractor. Evaporation of the solvent left a residue that was washed with

acetone and added to the filtrant. Purification by sublimation gave 3.87 g (70% yield) of a white powder.

2.2.8 3-Hydroxy-2-methyl-1-ethyl-4-pyridinone, Hmepp. A solution of maltol (2.52 g, 20.0 mmol), 70% ethylamine in water (13.3 g, 206 mmol) and 40 mL of water was cooled in an ice bath. 30 mL of 6 N HCl was slowly added and the pH adjusted to 9.8. The solution was heated for 24 hours, transferred to a continuous liquid-liquid extractor, and the product was extracted into 100 mL CH_2Cl_2 for 6 hours. Evaporation of the solvent left a brown solid that was washed with cold acetone. Sublimation gave 1.80 g (58% yield) of a white powder. Mp 205 °C dec.

2.3 Discussion of the Synthetic Procedure

Initially, the ammonolysis of maltol was attempted under the same conditions as reported herein for its benzyl ether derivative Bzma. The resulting failure to observe any conversion to Hmpp confirmed the utility of employing a blocking group. Method A (Fig.2.4) can be divided into three steps: blocking of the ring hydroxyl group, the ring conversion reaction, and deblocking to give the 3-hydroxy-4-pyridinone. The blocking reaction is a Williamson ether synthesis with maltol going to Bzma (an oil) in high yield.

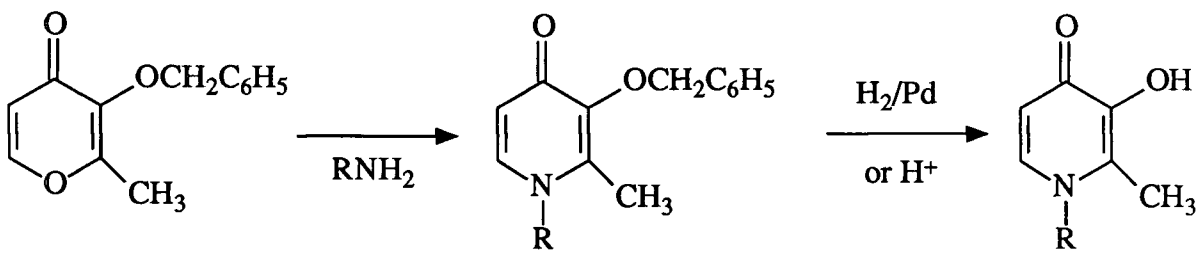

Figure 2.4. The schematic representation of Method A.

The conversion reaction was done at ambient temperature and the maximum yield was obtained after three days. A similar procedure allowed seven days but the yield for Hdpp was the same as in Method A (~50%).[63] Attempts were made to speed up the reaction by refluxing, but product isolation was complicated by the resulting tarry byproducts and yields were significantly lower. The reaction was done in alcohol/water mixtures because of the hydrophobicity of Bzma and this may have retarded the reaction; an earlier study had concluded that the conversion reaction was more efficient in water than in alcohol.[51] In the synthesis of Hmpp, the 4-pyridinone benzyl ether (Bzmpp) was isolated as an analytically pure solid when triturated by acetone and recrystallized from ethanol. The other benzyloxy intermediates only formed as oils (probably due to the lipophilic N-alkyl substituents) and the preparations proceeded directly to the deblocking step.

For Hmpp, deblocking was done by catalytic hydrogenation or by acid hydrolysis in 40% HBr in acetic acid, with the latter giving the greater yield. The results were reversed with Hdpp, and hydrogenation gave better results. Acid hydrolysis with 6 N HCl was used for Hmhpp, and H_2exn required concentrated HCl to remove the benzyl blocking group. Restricted access to the hydrogenation apparatus and the need for more rigorous deblocking left acid hydrolysis as the method most often employed. The conversion reaction was done with a five-fold excess of amine, and the unreacted amine was removed by rotary evaporation. For 1,2-diaminohexane this was insufficient and acid hydrolysis gave the dihydrogenchloride salt of the precursor amine as a byproduct. Separation of the product was difficult and undoubtedly contributed to the poorer yield for H_2exn compared to that for Hmhpp (18 vs. 48%). The problem of salt formation was a complicating factor in all the preparations albeit to a lesser extent.

The least desirable aspect of Method A was the time required as the three steps took up to five days to complete. A possibility for shortening the procedure would be to heat the reaction in a sealed glass tube: maltol and its 3-methoxy derivative gave 35 and 69% yields

respectively when heated with aniline in sealed tubes (40 hours at 150 °C).[65] Our efforts with sealed vessels were unsuccessful as both maltol and Bzma failed to react with either ammonia or *n*-hexylamine. The decision to forego further experimentation with this technique was facilitated by the physical restrictions of the glass tubes; this limitation led to recent attempts to circumvent sealed tube reactions in a study with kojic acid and arylamines.[66] Another way to speed up the procedure would be the elimination of the blocking step. This step was included to avoid deprotonation of the ring hydroxyl group as the increased electron-donating capacity of the O^- anion would impede formation of the 4-pyrone resonance hybrid most susceptible to nucleophilic attack. Instead of replacing the proton, the ionic state of maltol could be controlled by buffering the reaction at a pH < the pK_a of the hydroxyl proton.

Hdpp was obtained in a 55% yield from a procedure employing a methylammonium acetate buffer. The reaction was done at slightly acidic, neutral, and slightly basic pH with the latter giving the best results.[62] The pH was not specified but repeating the preparation gave an initial pH of 9; however, we were unable to achieve reasonable yields for Hdpp or Hmepp with this procedure. It was felt the problem lay with the acetate buffer (and with the chromatographic separation step this necessitated) and the results encouraged further experimentation with buffered systems. Recently the conversion reaction was done without blocking or buffering.[67] This simple preparation gave a 50% yield for the reaction of maltol with methylamine, but the results were poorer with ethyl- and *n*-propylamine (24% and 21% yield, respectively) showing once more the inconsistency of the conversion reaction. This limitation made it worthwhile to continue to look for a procedure that would have wider applicability than the above preparations and that would be faster than Method A. But "method" is the wrong word; rather what is reported herein as Method B is simply an experimental strategy that recognizes the primary importance of the ionic state of the reactants (and consequently the solution pH) to the success of the conversion reaction.

The utility of this strategy can be demonstrated by examining the preparation of Hdpp without blocking or buffering.[67] The ratio of reactants was 3:1 methylamine to maltol; given the concentrations used, the initial pH was 11.5 and maltol would be 99.6% ionized. At the start of the reaction there was essentially no unionized or reactive maltol present. As the reaction was heated, the concentration of the volatile methylamine was reduced and after the prescribed 5 hours of refluxing the pH was 8. At this pH, methylamine would be 99% ionized and unreactive. Somewhere in between these two extremes there is a pH region where the nucleophilic attack mechanism is operable but this preparation does not control the time spent at this optimal pH. As well, the hydroxide ion is a nucleophile able to cleave 4-pyrones[68] so the avoidance of side reactions is another reason for controlling the solution pH.

A simple way to control the pH without buffering would be the slow addition of base and this was done in the preparation of Hdpp as reported in Method B. Methylamine was added to an aqueous maltol solution over 4 hours and because of the volatility of the amine (Bp -6.3 °C), the reaction was heated at 50 °C overnight rather than refluxed. This simple preparation gave higher yields (70 vs. 52%) and was faster than the preparation in Method A. It was a cleaner preparation than the other syntheses of Hdpp (including the repeats of literature preparations) and gave microcrystalline precipitate directly from the reaction mixture.

The reaction with ammonia provided a better trial for this strategy since every ammonolysis of 3-hydroxy-4-pyrones of which we are aware employed a blocking group, a sealed reaction vessel, or both. This is probably due to the volatility of ammonia (Bp -33.4 °C) and its reduced nucleophilicity compared to alkylamines. In retrospect, our choice of ammonolysis rather than aminolysis to explore the necessity of employing a blocking group was an unfortunate one. Consistent with the difficulty of this reaction, attempts to prepare Hmpp simply by the slow addition of ammonia ended in failure; better

results were obtained with an ammonium chloride buffer. Buffering at pH 7.5 and 8.5 produced no reaction (monitored by TLC) but a significant decrease in the amount of maltol occurred upon overnight refluxing at pH 9.3. These results coupled with the failure of the unbuffered reaction (pH > 10) indicated a narrow range of optimum reactivity.

For the Hmpp preparation in Method B, the solution was buffered at pH 9.3 with initial concentrations such that the ratio of unionized reactants would be 15:1 ammonia to maltol. This was a one pot synthesis that gave the same yield (48%) as in Method A but was again a simpler and faster preparation. The N-ethyl derivative Hmepp was prepared in an analogous manner to Hmpp. The buffered preparation gave a higher yield (58%) than either Method A (35%) or the unbuffered preparation cited previously (24%).[67]

By controlling the ionic state of the reactants it is possible to convert maltol to its 3-hydroxy-4-pyridinone analogues without using a blocking group. The yields are the same or better and the preparations are simpler and faster for Method B when compared to Method A. The routine synthesis of 3-hydroxy-4-pyridinones in our laboratory is now done without a blocking group, as are the exploratory efforts to synthesize new pyridinone ligands.

2.4 Characterization of the 3-Hydroxy-4-Pyridinone Ligands

The ligands were characterized by elemental analysis, infrared (IR) and proton NMR spectroscopy, and electron impact mass spectrometry (EI-MS). The characterization data were completely consistent with the structures as shown in Figure 2.3. Particular attention was paid to the hydrogen bonding (H-bonding) in these compounds. The IR spectra indicated that the compounds were H-bonded polymers in the solid state and that the intermolecular H-bonds involved the hydroxyl and the carbonyl moieties. The IR

results for Hmpp showed the cyclic secondary amine was also a H-bond donor; a proton NMR experiment indicated the H-bonding persisted in solution.

The elemental analyses (C, H, N) were performed by Mr. Peter Borda of the Microanalytical Laboratory of this Department. The IR spectra were recorded with a Perkin Elmer PE 783 in the range 4000-200 cm^{-1}. All samples were prepared as KBr disks and spectra were referenced to polystyrene film. The proton NMR spectra were recorded with a Bruker WP-80 and a WP-400 instrument. The 80 MHz instrument was run by the author, and spectra at 400 MHz were supplied by the U.B.C. NMR service. The EI-MS was performed on a Kratos MS 50 spectrometer and all mass spectra were supplied by the U.B.C. mass spectrometry service.

2.4.1 Elemental Analysis

Prior to submission for analysis, all samples were purified either by recrystallization or by sublimation in vacuo (0.03 torr) with heating. The temperatures for sublimation were relatively mild (<140 °C) except with H_2exn. This compound was too insoluble for recrystallization and the analyzed sample was sublimed at > 285 °C using a Wood's metal bath.

Table 2.1. Results of the ligand elemental analyses (Found/[Calculated]).

	Hmpp $C_6H_7NO_2$	Hdpp $C_7H_9NO_2$	Hmepp $C_8H_{11}NO_2$	Hmhpp $C_{12}H_{19}NO_2$	H_2exn $C_{18}H_{24}N_2O_4$
%C	57.58 [57.57]	60.45 [60.41]	62.56 [62.72]	68.56 [68.87]	64.81 [65.03]
%H	5.70 [5.65]	6.49 [6.53]	7.28 [7.25]	9.01 [9.15]	7.19 [7.29]
%N	11.23 [11.24]	10.00 [10.07]	8.98 [9.14]	6.61 [6.69]	8.40 [8.43]

2.4.2 Infrared Spectroscopy

Of the spectroscopic techniques employed in the study of these compounds, IR is the most useful as it affords a facile confirmation of the outcome of the conversion reaction. The ring skeleton vibrational modes of the pyridinones and the pyrones are related to those found in benzene.[42] This typically results in four ring-stretching modes between 1650 and 1400 cm^{-1}, and the pattern changes predictably when the cyclic oxygen is replaced by nitrogen. An examination of the IR spectrum readily confirms the transformation of maltol to the corresponding 3-hydroxy-4-pyridinone.

In the 1960's there were a number of IR spectroscopic studies on the 4-pyridinones motivated primarily by the difficulty of assigning the carbonyl stretching mode in these compounds.[69-71] Although none of these studies included any 3-hydroxy derivatives, it was possible to make tentative spectral assignments based on this work. The assignments in Tables 2.2 and 2.3 were supported by reference to Bellamy's review of structural correlations in the infrared.[72] Hmpp is of special interest because of the additional H-bond donor in this compound; the assignments for the modes in Hmpp affected by H-bonding are included with those of the benzyl ether intermediate (Bzmpp), and the dideuterated analogue, d_2-Hmpp in Table 2.2. Deuteration was by repeated crystallization from D_2O and was undertaken to determine the relative strength of the H-bonds. The spectral assignments for the other compounds are in Table 2.3. The IR spectrum of Hmpp from 1700 to 300 cm^{-1} is reproduced as Figure 2.5. The abbreviations used for the vibrational modes are: ν, stretching; δ, in-plane bend; π, out-of-plane bend; as, asymmetric; sy, symmetric.

The assignment of ν_{OH} in Hmpp is confirmed by Bzmpp where the 3270 cm^{-1} band disappears and by d_2-mpp, where it shifts to 2420 cm^{-1}. This gives a ν_{OH}/ν_{OD} of

1.35, indicative of a relatively weak H-bond. The theoretical ratio is 1.375 (from the reduced masses) and for free OH it is 1.355.[73] This ratio falls systematically as the strength of the H-bond increases and can reach unity for very short H-bonds.[74] A combination of a lower zero point energy for H than D, and a weaker O···D···O than O···H···O interaction explains this low ratio.[74] In the N-alkyl derivatives the ν_{OH} drops below 3200 cm^{-1} which suggests stronger H-bonding than in Hmpp; this is suppported by the lower $\nu_{C=O}$ in these compounds, e.g., 1645 cm^{-1} in Hmpp and 1630 cm^{-1} in Hdpp. In all cases the bands are broad and within the range for normal polymeric intermolecular H-bonding.[72]

The assignment of ν_{NH} is confirmed by Bzmpp, d_2-Hmpp, and Hdpp: the band is at 2800 cm^{-1} in Hmpp, shifts to 2650 cm^{-1} on benzylation, shifts to 2210-2150 cm^{-1} (split, mean = 2180 cm^{-1}) on deuteration, and finally disappears on methylation. The ratio (ν_{NH}/ν_{ND}) is 1.28 and splitting of ν_{ND} is not without precedent, as it is reported in deuterio-2-pyridinone.[75] The authors list a 3100 cm^{-1} band (in KBr) for the protio compound which supports our assignment, and also state that the 2885 cm^{-1} ν_{NH} band for 2-thiapyridinone is the strongest NH hydrogen bonding yet recorded for other than zwitterionic structures. The deuteration ratio for the thiapyridinone is 1.29, and the typical N···H···S stretch appears at 3160 cm^{-1}.

It is impossible to separate the $\nu_{C=O}$ and the higher energy ν_{ring} stretches in any of the compounds. The bands are extensively coupled and there is no mode which is localized solely in the carbonyl bond.[76] The highest wave number band has the most C=O character and the relatively low energy of this band (below 1650 cm^{-1} in all spectra) indicates it is acting as a H-bond acceptor. In the δ_{CH} region, weak to medium intensity bands are observed with additional bands for the compounds with N-substitution consistent with the presence of additional methyl and methylene groups. There is extensive mechanical coupling of the δ_{OH} and ν_{CO} modes in the region 1325 to 1235 cm^{-1}

so that an unambiguous assignment is not possible.[74,77] The δ_{Ring} and π_{Ring} assignments correlate well with the literature and the sharp out-of-plane bending mode (ca. 820 cm^{-1}) is the most distinctive feature of the lower energy region in all of the spectra.

Table 2.2. Infrared bands for Hmpp and substituted analogues (cm^{-1}).

Assignment	Hmpp	d_2-Hmpp	Bzmpp
$\nu_{OH\ (D)}$	3270 b	2420	
$\nu_{NH\ (D)}$	2800 b	2180	2650 b
$\nu_{C=O}$	1645	1630	1630 sh
and	1620	1550	1620
ν_{Ring}	1540	1540 sh	1535
	1500	1490	1500
	1420 w	1420 w	1410
ν_{CO} and	1300,1270	1325	1190 (ν_{COC})
$\delta_{OH\ (D)}$	1245	900 b	
δ_{Ring}	1225	1245 sp	1215 sp
	1110	1150	1110
	1045	1090	1050

Table 2.3. Selected infrared absorption bands (cm^{-1}). All bands are strong except where noted.[a]

Assignment	Hmpp	Hdpp	Hmepp	Hmhpp	H_2exn
ν_{OH} (b)	3270	3150	3180	3195	3195
ν_{CHring} (w)	3100	3010	3040	3060	3060
$\nu_{CH3(2)}$	2920 w	2940 w	2980 w	2960,2935	2960
				2860	2890
$\nu_{C=O}$	1645	1630	1630	1630	1630
and	1620	1565	1575	1580	1580
ν_{Ring}	1540	1530	1530	1530	1530
	1500	1515	1510	1510	1505
	1420 w	1400 w	1405 w	1405 w	1400 m
δ_{asCH}	1450 w	1460	1450 w	1465 w	1460 w
δ_{syCH}	1380	1380 m	1365	1380 w	1380 w
		1335		1350	1360 m
ν_{CO} and	1300, 1270	1280	1260	1270 sh	1300,1280
δ_{OH}	1245	1250 b	1230	1240 b	1235 b
δ_{Ring} (w)	1225	1230	1250	1220	1220
	1110	1125	1135	1170	1170
	1045	1055	1040	1130	1040
		1030		1040	
π_{Ring}	830	820	830	850	850

[a] m, medium absorption; w, weak absorption; sp, split band; b, broad band; sh, shoulder.

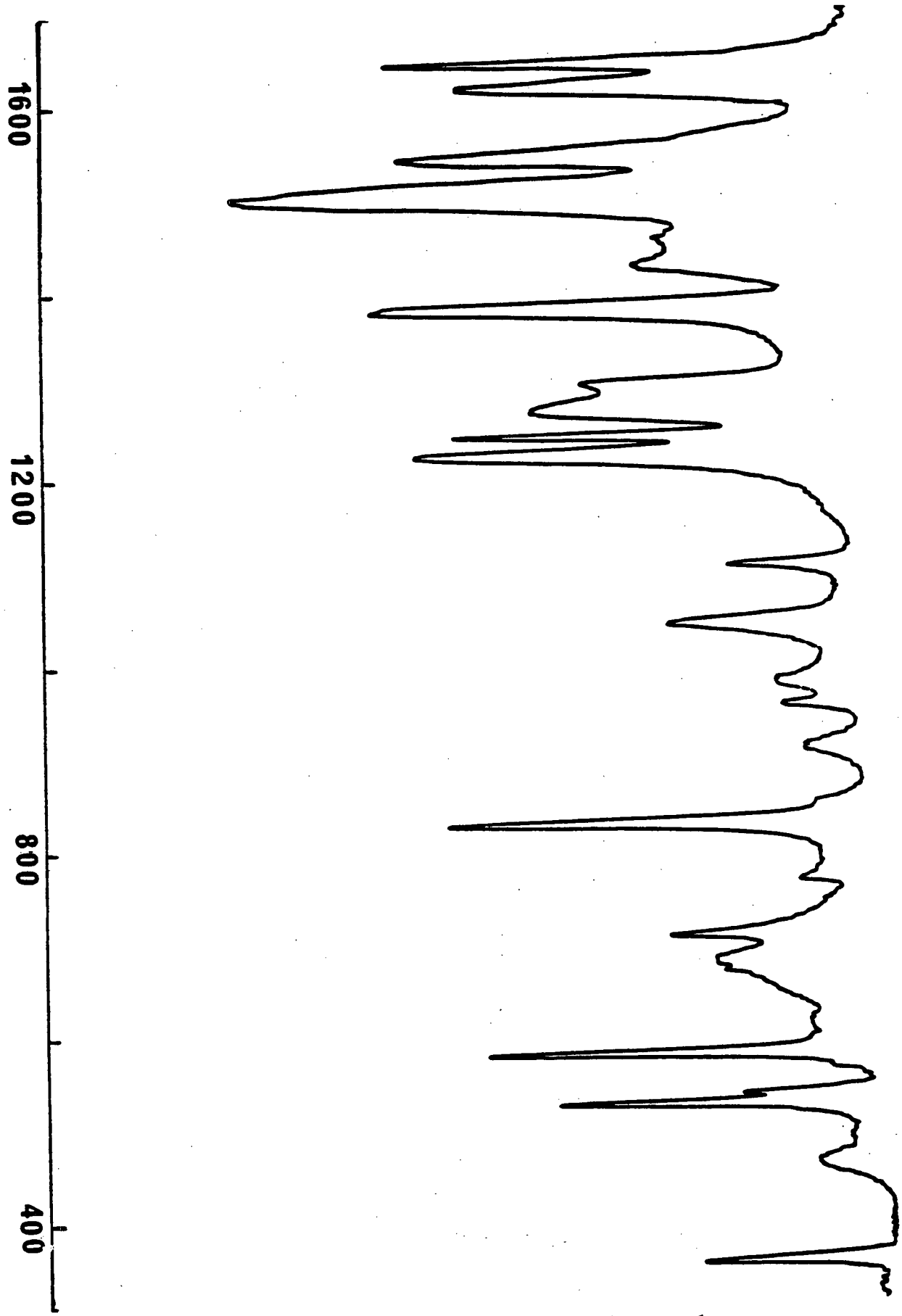

Figure 2.5. Infrared spectrum of Hmpp from 1700 to 300 cm^{-1} (KBr disk).

2.4.3 Proton NMR Spectroscopy

The spectra of Hmpp, Hdpp, and Hmepp were recorded in D_2O; the lipophilic Hmhpp and the insoluble H_2exn required 20% CD_3COOD/D_2O. The acidic NH and OH protons were detectable if the samples were rigorously dried and the spectra were recorded in aprotic solvents: $(CD_3)_2SO$ for Hmpp and Hdpp, and $CDCl_3$ for Hmepp and Hmhpp. H_2exn was only soluble in acidic solution so it was not possible to detect the hydroxyl proton signals. The spectra in D_2O were referenced to an external $(CH_3)_3Si(CH_2)_3SO_3Na$ (DSS) signal and the spectra in aprotic solvents were internally referenced to the solvent signal. The chemical shifts listed in Table 2.4 were recorded at 400 MHz except those of the OH protons that were at 80 MHz.

The spectra have AB doublets for the ring protons ($J_{a,b}$ of 7 to 8 Hz), a singlet for the ring methyl group, and a series of signals for the methyl and methylene protons of the R substituent. The signal from the protons on the carbon directly attached to the ring nitrogen is shifted downfield from that of the ring methyl group. Deshielding by the electronegative nitrogen is the reason for this and for assigning the lowfield doublet to H_a.[78] For Hdpp and Hmepp, the signals from the alkyl protons are easily assigned. With the exception of the $CH_{2d,e}$ methylene protons in Hmhpp, we did not attempt to resolve the second order spectra of the alkyl protons in Hmhpp or H_2exn. In all cases, peak integrations are consistent with the assignments as given in Table 2.4.

In the solid state, Hmpp forms intermolecular H-bonds and this interaction persists in solution as evidenced by the spectra recorded in $(CD_3)_2SO$. As the sample concentration is increased, the OH resonance shifts downfield from 5.64 ppm at 0.03 M to 6.90 ppm at 0.09 M. The direction of the shift is indicative of H-bonding and a dependence on concentration is typical of intermolecular H-bonding. The OH chemical shift is also

affected by the concentration of water in the solvent. The spectrum of an Hmpp sample (0.09 M) prepared in a drybox under N_2 is reproduced as Figure 2.6 and the OH resonance is assigned to the broad peak at 6.90 ppm; leaving the NMR tube under ambient atmosphere for several days caused the OH resonance to shift to 6.32 ppm. Similar results were obtained with a 0.03 M solution of Hmpp and with Hdpp samples. This shift is probably due to the diffusion of atmospheric water into the previously dry solvent and the upfield direction of the shift suggests the intermolecular H-bonds are stronger than those between the 3-hydroxy-4-pyridinone and water.

The NH resonance in Hmpp is assigned to the broad signal at 11.35 ppm, based on a peak in Bzmpp at 11.30 ppm (both in $(CD_3)_2SO$ at 80 MHz). The addition of a drop of D_2O to NMR samples of Hmpp results in the loss of both acidic proton signals and the loss of the second order coupling to H_a which appears as a broad, less well resolved doublet only with this compound (see Fig. 2.6). The presence of an NH chemical shift of 12.05 ppm in 2-pyridinone has been taken to suggest that the compound exists as H-bonded dimers in solution[79] just as it does in the solid state.[80] Our results for Hmpp also indicate the existence of intermolecular H-bonded arrays in solution with both the NH and OH acting as proton donors. The IR spectra and the crystallographic results (see Chapter III) clearly show that this is the case in the solid state.

Table 2.4. Proton NMR chemical shift (δ) data for the free ligands at 400 MHz (ppm).

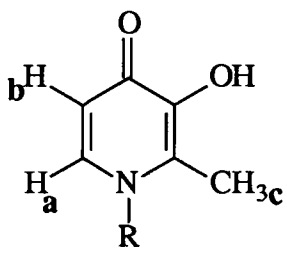

R = H

CH_{3} **d**

CH_{2} **d** CH_{3} **e**

CH_{2} **d** CH_{2} **e** CH_{2} **f** CH_{2} **g** CH_{2} **h** CH_{3} **i**

CH_{2} **d** CH_{2} **e** CH_{2} **f** CH_{2} **g** CH_{2} **h** CH_{2} **i**

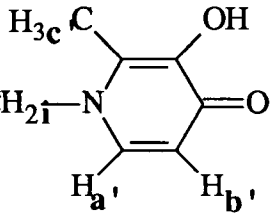

Assignment	Hmpp	Hdpp	Hmepp	Hmhpp	H2exn**
OH	6.90	6.35	6.43	5.96	
H_a (d)	7.58	7.58	7.56	7.57	7.55
H_b (d)	6.51	6.46	6.43	6.71	6.69
CH_{3c} (s)	2.34	2.36	2.33	2.16	2.13
CH_{2d}		*3.73 (s)	4.00 (q)	3.87 (t)	x3.87 (t)
CH_{2e}			*1.26 (t)	1.37 (tt)	y1.37 (m)
$CH_{2f,g,h}$				0.85 (m)	z0.93 (m)
CH_{3i}				0.38 (m)	

abbreviations: s = singlet; d = doublet; q = quartet; t = triplet; tt = triplet of triplets; m = multiplet.

* Read CH_3.

** For H_2exn, the two rings are apparently equivalent, e.g. read: $H_{a,a'}$ with integral equal to two protons.

x Read $CH_{2d,i}$ with integral equal to four protons.

y Read $CH_{2e,h}$ " "

z Read $CH_{2f,g}$ " "

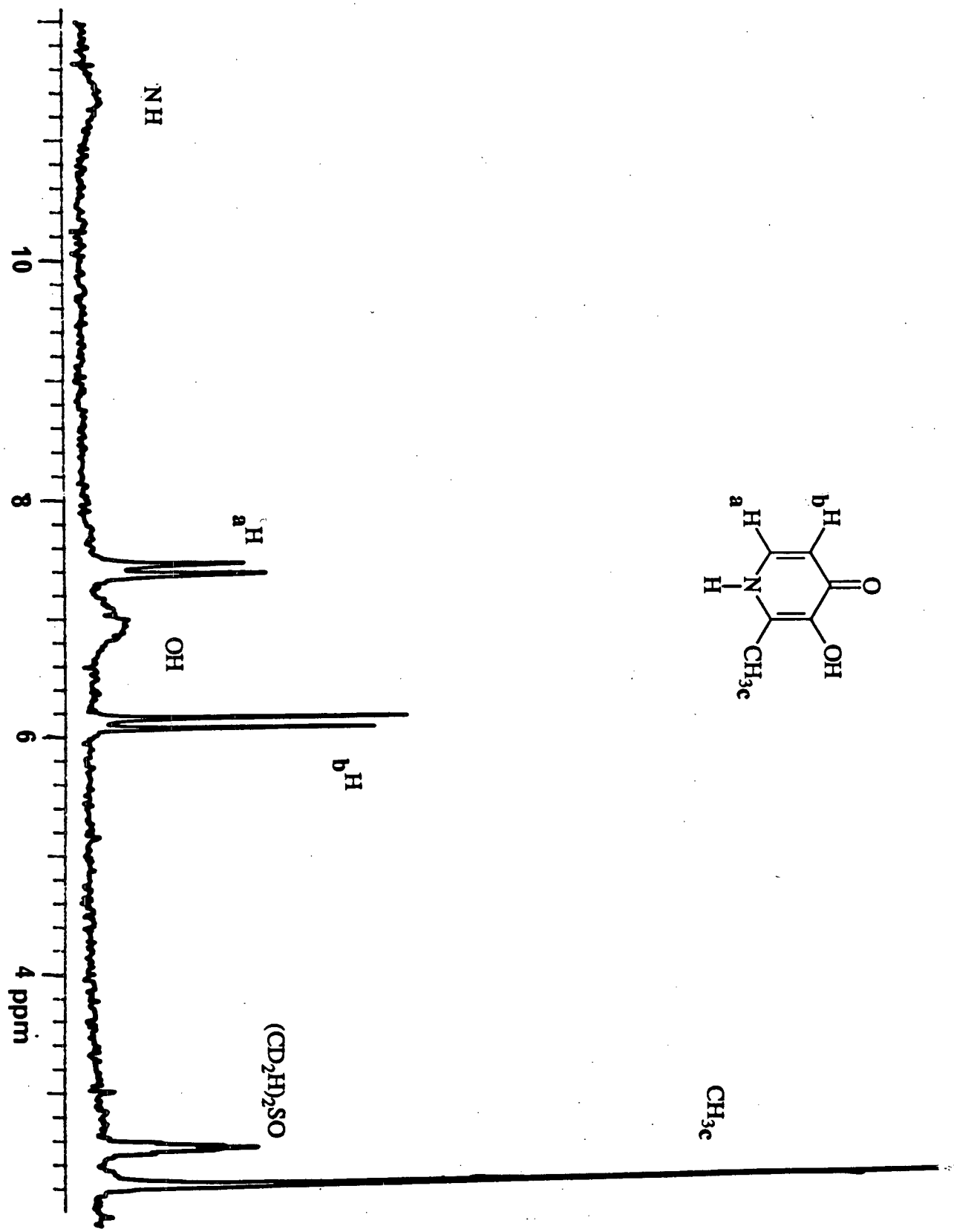

Figure 2.6. Proton NMR spectrum of Hmpp in $(CD_3)_2SO$ at 80 MHz.

2.4.4 Electron Impact Mass Spectrometry

The molecular ions, base peaks, and selected fragment ions for the compounds are listed in Table 2.5 and the mass spectrum of H_2exn is reproduced as Figure 2.7. Some assignments were made by comparison with the literature on 2-pyridinones because of the scant work available on the 4-pyridinones.[81] The ring fragments exclusively by the loss of CO (M-28) and $HCO^{\bullet}$ (M-29) and not by the loss of HCN (M-27) or CH_3CN (M-41), as is common in the 2-pyridinones. 3-Hydroxy-2-pyridinone[82] fragments with the loss of H_2O (M-18) and this did not occur in any of the 3-hydroxy-4-pyridinones.

The molecular radical cation ($M^{\ddagger}$) is present in all the spectra and this is probably a result of the ability of the ring nitrogen to localize positive charge. In the spectrum of Hmpp, the $M^{\ddagger}$ at *m/z* 125 is the base peak and *m/z* 97 and 96 are due to the loss of CO and of HCO respectively. The *m/z* 125 occurs in four of the five spectra and is the base peak in three; the prominence of the ring radical cation is due to the stability of the dihydroxypyridinium moiety which is known to be favored in the gas phase.[83] Loss of CO and $HCO^{\bullet}$ results in the *m/z* 111 and 110 peaks in Hdpp and the *m/z* 125 and 124 peaks in Hmepp. Hmepp can also fragment by cleavage of the exocyclic N-C bond with hydrogen migration to give the ring molecular cation at *m/z* 125; loss of CO and $HCO^{\bullet}$ from this ion is the best explanation for the prominent peaks at *m/z* 97 and 96 (base peak in this spectrum). This fragmentation mode is not operable with the N-methyl group so the Hdpp spectrum was without a *m/z* 125 peak.

The loss of carbonyl fragments from the $M^{\ddagger}$ is not observed in the spectra of either Hmhpp or H_2exn. The N-hexyl group in Hmhpp fragments by successive loss of methylene groups and again (by hydrogen migration) the ring radical cation is the base peak. The bispyridinone H_2exn fragments through loss of one ring to give a *m/z* 208 peak

followed by the same methylene cascade as in Hmhpp. The base peak is *m/z* 125 and both spectra have peaks at *m/z* 97 and 96. The least ambiguous spectroscopic evidence for the structure of H_2exn is provided by its mass spectrum as the IR and proton NMR spectra afford little distinction between the mono- and bispyridinone.

Table 2.5. Mass spectral data (*m/z*) with the percent relative intensity in parenthesis.

Ligand	M^+	M-CO	M-HCO	Fragment Peaks			
Hmpp	125*	97 (9)	96 (47)				
Hdpp	139 (98)	110*	111 (25)				
Hmepp	153 (74)	125 (91)	124 (28)	97 (58)	96*		
Hmhpp	209 (37)			125*	97 (14)	96 (20)	
H_2exn	332 (15)			208 (64)	125*	97 (10)	96 (31)

* Base peak (relative intensity = 100%).

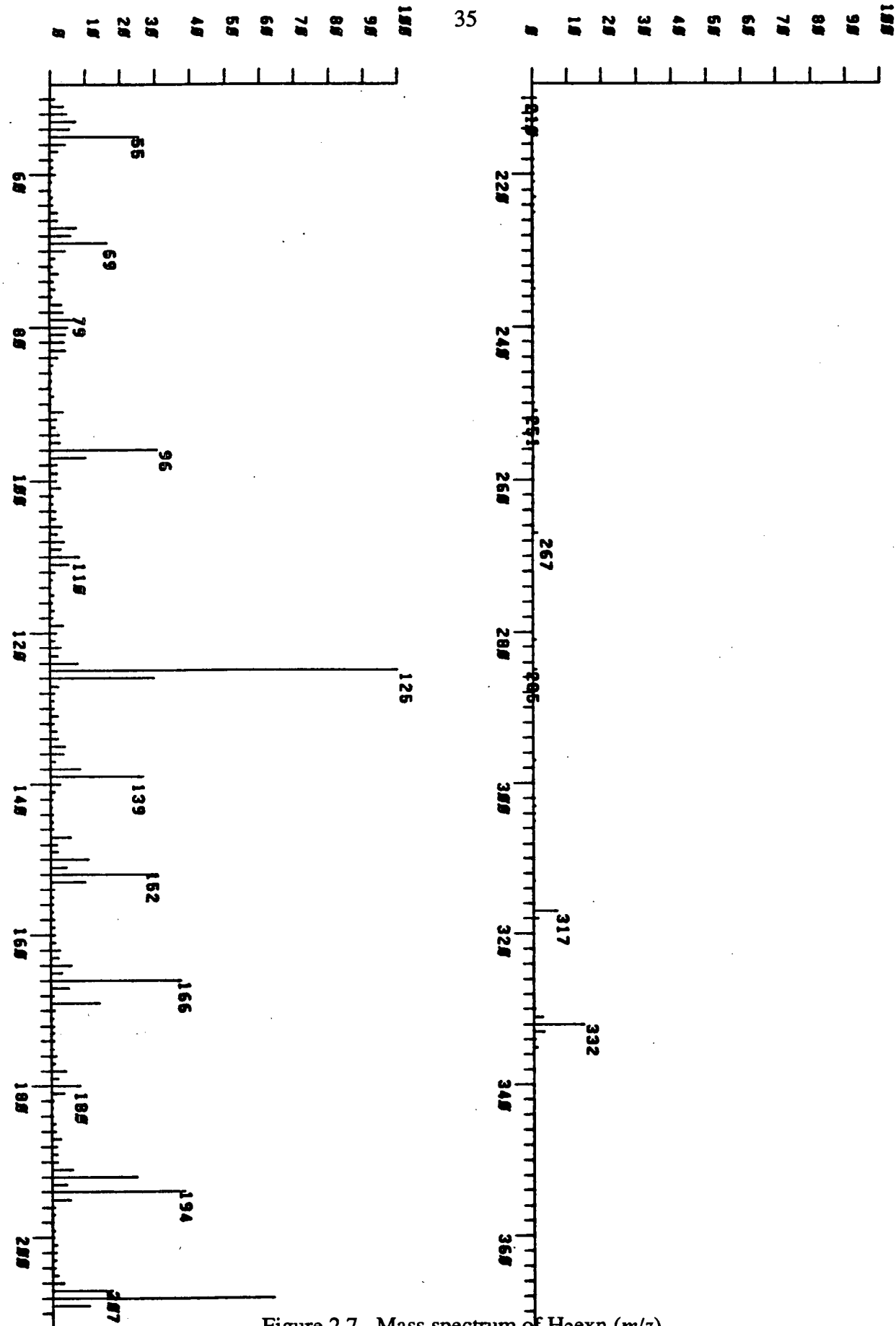

Figure 2.7. Mass spectrum of H_2exn (*m*/*z*).

B. Tris(3-Hydroxy-4-Pyridinonato) Metal Complexes

2.5 Introduction

With the exception of H_2exn, the conjugate bases of the 3-hydroxy-4-pyridinones are anionic bidentate ligands that can chelate a metal ion via the deprotonated 3-hydroxyl and the carbonyl oxygens. Each ligand would form a five-membered chelate ring with the metal center and the tris-ligand metal complexes would be of neutral charge.

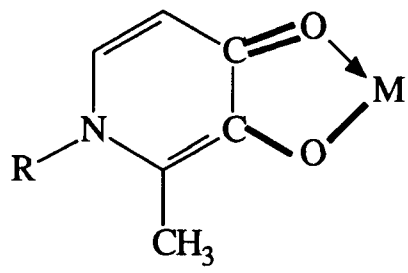

Figure 2.8. Five-membered chelate ring.

We refer to H_2exn as a "potentially" tetradentate ligand because it contains two bidentate moieties; however, the position of the oxygen atoms on the ring and the length of the hexyl bridge make it virtually impossible for both rings to chelate one metal center. H_2exn could chelate two metals to give a M_2L_3 dimer as was the case for a structurally similar diprotic tetradentate ligand containing two 1-hydroxy-2-pyridinone rings.[84]

Ligands with oxygen donor atoms are usually hard bases. Trivalent Al and Ga easily fit the definition of hard acids as acceptor atoms of high positive charge and small size. Therefore, the reaction of the 3-hydroxy-4-pyridinones with Al and Ga should conform to the Hard and Soft Acid Base (HSAB) principle, i.e., hard acids prefer to

coordinate to hard bases.[85] The HSAB principle is a generalization based on experimental facts; however, a theoretical derivation has been developed for this venerable canon of inorganic chemistry.[86] The derivation is based in part on the concept of absolute hardness (η) which has an operational (and approximate) definition of $\eta = \frac{(I - A)}{2}$ where I is ionization potential and A is electron affinity. This work has also produced a chemical definition of hardness as "the resistance of the chemical potential to change in the number of electrons".

Using the η values, it is possible to rank metal cations by their relative hardness. To demonstrate the utility of this, the η values and the charge to effective ionic radius (C/IR) ratios (based on data from ref. 30) are compared for several six coordinate trivalent metal ions in Table 2.6. (The left hand column is included for perspective: B^{3+} has the highest η value, and Ca^{2+} is a hard acid, Ag^{1+} is a soft acid, and Cu^{2+} is classed as borderline in the earlier classification system.[85]) The C/IR ratio has been used to indicate the relative hardness of metal ions and the η values allow a greater discrimination of this property. The first row transition metals (all high spin) have similar C/IR ratios but Fe^{3+} is significantly harder than its neighbors, as expected for its d^5 electron configuration and as indicated by the η values. By either the η values or the charge to ionic radius ratios, the order of hardness for the group 13 metals is Al >> Ga > In.

Table 2.6. Comparison of η values[86] (eV) and C/IR ratio ($Å^{-1}$) for selected trivalent metal ions.

	η		C/IR	η		C/IR	η
B^{3+}	111	Cr^{3+}	4.88	9.1	Al^{3+}	5.61	45.8
Ca^{2+}	19.5	Mn^{3+}	4.65	8.8	Ga^{3+}	4.84	17
Cu^{2+}	8.27	Fe^{3+}	4.65	12.1	In^{3+}	3.75	13
Ag^{1+}	6.96	Co^{3+}	4.92	8.9	Tl^{3+}	3.34	10.4

Another measure of the relative acidity of a metal ion is the first dissociation constant of the hexaaquo species defined as:

$$[M(H_2O)_6]^{3+} \underset{pKa}{\rightleftharpoons} [M(H_2O)_5OH]^{2+} + H^+$$

Based on pK_a values of 2.6, 4.0, and 5.0,[25] the order of acid strength is Ga > In > Al. The hardness of Al is exaggerated by both of the scales in Table 2.6 and the distortion is greatest in the absolute hardness value. Aluminum's large η value is due to its very large fourth ionization potential which requires the removal of an electron from an inert gas (Ne) core. The ionization potentials of Ga^{3+} and In^{3+} are based on the removal of a 3d and a 4d electron, respectively. Not surprisingly, the ionization potential for Al^{3+} is almost twice that of Ga^{3+} or In^{3+} (11,563 vs. 6150 and 5571 kJ mol^{-1}).[87] The question of the chemical relevance of the fourth ionization potential of Al was raised by the developers of the absolute hardness ranking,[86] and it is clear that the η values do not accurately predict the relative acidity of the group 13 metals. This is in contrast to the situation with the first row transition metals where the ionization potentials are due to the removal of valence electrons from the same shell.

The reason for the order of the hexaaquo pK_a values can be deduced from the third ionization potential of these metals. Instead of decreasing on going from Al to Ga it increases from 2744 to 2962 kJ mol^{-1}, and the value for In is only slightly lower than that of Al (2704 kJ mol^{-1}). The reason given for this is d-block contraction in atomic size and a higher effective nuclear charge for Ga and, to a lesser degree, for indium.[88] The electrons of the filled d shells do not completely shield the 10 added positive charges on the nucleus. When this is contrasted to the shielding afforded by the Ne core of Al, the reduced acidity of Al^{3+} (or the enhanced acidity of Ga^{3+} and In^{3+}) is quite understandable.

Regardless of the scale that is used, however, the group 13 metals are hard Lewis acids and any aqueous synthetic chemistry with Al or Ga requires the consideration of their pH dependent speciation. The complexity of their aqueous behavior can be attributed to the affinity of the hard base water ($\eta = 9.5$) for these hard metal ions. The following equations stress the pH dependence of hydroxide formation.[89]

$$Al(OH)_3 + 3\,H^+ \rightleftharpoons Al^{3+} + 3\,H_2O$$

$$K_{sol} = \frac{[Al^{3+}]}{[H^+]^3} = 10^{10.7}$$

$$[Al(H_2O)_6]^{3+} = 10^{10.7} \times 10^{-3pH}$$

From the final equation, 3×10^{-12} M is the highest concentration of free Al allowed by amorphous $Al(OH)_3$ at pH 7.4. The practical consequence is that the typical synthetic concentrations (mM) are supersaturated in $Al(OH)_3$ and a similar situation pertains with Ga. Unless a ligand has a high affinity for these metals, a gelatinous precipitate will form. Work in our laboratory with 3-hydroxy-4-pyrones had indicated that the α-hydroxyketone group was a strong enough binder of Al and Ga to preclude hydroxide formation at neutral pH and this was confirmed by the large overall formation constant β_3 reported for $Al(ma)_3$.[59] (For a definition of β_3 refer to Section 5.7.) The 3-hydroxy-4-pyrones are stronger acids than their pyridinone analogues because of the heterocyclic oxygen's greater capacity (compared to that of nitrogen) for stabilizing the negative charge of the deprotonated hydroxyl anion. The 3-hydroxy-4-pyridinone ligands used in this study have a hydroxyl pK_a ~1 pH unit higher than maltol. This increased basicity ensured there would be no hydroxide formation in the synthesis of the tris-ligand Al and Ga complexes.

There have been a number of aqueous solution studies of both of these metals with bidentate oxygen containing ligands, e.g., Al with salicylate ions[90] and with hydroxy carboxylic acids[91] and Ga with hydroxyaromatic ligands.[92] Recent interest in the biological and environmental roles of Al produced several studies on its aqueous speciation with the potentially tridentate citric acid.[93,94] Potentiometric studies indicate what ligands are good binders of these metals but do not afford any synthetic precedent. The field of Fe coordination chemistry is probably the best place to look for relevant synthetic studies as high spin Fe^{3+} is close in size and electronic properties to Ga^{3+} (see Table 2.6). The most pertinent work was Raymond's synthesis and structural characterization of Fe^{3+} complexes with 1-hydroxy-2- and 3-hydroxy-2-pyridinones.[95] Raymond has also reported the synthesis of Ga complexes with catecholate and benzohydroxamate ligands.[34]

Coordination chemistry with the 3-hydroxy-4-pyridinone ligands provides much less fertile ground as regards synthetic antecedents. In the mid 70's, N-aryl derivatives were touted as extractants for the separation of ^{67}Ga and ^{66}Zn radionuclides.[96] At this same time the stability constants of mimosine (and several related compounds) with a number of divalent metal ions were determined.[97,98] Another study[99] reported a log β_3 of 29.2 for tris(mimosinato)aluminum(III), although their methodology was questioned.[97] Several N-substituted-3-hydroxy-4-pyridinones have been evaluated as chelating agents for the treatment of iron overload diseases and a large formation constant (log β_3 = 34.5) was determined for $Fe(dpp)_3$.[100] This result was supported by the log β_3 of 35.1 found for the Fe^{3+} complex with 3,4-dihydroxypyridine.[95]

Based on our results with the 3-hydroxy-4-pyrones and the above literature, the synthesis of Al and Ga complexes was attempted with the 3-hydroxy-4-pyridinone ligands prepared in our laboratory and with L-mimosine (abbreviated as mimo). The latter was included to ascertain what effect the amino acid substituent would have on the synthesis of the tris-ligand metal complexes. It was also felt the $M(mimo)_3$ complexes could have an

interesting biodistribution as mimosine is the 4-pyridinone analogue of the catechol L-dopa, a compound that readily enters the brain (see Chapter I).

Figure 2.9 is a diagrammatic representation of the tris(3-hydroxy-4-pyridinonato) metal complexes that were successfully isolated and characterized in this study. $M(mpp)_3$, $M(dpp)_3$, and $M(mhpp)_3$ have been reported by this laboratory[101] and this is the first report of the synthesis of $M(mepp)_3$ and $Ga(mimo)_3$ of which we are aware.

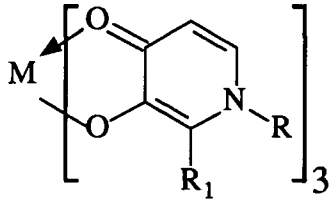

$R_1 = CH_3$	R = H	$M(mpp)_3$
	CH_3	$M(dpp)_3$
	CH_2CH_3	$M(mepp)_3$
	$(CH_2)_5CH_3$	$M(mhpp)_3$
$R_1 = H$	$CH_2CH(NH_2)CO_2H$	$M(mimo)_3$

Figure 2.9. Tris(N-substituted-3-hydroxy-4-pyridinonato) metal complexes.

2.6 Material and Methods

The preparations were the same for Al and Ga with any given ligand; the details are given for the Al preparations and only the reactant concentrations and yields are given for the corresponding Ga preparations. The only difference of synthetic importance was the reduced aqueous solubility of the Ga complexes. For a given ligand, the Ga complex was ~50% less soluble than its Al analogue and this necessitated only minor adjustments in the preparations.

Unless stated otherwise, the reported yields were for analytically pure compound. Mimosine was available commercially (Sigma, approx. 99%) and was used without further purification. The other ligands were prepared and purified as described in Section 2.2.

2.6.1 Tris(3-hydroxy-2-methyl-4-pyridinonato)aluminum(III), $Al(mpp)_3$. Hmpp (1.25 g, 10.0 mmol) and $Al(NO_3)_3 \cdot 9H_2O$ (1.24 g, 3.30 mmol) were dissolved in 20 mL water. The pH was raised to 8 with 2 M NaOH and the volume reduced to 10 mL by heating at 70 °C. While the suspension was still hot, the pink solid was collected by filtration and gave 1.06 g (83% yield). Mp 310 °C dec.

2.6.2 Tris(3-hydroxy-2-methyl-4-pyridinonato)gallium(III), $Ga(mpp)_3$. To Hmpp (1.09 g, 8.70 mmol) in 20 mL H_2O was added 1.45 M $GaCl_3$ (2.00 mL, 2.90 mmol). Yield 1.13 g, 88%. Mp 290 °C dec.

2.6.3 Tris(3-hydroxy-1,2-dimethyl-4-pyridinonato)aluminum(III), $Al(dpp)_3$. Hdpp (1.69 g, 12.2 mmol) and $Al(NO_3)_3 \cdot 9H_2O$ (1.52 g, 4.05 mmol) were dissolved in 50 mL water. The pH was raised to 8 with 12 M NH_4OH and the volume reduced to 20 mL by heating at 70° C. The pale pink product was collected after overnight cooling at 20 °C and gave 1.39 g (79% yield). Mp 300 °C dec.

2.6.4 Tris(3-hydroxy-1,2-dimethyl-4-pyridinonato)gallium(III), $Ga(dpp)_3$. To Hdpp (1.22 g, 8.80 mmol) in 20 mL water was added 1.45 M $GaCl_3$ (2.00 mL, 2.90 mmol). Yield 1.10 g, 79%. Mp 280 °C dec.

2.6.5 Tris(3-hydroxy-2-methyl-1-hexyl-4-pyridinonato)aluminum(III), $Al(mhpp)_3$. Hmhpp (0.86 g, 4.1 mmol) and $AlCl_3 \cdot 6H_2O$ (0.33g, 1.3 mmol) were dissolved in 40 mL (1:1) methanol/water. Deprotonation by the addition of 12 M NH_4OH (2 mL) was followed by heating at 80 °C for one hour to remove excess ammonia and methanol. The product

was extracted into CH_2Cl_2 (2 x 50 mL) and the solution was dried over $MgSO_4$. Vacuum distillation left a brown oil that was triturated with hexanes. Drying in vacuo (18 hours) gave 590 mg of a yellow powder (67% yield). Purification was by sublimation (300 °C, 10^{-2} torr). Mp 305 °C dec.

2.6.6 Tris(3–hydroxy–2–methyl–1–hexyl–4–pyridinonato)gallium(III), $Ga(mhpp)_3$. To Hmhpp (0.63 g, 3.0 mmol) in 40 mL (1:1) methanol/water was added 1.45 M $GaCl_3$ (0.69 mL, 1.0 mmol). Yield 0.50 g, 71% . Mp 285 °C dec.

2.6.7 Tris(3-hydroxy-2-methyl-1-ethyl-4-pyridinonato)aluminum(III), $Al(mepp)_3$. Hmepp (422 mg, 2.89 mmol) and $Al(NO_3)_3 \cdot 9H_20$ (360 mg, 0.96 mmol) were dissolved in 25 mL of water forming a pale pink solution of pH 2.2. The pH was raised to 7 by the slow addition of 2N NaOH and then the solution was heated at 70 °C for 30 minutes. The cloudy yellow solution was transferred to a liquid-liquid extractor and the product extracted into 75 mL CH_2Cl_2 over 12 hours. The organic layer was removed in vacuo. The pink solid was washed with diethyl ether and gave 425 mg (92% yield). Mp 250 °C dec.

2.6.8 Tris(3-hydroxy-2-methyl-1-ethyl-4-pyridinonato)gallium(III), $Ga(mepp)_3$. To Hmepp (669 mg, 4.37 mmol) dissolved in 15 mL of water was added 1 mL of 1.45 M $Ga(Cl_3)$ aqueous solution. Yield 652 mg, 85%. Mp 240 °C dec.

2.6.9 Tris(mimosinato)aluminum(III), $Al(mimo)_3$. L-mimosine (591 mg, 2.98 mmol) and $Al(NO_3)_3 \cdot 9H_2O$ (371 mg, 0.99 mmol) were dissolved in 25 mL of water forming an orange colored solution of pH 1.8. Concentrated NH_4OH was slowly added to bring to pH 6.5 and the yellow solution was left stirring at 20 °C for 1 hour. Methanol was added until cloudy and the solution was cooled at 5 °C for 16 hours. The pink precipitate was collected, the filtrate was concentrated to 15 mL in vacuo, and the precipitation procedure was repeated a second time. The two precipitates were combined giving 510 mg (83% yield). Mp 250 °C dec.

2.6.10 Tris(mimosinato)gallium(III) hydrate, $Ga(mimo)_3 \cdot H_2O$. To L-mimosine (593 mg, 2.99 mmol) dissolved in 25 mL of water was added 1.45 M $GaCl_3$ aqueous solution (0.69 mL, 1.00 mmol). Yield 571 mg, 86%. Mp 240 °C dec.

2.7 Discussion of the Synthetic Procedure

The preparation of the tris(3-hydroxy-4-pyridinonato) Al and Ga complexes was relatively straightforward (Fig. 2.10). The 3:1 stoichiometry was closely maintained as the formation of the tris-ligand metal complexes was thermodynamically favored and it was not necessary to use an excess of ligand to push the reaction to completion. The preparations were in water except for $M(mhpp)_3$; because of the lipophilic N-hexyl substituent, a 1:1 methanol to water solution was used. To overcome purification problems with several of the preparations, other solvents (methanol, ethanol, acetone) were tried but the best results were obtained in water. The heating step was ostensibly included to ensure complete reaction but its primary utility became that of volume reduction to induce precipitation of the tris-ligand metal complexes.

$$3\,HL + MX_3 \xrightarrow[\Delta]{\text{raise to pH 8 with BOH}} ML_3 + 3\,BX + 3\,H_2O$$

HL = 3-hydroxy-4-pyridinone ligand M = Al or Ga X = NO_3 or Cl B = Na or NH_4

Figure 2.10. Equation for the formation of the tris-ligand metal complexes.

All of the complexes were prepared in good yield (70 to 90%), and at no time were any side reactions observed. The only synthetic complication was the separation of the products from the salt formed in the neutralization process. This separation was effected either by solvent extraction or by fractional crystallization in those cases where the solubility properties of the complexes precluded simple extraction. $M(mpp)_3$, $M(dpp)_3$ and $M(mimo)_3$ were only soluble in protic solvents and they were isolated by fractional crystallization.

The initial preparations of $Al(mpp)_3$ used $AlCl_3 \cdot 6H_2O$ with NaOH as the base. The reaction mixture was concentrated (at 70 °C) until $Al(mpp)_3$ precipitated thereby taking advantage of the large difference in solubility between the product and the byproduct salt ($Al(mpp)_3$ was predicted to be soluble at the mM level). The solution was cooled and filtered; the IR and proton NMR spectra of the precipitate were consistent with the $Al(mpp)_3$ formulation and showed no proton containing impurities. However, the analytical results were indicative of a non-carbon containing contaminant (%C expected 54.18, found 46.93) and the likely cause was coprecipitation of NaCl. The preparation was repeated using $Al(NO_3)_3$ since $NaNO_3$ is twice as water soluble as NaCl, and NO_3^- has a strong sharp IR band at 1380 cm^{-1} (a region free of ligand absorbances) whereas Cl^- is invisible in the IR.

A simple experiment showed that NO_3^- was present in the precipitate and offered an easy purification method: the IR spectrum of the initial precipitate had the distinctive 1380 cm^{-1} band but if the solution was concentrated further and filtered while still hot (70 °C), this band disappeared only to reappear when the solution was allowed to cool to 20 °C before filtering. The hot (on the left) and the cold (on the right) $Al(mpp)_3$ precipitate IR spectra are reproduced as Figure 2.11 (the NO_3^- band at 1380 cm^{-1} is marked with an asterisk). The simple expedient of hot filtration gave analytically pure product in 83% yield. The $Al(mpp)_3$ preparation set the pattern for the rest of the Al complexes in that

$Al(NO)_3$ was used as the starting material to take advantage of the IR visibility of NO_3^-. As the most convenient source of Ga was the chloride salt (obtained by dissolving the metal in HCl), the reaction conditions were optimized for the Al preparation before being repeated with $GaCl_3$.

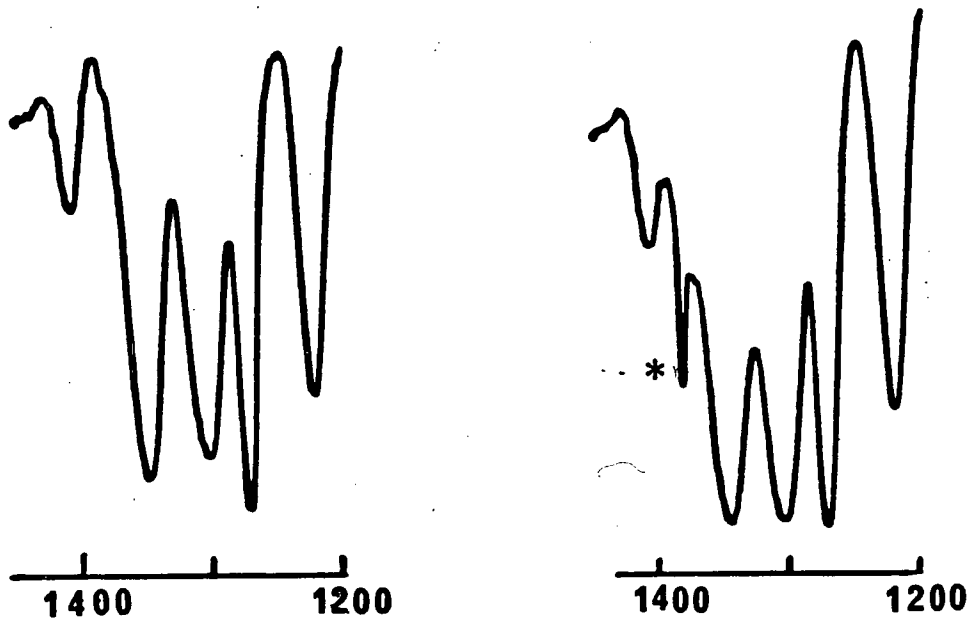

Figure 2.11. The IR spectra of $Al(mpp)_3$ from 1450 to 1200 cm^{-1}.

$Al(dpp)_3$ did not precipitate from a hot solution (due to its high solubility temperature coefficient) but overnight cooling at 20 °C gave the pure product in good yield. To avoid problems with coprecipitation, the reaction mixture was more dilute than with $Al(mpp)_3$ and NH_4OH was used as the base (NH_4^+ salts are more water soluble than Na^+ salts). In the preparation of $Al(mimo)_3$, fractional crystallization from hot water did not work nor was it possible to induce precipitation by cooling as the complex was too water soluble. Better results were obtained by using methanol as a second solvent; when precipitation was allowed to proceed slowly (16 hours), an analytically pure product was obtained.

Fractional crystallization gave low yields (50%) of $Al(mepp)_3$. Although this complex is not soluble to a measurable extent in any aprotic solvents, it was possible to isolate pure product in yields > 85% by continuous liquid-liquid extraction with CH_2Cl_2. $Al(mhpp)_3$ is quite lipophilic and forms an intractable gummy solid in water. Its preparation from $Al(CH_3)_3$ was attempted using anhydrous organic solvents and a *Schlenk* line. The product was isolated in low yield (10%) but the results did not justify the complications inherent in a highly reactive starting material. Further experimentation using $Al(NO_3)_3$, alcohol-water mixtures, and product extraction with CH_2Cl_2 produced a reasonable preparation. The yields were somewhat low (70%) and sublimation (300 °C, 0.08 torr) was needed to give samples suitable for analysis.

Despite considerable effort, we were unable to isolate any metal-ligand complexes with the H_2exn ligand. Reactions using a 3:2 stoichiometry invariably gave precipitates that were so insoluble as to defy characterization or purification. The mass spectra of a sample from an Al reaction did give an Al_2L_3 molecular ion but this was the sole piece of structural evidence to emerge from this work. The insolubility of the products proved to be an insurmountable problem.

H_2exn itself is only soluble in acidic solution; this is rather surprising since Hmhpp is readily soluble in organic solvents and the other ligands all have appreciable water solubility. The anomalous behavior of the bispyridinone may be due to the formation of H-bonded dimeric units. The hydrophilic sites in the molecule (the α-hydroxyketone moieties) would be involved in intermolecular H-bonds and the hexyl bridge is hydrophobic: the result would be water insolubility. The polar H-bonds would make the complex lipophobic: the result would be complete insolubility. A similar argument could explain the insolubility of the metal complexation reaction precipitate, as the M_2L_3 dimer would have hydrophobic hexyl bridges and lipophobic metal centers.

It is also possible for H_2exn to polymerize by forming H-bonded chains rather than dimeric units. The monopyridinones would be much less likely to form chains and this may offer a better explanation for the higher melting point and sublimation temperature (both near 300 °C), and for the decreased solubility of H_2exn when compared to the other ligands. In the metal complexation reaction, oligimers could be formed rather than dimers. Whether due to dimerization or polymerization, the established insolubility of H_2exn and the conjectured insolubility of its M_2L_3 dimer is reasonable.

2.8 Characterization of the Tris(3-Hydroxy-4-Pyridinonato) Metal Complexes

The IR and proton NMR spectra of the tris-ligand metal complexes show diagnostic changes from those of the free ligands. The changes are consistent with metal chelation via the deprotonated hydroxyl and the carbonyl oxygen atoms. The elemental analyses and the molecular ions in the mass spectra are consistent with an ML_3 formulation. The spectra of the free ligands were analyzed in some detail; therefore, only the differences between the free and complexed ligand need be addressed in this section.

Unlike the free ligands, the tris-ligand metal complexes are not volatile enough for EI-MS but rather require positive ion fast atom bombardment (FAB) ionization. All the spectra were recorded with an AEI MS 9 and the samples were introduced on a copper tipped probe in either a glycerol or a thioglycerol matrix dependent on solubility. With this exception, the instrumentation and conditions are the same as those reported for the characterization of the free ligands (see Section 2.4).

2.8.1 Elemental Analysis

The samples were submitted for analysis under N_2 because the tris-ligand metal complexes were hygroscopic. Rigorous drying was required to remove water from the recrystallized products: heating in vacuo (0.05 torr) at $\geq$ 65 °C for a minimum of 12 hours. Those samples that were sublimed were not subjected to further drying.

Table 2.7. Results of elemental analyses (Found [Calculated])

Compound	Formula	%C	%H	%N
$Al(mpp)_3$	$[C_{18}H_{18}AlN_3O_6]$	53.89 [54.13]	4.69 [4.55]	10.60 [10.52]
$Ga(mpp)_3$	$[C_{18}H_{18}GaN_3O_6]$	48.65 [48.90]	4.29 [4.11]	9.53 [9.51]
$Al(dpp)_3$	$[C_{21}H_{24}AlN_3O_6]$	57.40 [57.13]	5.54 [5.49]	9.67 [9.52]
$Ga(dpp)_3$	$[C_{21}H_{24}GaN_3O_6]$	51.98 [52.09]	5.10 [5.01]	8.54 [8.68]
$Al(mepp)_3$	$[C_{24}H_{30}AlN_3O_6]$	59.72 [59.61]	6.25 [6.27]	8.90 [8.69]
$Ga(mepp)_3 \cdot H_2O$	$[C_{24}H_{32}GaN_3O_7]$	53.52 [53.85]	6.00 [5.85]	7.72 [7.85]
$Al(mimo)_3$	$[C_{24}H_{27}AlN_6O_{12}]$	46.61 [46.60]	4.60 [4.41]	13.52 [13.59]
$Ga(mimo)_3 \cdot H_2O$	$[C_{24}H_{29}GaN_6O_{13}]$	42.18 [42.43]	4.08 [4.31]	12.20 [12.37]
$Al(mhpp)_3$	$[C_{36}H_{54}AlN_3O_6]$	66.50 [66.34]	8.19 [8.35]	6.34 [6.45]
$Ga(mhpp)_3$	$[C_{36}H_{54}GaN_3O_6]$	62.42 [62.25]	7.94 [7.85]	5.93 [6.05]

2.8.2 Infrared Spectroscopy

IR studies on pyridine derivatives show that the substituents vibrate largely independently of the ring.[42] The free ligand IR spectra were consistent with this conclusion and predictably, the spectra of the tris-ligand metal complexes and the corresponding free ligand are quite similar. The bands are broadened somewhat but the general features of the spectra are the same. Also, the spectra of the Al and Ga complexes with any given ligand are virtually identical above 800 cm^{-1} (all bands are within ± 5 cm^{-1}).

There are, however, three diagnostic differences between the spectra of the free and complexed ligand: the appearance of three new bands below 800 cm^{-1}, the loss of ν_{OH}, and the bathochromic shift of $\nu_{C=O}$. The three new bands (Table 2.8) are tentatively assigned as ν_{M-O} but they are probably also coupled to the ring deformation modes.[102] This is the only region of the spectrum where distinctions due to the difference in mass between the two metal ions are observable as at least one of the bands is consistently at lower energy in the Ga complexes. Figure 2.12 is a comparison of the spectra of Hmpp (top), $Al(mpp)_3$ (middle), and $Ga(mpp)_3$ (bottom) from 900 to 300 cm^{-1} (the ν_{M-O} bands are marked with asterisks). The zwitterionic amino acid moiety obscures the IR spectrum of mimosine but the low energy region is clean enough to be of diagnostic utility in assigning the ν_{M-O} of the $M(mimo)_3$ complexes.

The loss of the ν_{OH} is the most noticeable change in the spectra of $M(dpp)_3$, $M(mepp)_3$, and $M(mhpp)_3$. The region above 3100 cm^{-1} has only the ubiquitous band at 3450 cm^{-1} due to water. For $M(mpp)_3$, the band at 3280 cm^{-1} is assigned as ν_{NH} with the hypsochromic shift of this mode (at 2800 cm^{-1} in Hmpp) ascribed to the absence of NH

intermolecular H-bonds. The assignment is not unusual for this mode[72] and the band is much sharper in the tris-ligand metal complex than in the free ligand.

Table 2.8. Assignment of $\nu_{M\text{-}O}$ (cm^{-1}, KBr disks)

M(mpp)3		M(dpp)3		M(mepp)3		M(mhpp)3		M(mimo)3	
Al	Ga	Al	Ga	Al	Ga	Al	Ga	Al	Ga
735	730	710	710	705	705	720	720	660	655 b
640	625	575	570	580	565	580	570	620	600 b
460	365 b	440	370	460	410	475 b	340 b	440	< 300

The characteristic four band pattern of mixed $\nu_{C=O}$ and ν_{Ring} is shifted upon formation of the tris(3-hydroxy-4-pyridinonato) metal complexes (Table 2.9), with the most pronounced bathochromic shift occurring for the highest energy band (ca. 30 cm^{-1}). The superimposed spectra of Al(dpp$_3$ (on top) and Hdpp (on bottom) in Figure 2.13 illustrate the changes typically observed.

Table 2.9. Characteristic infrared absorptions (cm^{-1}). All are sharp and strong except as noted.

Assignment	M(mpp)3	M(dpp)3	M(mepp)3	M(mhpp)3
$\nu_{C=O}$	1620	1605	1600	1605
and	1595	1560	1555	1560
ν_{Ring}	1535 sh	1515	1515	1520
	1505 b	1495	1490	1490

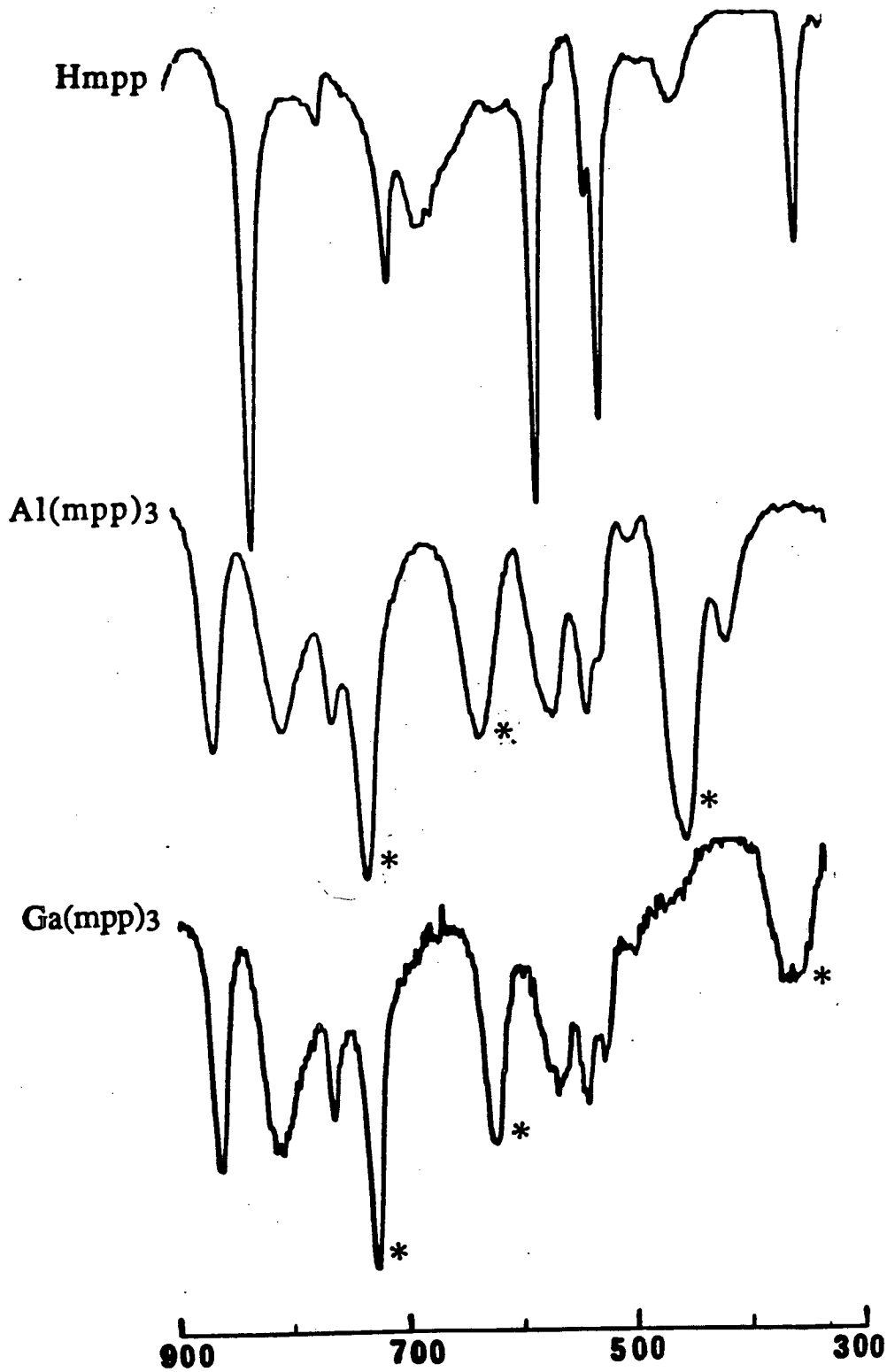

Figure 2.12. IR spectra of Hmpp and M(mpp)$_3$ complexes from 900 to 300 cm^{-1}.

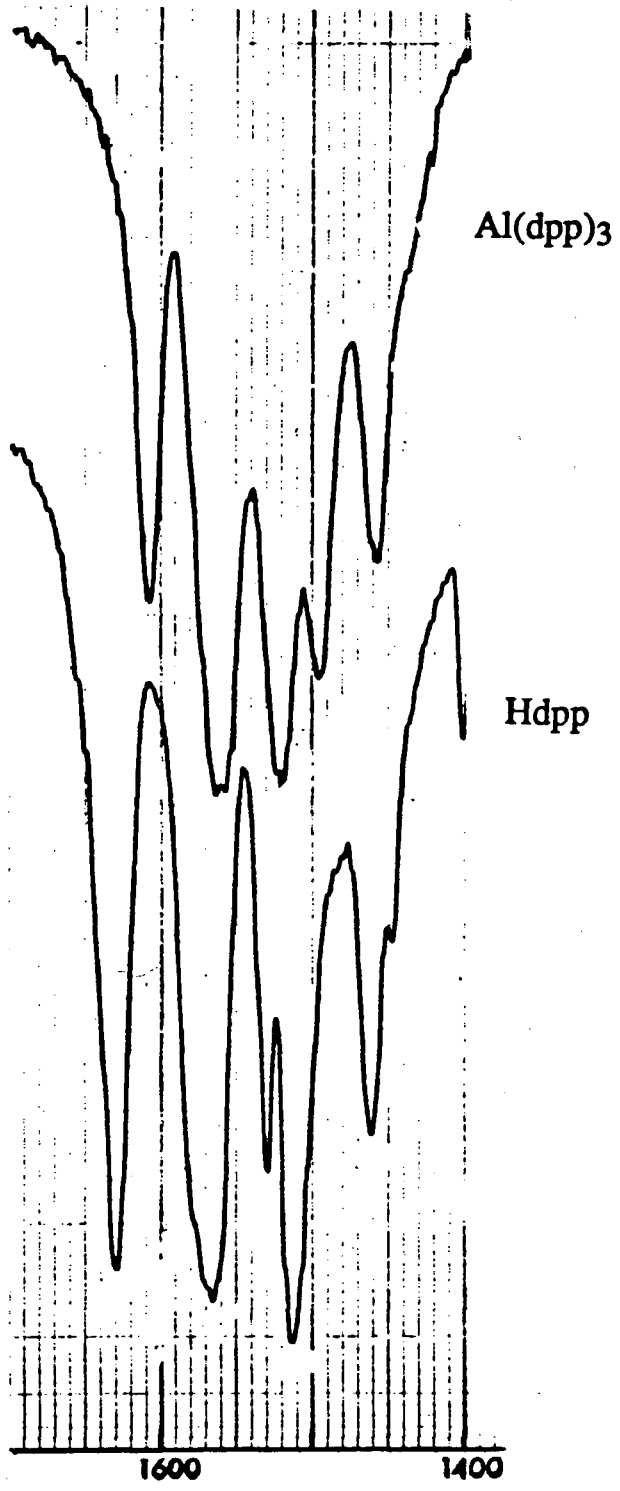

Figure 2.13. IR spectra of $Al(dpp)_3$ and Hdpp from 1700 to 1400 cm^{-1}.

2.8.2 Proton NMR Spectroscopy

The spectral changes on formation of the tris(3-hydroxy-4-pyridinonato) metal complexes are minor, but there is a diagnostic shift in the resonances of the ring protons. The resonances are closer together and the H_a signal is shifted slightly upfield (typically ca. 15 Hz). The alkyl proton resonances are also shifted but in a less consistent fashion. Under the same conditions as described previously for the free ligands, the OH resonances are absent in all the tris-ligand metal complexes. The NH signal is at 12.02 and 12.07 ppm respectively for Al- and $Ga(mpp)_3$ (in $(CD_3)_2SO$ at 80 MHz).

An exchange process is occurring in the tris-ligand Al complexes at ambient temperature; however, the chemical shift changes are small (from 8 to 20 Hz at 400 MHz) and are only observable on higher field strength instruments. This is another instance where a difference between the metals is observed as only the averaged spectrum is observed for the Ga complexes at the ambient probe temperature (typically 18 °C); this was not unexpected as Ga is known to be more labile than Al.[103] (The temperature-dependent NMR of the tris(3-hydroxy-4-pyridinonato) Al and Ga complexes is addressed in Chapter IV.) The fluxionality of the Al complexes results in overlapping signals so the chemical shift of the central signal is reported. The spectral assignments for all but the $M(mimo)_3$ complexes are listed in Table 2.11 and the peak integrations are consistent with the assignments.

It is possible for mimosine to chelate via the amino acid nitrogen and oxygen atoms although this was considered to be unlikely given the relative softness of nitrogen. The IR spectra are indicative of chelation by the α-hydroxyketone moiety, but the broadness of the amino acid bands in both the free and complexed ligand makes it impossible to rule out

entirely binding at this site. The compounds are not soluble in aprotic solvents so it was not possible to look for the acidic protons by NMR; however, comparison of the chemical shifts of free and complexed mimosine in D_2O (Table 2.10) shows the same small shifts in the H_a and H_b resonances that were seen with the other ligands. The H_c resonance (mimosine is the only ligand in this study without a 2-methyl substituent) is shifted upfield so that it is between the AB doublets, rather than downfield of them, in the $M(mimo)_3$ complexes. The exocyclic proton signals, found as three multiplets from 4.2 to 4.7 ppm that each integrate as one proton, are broadened but they did not shift significantly on chelation. The similarity in the movement of the ring proton signals indicates that mimosine is chelating the metals in an fashion analogous to the other 3-hydroxy-4-pyridinone ligands employed in this study.

Table 2.10. ^1H NMR chemical shifts (δ) for mimosine and $M(mimo)_3$ complexes (ppm). Recorded at 400 MHz.

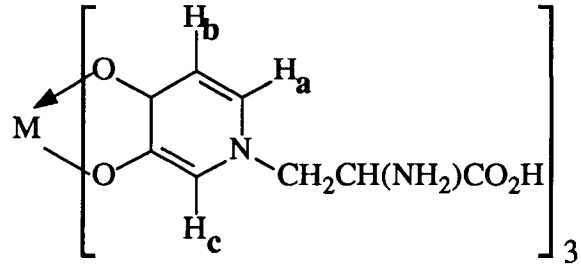

Assignment	Mimosine	$Al(mimo)_3$	$Ga(mimo)_3$
H_a (d)	7.78	7.73	7.72
H_c (s)	7.82	7.46	7.54
H_b (d)	6.85	6.72	6.77

Table 2.11. ^1H NMR chemical shifts (δ) for the tris-ligand metal complexes (ppm). Recorded at 400 MHz.

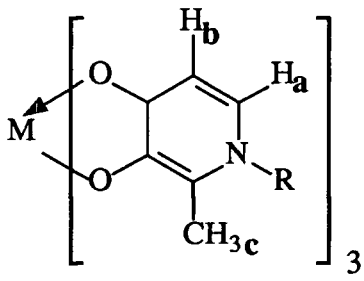

R =		
H		$M(mpp)_3$
CH_3 **d**		$M(dpp)_3$
CH_2**d** CH_3 **e**		$M(mepp)_3$
CH_2**d** CH_2**e** CH_2**f** CH_2**g** CH_2**h** CH_3**i**		$M(mhpp)_3$

	$M(mpp)_3$		$M(dpp)_3$		$M(mepp)_3$		$M(mhpp)_3$	
	Al	Ga	Al	Ga	Al	Ga	Al	Ga
H_a (d)	7.50	7.48	7.56	7.49	7.53	7.52	7.02	7.24
H_b (d)	6.56	6.61	6.50	6.47	6.48	6.54	6.48	6.70
CH_{3c} (s)	2.31	2.34	2.35	2.43	2.32	2.36	2.38	2.56
CH_{2d}			3.81*	3.80 s*	4.08	4.08 q	3.82	3.96 t
CH_{2e}					1.30*	1.30*	1.66	1.73 m
$CH_{2f,g,h}$							1.27	1.30 m
CH_{3i}							0.85	0.87 m

* Read CH_3.

All recorded in D_2O except: @ = CD_3OD; # = $CDCl_3$.

D_2O spectra externally referenced to DSS; spectra in other solvents are internally referenced.

Abbreviations: s = singlet; d = doublet; q = quartet; t = triplet; m = multiplet.

2.8.3 Mass Spectrometry

The FAB-MS spectral data are listed in Table 2.12. In every case the molecular ion is found as the HML_3^+ (HM^+) peak, and the ML_2^+ base peak is formed by the loss of one ligand. For the Ga complexes, the peaks are in the natural isotopic ratio of 3:2 ^{69}Ga to ^{71}Ga. The presence of peaks due to the matrix make the assignment of the spectra beyond this point profitless.

Table 2.12. Data from FAB-MS spectra of the tris-ligand metal complexes (*m/z*).

	M(mpp)$_3$		M(dpp)$_3$		M(mepp)$_3$		M(mhpp)$_3$		M(mimo)$_3$	
	Al	Ga	Al	Ga	Al	Ga	Al	Ga	Al	Ga
HML_3^+	400	444 442	442	486 484	484	528 526	652	695 693	619	662 660
ML_2^+	275	319 317	303	347 345	331	375 373	443	487 485	421	465 463

Chapter III Solid State Studies

A. 3-Hydroxy-4-Pyridinone Crystal Structures

3.1 Introduction

The structures of Hmpp, Hdpp, and Hmepp (Fig. 3.2) were established by single crystal X-ray diffraction. Apart from the obvious motive of structure confirmation, the crystallographic study was undertaken to establish the extent of double bond delocalization in these compounds, to determine if N-alkyl substitution increased the delocalization, and to discover what effect intermolecular H-bonding had on the crystal packing arrangement.

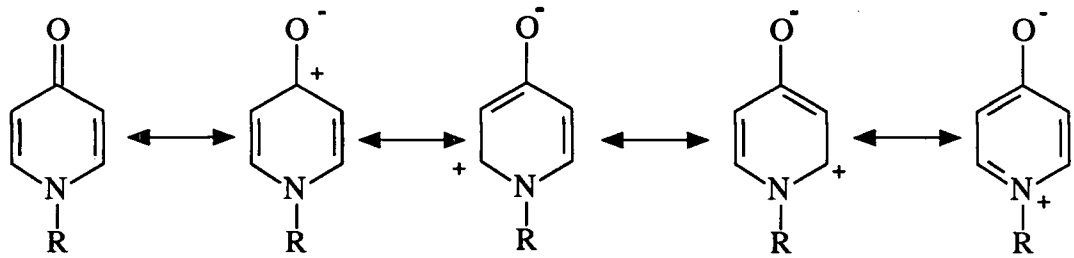

Figure 3.1. 4-pyridinone resonance forms.

There are several possible resonance forms for 4-pyridinone[104] (Fig.3.1) and this is of some importance when considering the potential stability of the tris(4-pyridinonato) metal complexes. A significant contribution from the resonance forms with a partial negative charge on the carbonyl oxygen might lead to complexes of increased stability as the bonding interactions with the hard acids Al and Ga are primarily electrostatic in nature.[105] Delocalization of the ring double bonds and a lengthening of the carbonyl bond

would be evidence of resonance hybridization in the 4-pyridinone ligands. It was thought that alkyl substitution at the ring nitrogen might enhance its ability to accommodate a positive charge thereby increasing the contribution from the pyridinium resonance form; the veracity of that supposition was examined by comparing the structures of Hmpp and its N-alkylated analogues.

Intermolecular H-bonding had been indicated by the IR and proton NMR spectra and not surprisingly, the 3-hydroxy-4-pyridinones crystallized as dimeric H-bonded units. Our interest in this interaction is due to the potential connection between H-bonding and the solubility properties of the ligands and the metal-ligand complexes. In addition, our research group would eventually like to enter the field of inclusion chemistry and extensively H-bonded structures have potential for the synthesis of clathrate compounds. Knowledge of the packing arrangement could be useful in determining the suitability of Hmpp, Hdpp, and Hmepp as host molecules.

The structures of Hmpp and Hdpp have been reported previously by this laboratory[60] and this is the first report of the structure of Hmepp. The single crystals of Hmpp were grown from a supersaturated water solution: a twice recrystallized sample of the ligand was dissolved in dilute acetic acid (pH 2), the pH was adjusted to 8 with 2 M NaOH, and overnight cooling at 10 °C gave crystals suitable for X-ray diffraction. Crystals of Hdpp could not be grown from water and were obtained by liquid-liquid diffusion from methanol with diethyl ether as the second solvent. Hmepp crystals were grown by slow evaporation from a dilute water solution.

All of the crystal structures in this thesis were determined by Dr. Steven J. Rettig of the U.B.C. structural chemistry laboratory. In all cases, the crystals were stable under ambient atmosphere and were mounted on glass fibers for X-ray diffraction.

Hmpp

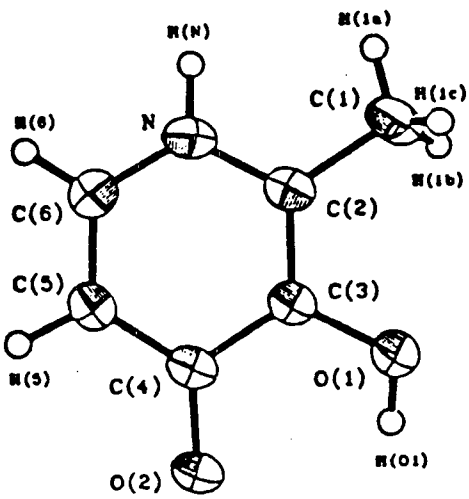

Hdpp

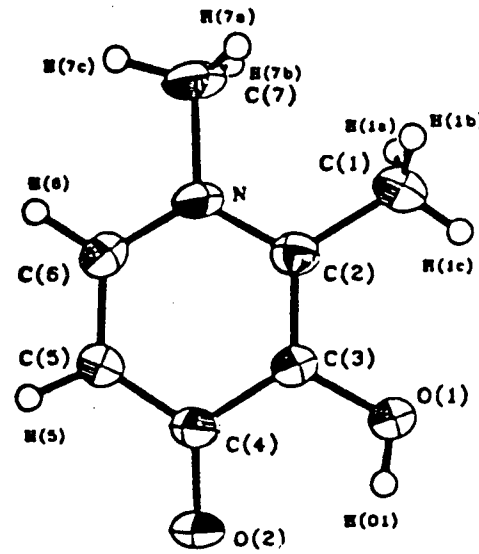

Hmepp

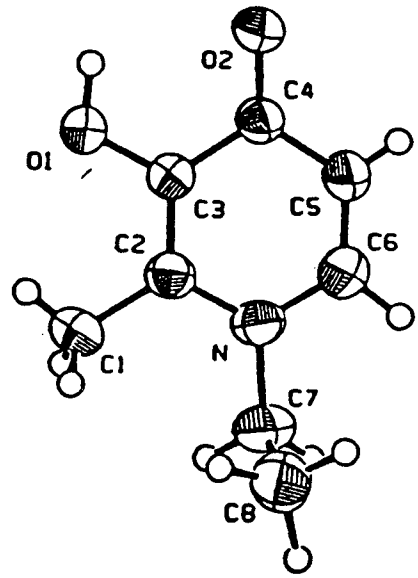

Figure 3.2. ORTEP view of Hmpp, Hdpp, and Hmepp.

Table 3.1. Bond lengths (Å) and angles (deg) for the free ligands (bond lengths in the upper and bond angles in the lower portion of the table). In this and all subsequent listings of bond parameters, the estimated standard deviation (esd) is in parenthesis after the data entry.

Atoms	Compound		
	Hmpp	Hdpp	Hmepp
O(1) - C(3)	1.358 (2)	1.360 (3)	1.357 (3)
O(2) - C(4)	1.280 (2)	1.272 (3)	1.258 (3)
N - C(2)	1.356 (2)	1.369 (4)	1.378 (3)
C(2) - C(3)	1.371 (2)	1.376 (4)	1.370 (3)
C(3) - C(4)	1.431 (2)	1.430 (4)	1.433 (3)
C(4) - C(5)	1.411 (2)	1.407 (4)	1.410 (3)
C(5) - C(6)	1.365 (2)	1.364 (4)	1.350 (4)
C(6) - N	1.345 (2)	1.352 (4)	1.351 (3)
C(2) - C(1)	1.493 (2)	1.489 (4)	1.490 (4)
N - C(7)		1.482 (4)	1.485 (3)
C(7) - C(8)			1.484 (4)
O(1) - C(3) - C(2)	117.8 (2)	118.2 (3)	118.3 (2)
O(1) - C(3) - C(4)	120.4 (2)	119.2 (2)	118.8 (2)
O(2) - C(4) - C(3)	120.0 (2)	120.5 (3)	121.3 (2)
O(2) - C(4) - C(5)	124.4 (2)	124.3 (3)	124.3 (2)
C(6) - N - C(2)	121.8 (2)	120.8 (2)	120.5 (2)
N - C(2) - C(3)	119.0 (2)	118.6 (3)	118.6 (2)
C(2) - C(3) - C(4)	121.8 (2)	122.5 (3)	122.9 (2)
C(3) - C(4) - C(5)	115.5 (2)	115.2 (3)	114.3 (2)
C(4) - C(5) - C(6)	120.7 (2)	121.1 (3)	121.9 (2)
C(5) - C(6) - N	121.1 (2)	121.7 (3)	121.8 (2)
N - C(2) - C(1)	118.3 (2)	119.0 (3)	120.0 (2)
C(1) - C(2) - C(3)	122.7 (2)	122.3 (3)	121.5 (2)
C(6) - N - C(7)		118.4 (3)	117.3 (2)
C(2) - N - C(7)		120.7 (3)	122.0 (2)
N - C(7) - C(8)			111.8 (2)

3.2 Results and Discussion

The six-membered pyridinone rings are slightly non-planar and the maximum deviations from the mean planes are 0.019(2) Å in Hmpp, 0.009(3) Å in Hdpp, and 0.013(3) Å in Hmepp; the distortions from planarity are toward a C(4) envelope, a C(2)-C(5) boat, and a N-C(4) boat respectively. An examination of the bond angles (Table 3.1) shows only minor differences between the three structures. N-alkylation results in a smaller intra-annular bond angle at nitrogen (C(2)–N–C(6)), and the C(3)-C(4)-C(5) angle is compressed in all three compounds to a minimum of 114.3° in Hmepp. This compression is indicative of the strength of the C=O bond (shortest in Hmepp) and is due in part to the lone pairs of electrons on the oxygen. The bulk of the N-alkyl groups predictably affects the position of the ring methyl group (C(1)) and this increases the N-C(2)-C(1) angle from 118.3° in Hmpp to 120° in Hmepp. The small changes in the bond angles involving the oxygen atoms are due to the packing of the H-bonded dimeric units.

The nitrogen coordination is planar within experimental error in all three compounds and the bond lengths indicate partial delocalization of the formal double bonds. By comparing the observed bond lengths with the values calculated (using the empirical relationship between bond order and bond length) for the double bond character consonant with the probable resonance forms, it is possible to relate double bond delocalization (as determined crystallographically) to the approximate contributions from each resonance hybrid.[106] Calculations of this nature were done for 2-pyridinone, a structural isomer of 4-pyridinone that is capable of similar resonance interactions involving the nitrogen lone pair of electrons.[80] The formula used was $R = \frac{R_1 - (R_1 - R_2) * 3x}{(2x + 1)}$ where R is the observed bond length, R_1 and R_2 are the standard carbon single- and double bond lengths

and x is the bond order expressed as the fraction of double bond character. The combination of 2-pyridinone resonance forms that gave the best agreement with the observed bond lengths are shown in Figure 3.3.

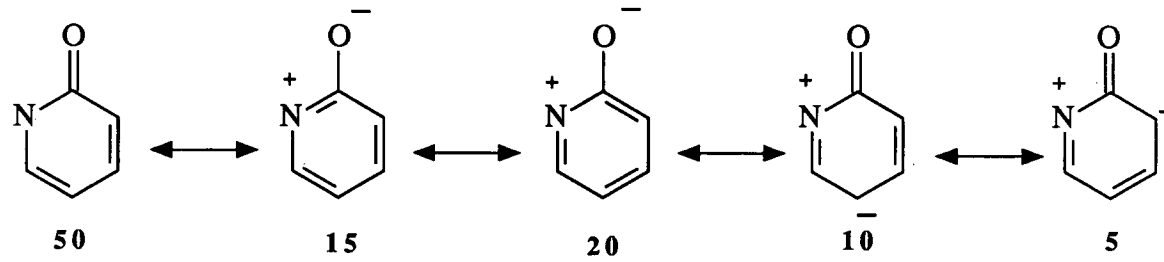

Figure 3.3. Resonance forms for 2-pyridinone (percent contribution is in bold type).

Analogous calculations were not done for the 3-hydroxy-4-pyridinones as a comparison of the bond lengths listed in Table 3.2 clearly indicates the similarity in the degree of double bond delocalization between Hmpp and 2-pyridinone. (Compound C was included to show that N-alkyl and hydroxy substitution did not appreciably alter bond delocalization in the 2-pyridinone ring.) The carbonyl bond is significantly longer in Hmpp and the similarity in the ring bond lengths is readily apparent; additionally, the mean of the six ring bonds is the same and Hmpp even has a slightly smaller standard deviation (σ). This indicates there is as much delocalization in Hmpp and suggests there may be as significant a contribution from the pyridinium resonance forms for Hmpp as was seen in 2-pyridinone (35%). Contrary to our expectations, N-alkylation did not increase the amount of double bond delocalization in the 4-pyridinones. Compared to Hmpp, there was no significant change in Hdpp bond lengths and the changes in Hmepp were indicative of a decrease rather than an increase as the C(5)=C(6) and C=O bonds were shorter and the C-N bonds were longer than in Hmpp (see Table 3.1).

Table 3.2. Comparison of bond lengths (Å). (The ring carbons are numbered as in Hmpp.)

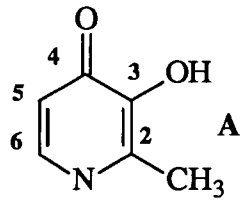

Hmpp

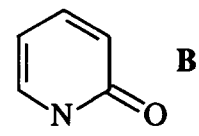

2-Pyridinone

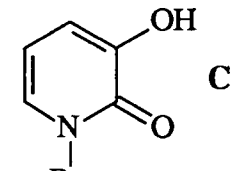

n- Bu

3-Hydroxy-1-butyl-2-pyridinone

Bond	Compound A	B#	C@
C=O	1.28	1.24	1.24
C(2)-C(3)	1.37*	1.44	1.43
C(3)-C(4)	1.43	1.33*	1.35*
C(4)-C(5)	1.41	1.42	1.41
C(5)-C(6)	1.37*	1.37*	1.33*
N-C(2)	1.36	1.40	1.37
N-C(6)	1.34	1.34	1.38
Mean (σ)	1.38 (0.033)	1.38 (0.044)	1.38 (0.038)

* Indicates the bonds that have the most double bond character.

\# Data from ref. 80.

@ Data from ref. 107.

The 3-hydroxy-4-pyridinones crystallized as centrosymmetric O-H···O=C hydrogen bonded dimeric units. (The dimeric unit from Hdpp is included as Figure 3.4 and the packing arrangements of Hmpp, Hdpp, and Hmepp are given as Figures 3.5, 3.6, and 3.7 respectively.) The dimeric units of Hdpp and Hmepp are separated from one another by normal van der Waals distances but in Hmpp each dimer is linked to four others by N-H···O=C hydrogen bonds to form a three-dimensional network. The strength of the

H-bonds can best be judged by examining both the H-bond parameters and the IR stretching frequencies (Table 3.3). In all three structures, the O-H···O bond lengths are intermediate (<2.70 Å[108]) and the angles are within the range typical for H-bonds (140-180°[109]). In Hmpp, the N-H···O distance and ν_{NH} indicate relatively strong nitrogen H-bonds;[108] the constraints imposed by the NH hydrogen bonding causes a weakening of the O-H···O bonds as indicated by the bond angle of 144° and by the ν_{OH} of 3270 cm^{-1} (ν_{OH} > 3200 cm^{-1} is classified as weak H-bonding[108]). A comparison of ν_{OH} in the three ligands supports the proposition that the weakening of the bonds between the dimeric units in Hmpp is due to the formation of the three-dimensional network.

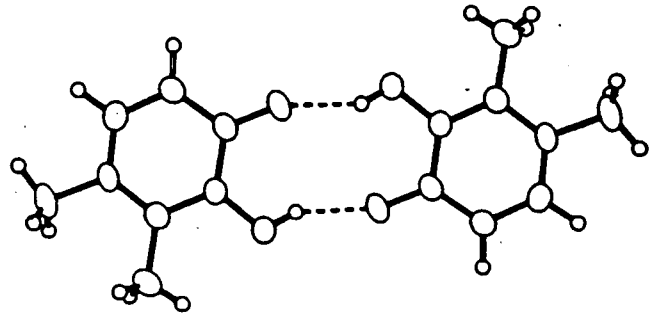

Figure 3.4 The Hdpp hydrogen bonded dimeric unit.

Table 3.3. A comparison of the free ligand H-bond parameters and the IR stretching frequencies. Values involving the nitrogen in Hmpp are in italics.

Atoms	Compound			
	Hmpp		Hdpp	Hmepp
H·····O (Å)	1.90 (3)	*1.90 (2)*	1.94 (5)	1.83 (4)
*(N)*O·····O (Å)	2.670 (2)	*2.796(2)*	2.692 (3)	2.659 (2)
*(N)*O-H·····O (deg)	144 (3)	*166 (2)*	154 (3)	150 (2)
$\nu_{(N)OH}$ (cm^{-1})	3270	*2800*	3150	3180

In the packing of the dimeric units, the alkyl groups are staggered to allow the closest spacing of the pyridinone rings and this is most readily seen in the unit cell of Hdpp (see Fig. 3.6). Comparing Hdpp to Hmepp shows that the N-ethyl group disrupts the stacking of the dimeric units; this is reflected in an increase in the volume of the unit cell (both compounds crystallized in the orthorhombic space group* *Pbca*) from 1312 $Å^3$ in Hdpp to 1628 $Å^3$ in Hmepp. The bulkier ethyl group also results in an appreciably lower calculated density for Hmepp (1.14 g/cm^3) than either Hmpp or Hdpp (1.42 and 1.41 g/cm^3, respectively). Despite the similarities in the strength of the H-bonds, the Hmepp crystal lattice appears to have been weakened due to the steric requirements of the N-ethyl group. This conclusion is supported by the lower melting point (205 vs. 260 °C) and the greater water solubility (five-fold increase at 25 °C) of Hmepp when compared to Hdpp.

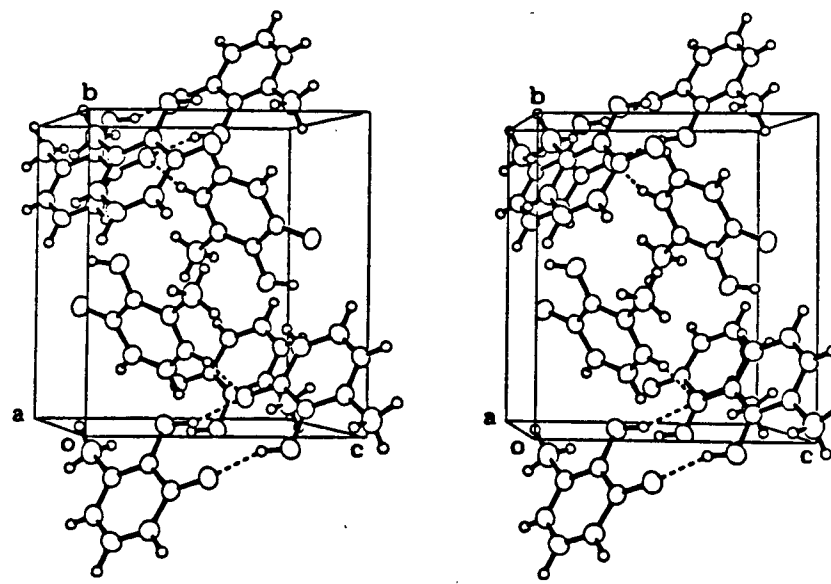

Figure 3.5. Stereoview of the packing arrangement in Hmpp.

* The crystallographic data (including the unit cell dimensions) for Hmpp, Hdpp, and Hmepp are in the Appendix as Table A.2.

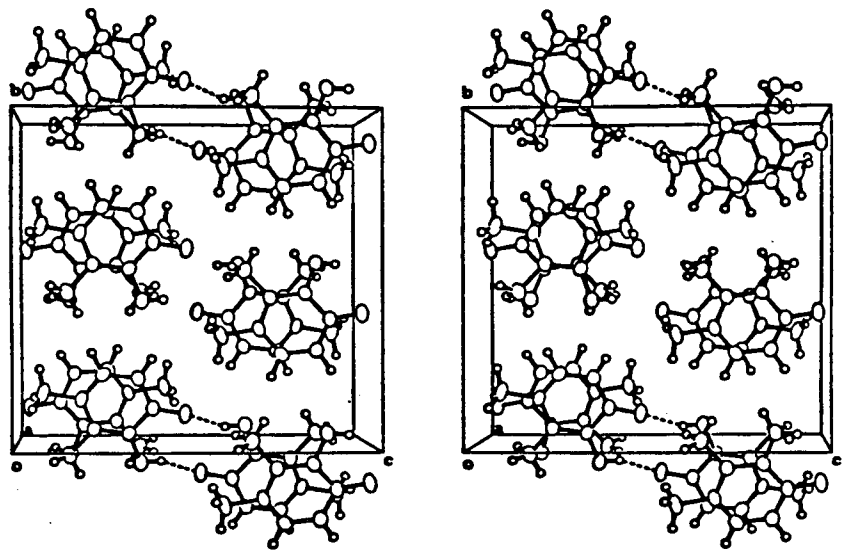

Figure 3.6. Stereoview of the packing arrangement in Hdpp.

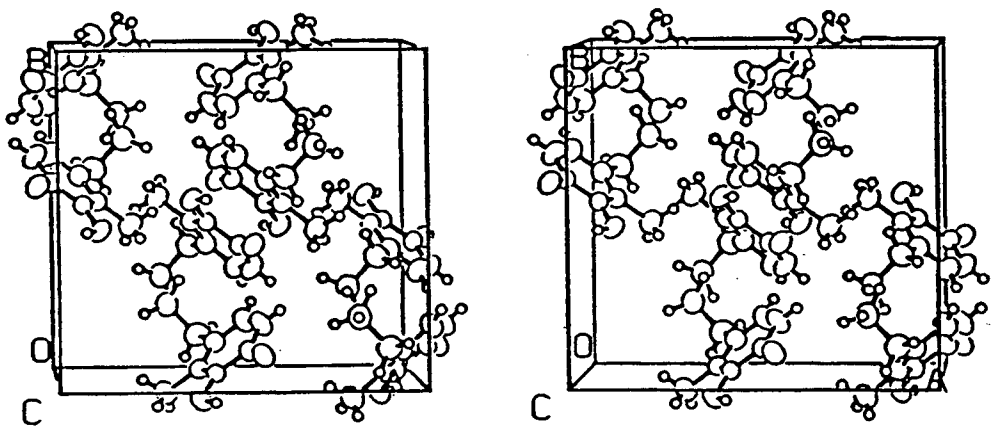

Figure 3.7. Stereoview of the packing arrangement in Hmepp.

B. $M(dpp)_3$ Crystal Structures

3.3 Introduction

The structures of Al-, Ga-, and $In(dpp)_3$ were determined; the *facial* (*fac*) isomers crystallize in the trigonal space group* $P\bar{3}$ and the empirical formula is $M(dpp)_3 \cdot 12H_2O$. The threefold symmetry of the *fac* isomers results in an asymmetric unit consisting of 1/3 of a metal ion, one ligand, and four water molecules. The water molecules form hexagonal rings that are H-bonded to the chelating oxygen atoms of the complexes by bridging waters. The water molecules do not coordinate the metal; rather they are structural waters[110] which form a three dimensional framework that is an important factor in determining the structure of the inorganic complex. The unit cell diagram (Figs. 3.8 and 3.9) accentuates the spatial relationship of the water channels to the tris(pyridinonato)metal portion of the structure (*fac*-$M(dpp)_3$ unit). The view perpendicular to the symmetry axes of the water channels and the *fac*-$M(dpp)_3$ units in Figure 3.10 affords the best perspective of the entire water network.

Because of the uniqueness and the structural importance of the water network, the Results and Discussion will be divided into two parts: the *fac*-$M(dpp)_3$ unit in Section 3.4.1 and the hexagonal water network in Section 3.4.2. The Al and Ga complexes are isostructural but due to a slight variation in the packing arrangement, the In complex is not crystallographically equivalent; however, the *fac*-$M(dpp)_3$ units of the three complexes are isostructural (Fig. 3.11) and the bonding parameters will be examined together. Despite

* The crystallographic data for the $M(dpp)_3$ complexes are in the Appendix as Table A.3.

the differences in packing, the water network is the same in all three compounds and will be addressed as such.

The single crystals were grown from supersaturated water solutions: an aqueous suspension was heated to 80 °C, filtered, and crystals formed after several days at 20 °C. The crystals were stable under ambient atmosphere and the integrity of the water network was exemplified by $Al(dpp)_3$ which successfully analyzed for 12 waters. The crystals were collected by filtration, dried overnight in a desiccator, and submitted for analysis under nitrogen: expected (found) C 38.35 (38.15); H 7.37 (7.39); N 6.39 (6.31). The strength of crystal lattice accounted for the rigorous conditions necessary to isolate the anhydrous compounds (see Section 2.8.1). To determine the importance of the lattice waters to the geometry of the *fac*-$M(dpp)_3$ units, numerous attempts were made to grow crystals from other solvents, either by liquid-liquid diffusion or by slow evaporation. The latter technique gave $In(dpp)_3$ crystals from 95% ethanol, but the complex again formed as the dodecahydrate. This was the only system that produced crystals suitable for X-ray diffraction.

The Al- and $Ga(dpp)_3$ structures were reported previously by this laboratory.[101,111] The synthesis of $In(dpp)_3$ was analogous to that of its congeners and the structure was reported in a study of In complexes.[112] Although my doctoral research did not involve the synthesis of indium complexes, the synthetic procedures were based on my work with the tris(3-hydroxy-4-pyridinone) Al and Ga complexes. I was directly involved in the growing of single crystals of $In(dpp)_3$ and the similarity of the three structures motivated the inclusion of the In complex in this thesis. A number of In complexes were also part of the octanol/water partition coefficient study that is included in Chapter V.

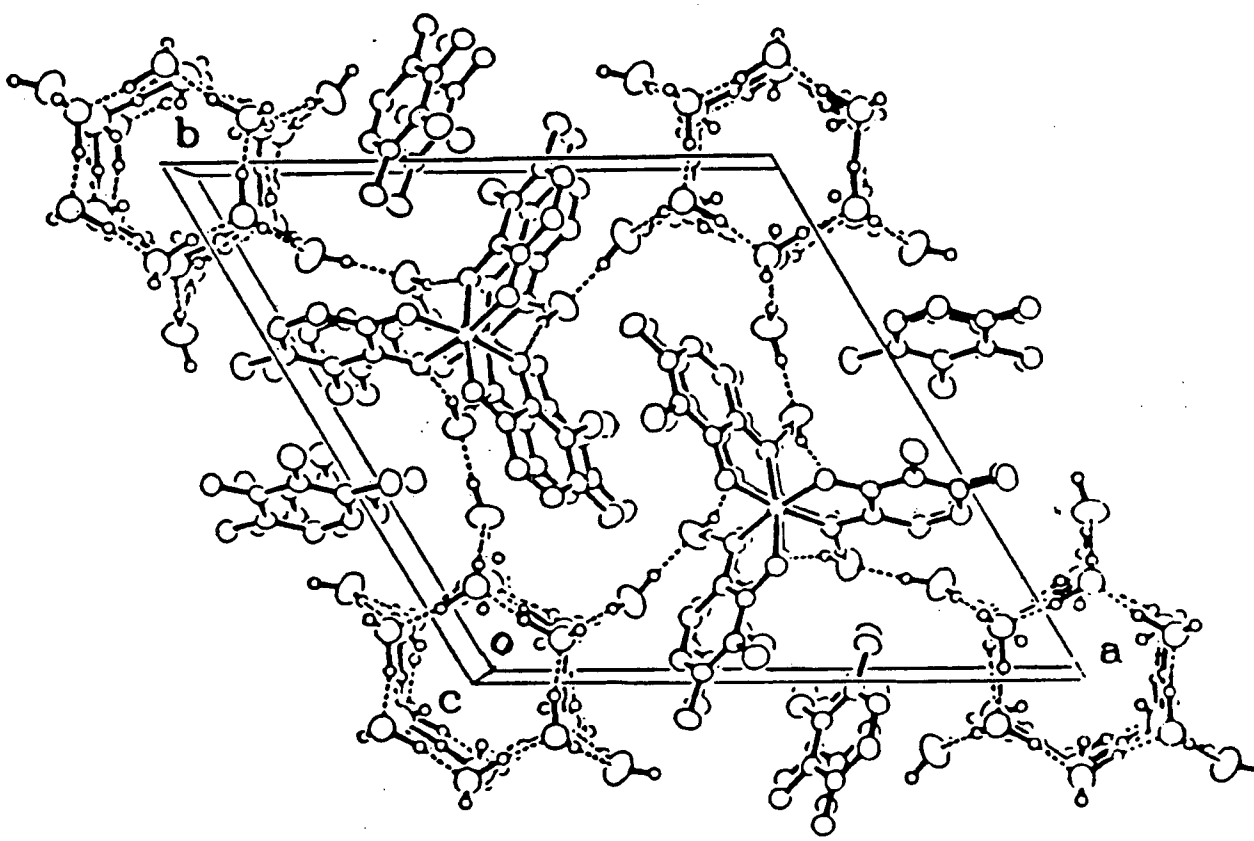

Figure 3.8. ORTEP view down the *c* axis of the unit cell packing of the $M(dpp)_3$ complexes (M = Al and Ga).

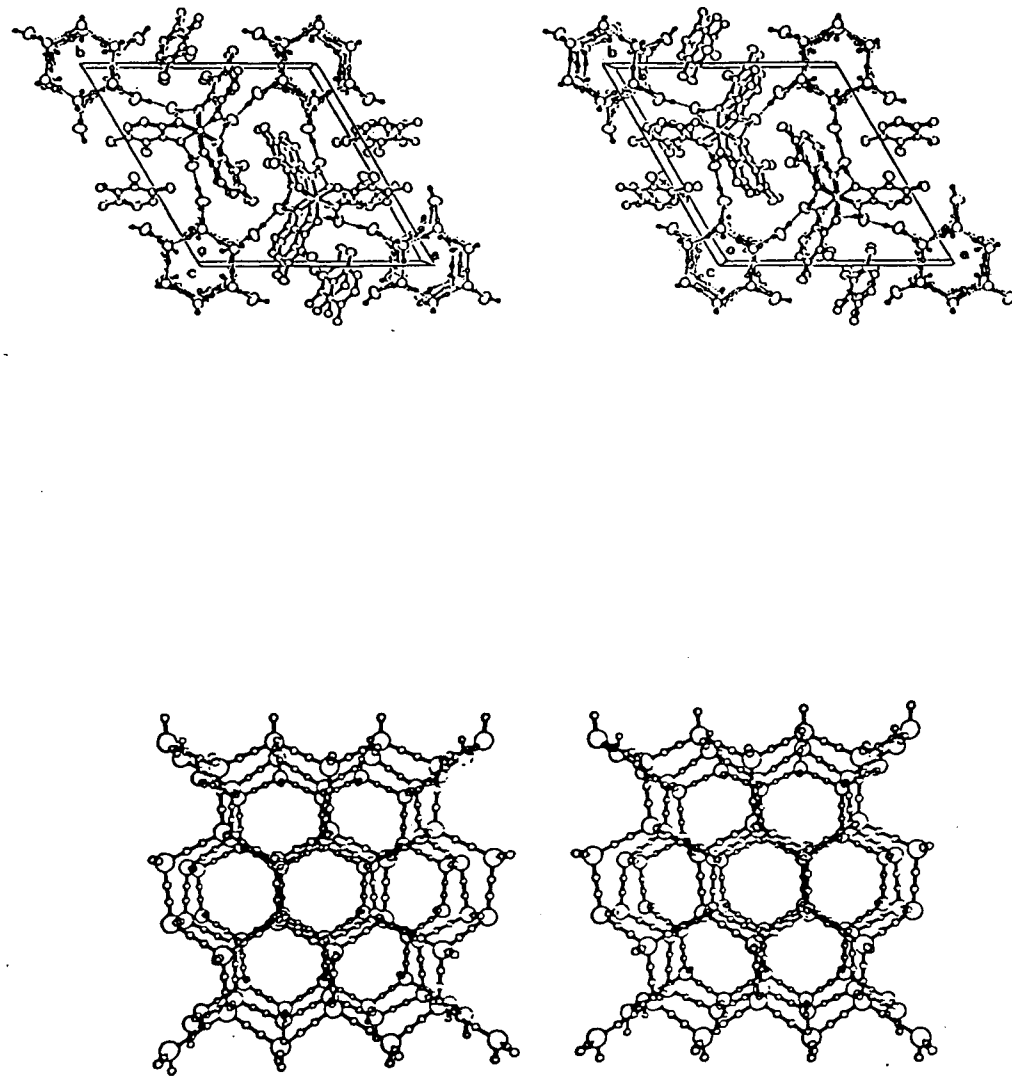

Figure 3.9. Stereoview of the unit cell packing in Al- and $Ga(dpp)_3$ (top) and stereoview of ice I_h from ref. 116 (bottom).

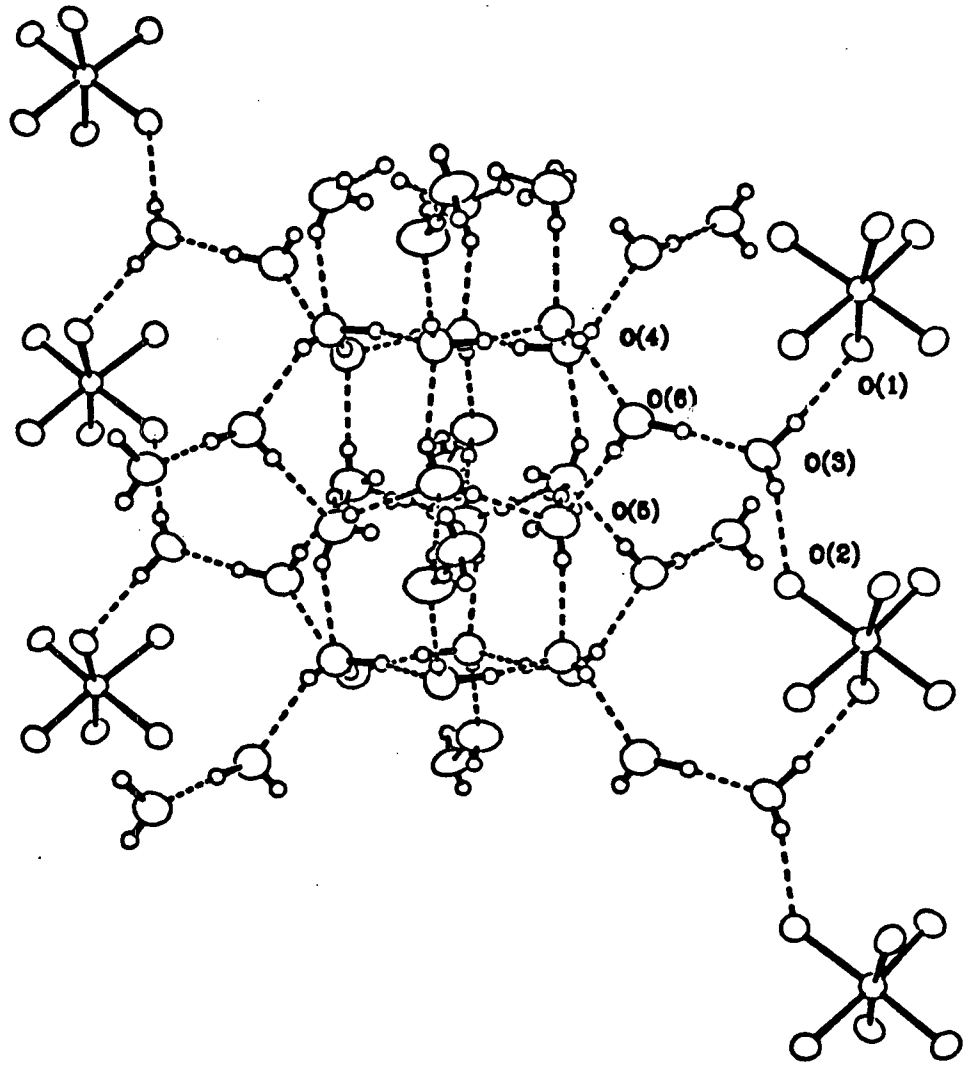

Figure 3.10. ORTEP view of a part of the H-bonding network of waters in $M(dpp)_3$. This view down the *a* axis shows all of the independent O atoms; all of the atoms in the $M(dpp)_3$ units are omitted except for the MO_6 octahedral coordination sphere.

3.4.1 The *fac*-M(dpp)$_3$ Unit

The ligand rings are planar within experimental error. There are no significant differences in the ring bond lengths between the Al and Ga complexes and only minor changes are seen in comparison to the In complex (Table 3.4). For In(dpp)$_3$, one C-N bond is longer but the other is shorter and the same relationship holds for the formal double bonds (C(2)-C(3) and C(5)-C(6)); this produces no net change in double bond delocalization. Comparison to the free ligand reveals only minor changes and the extent of ring double bond delocalization is essentially unaffected by metal chelation.

The delocalization in the C-O bonds is greater in the metal complexes than in the free ligand: the difference between O(1)-C(3) and O(2)-C(4) decreases from 0.088 Å in Hdpp to 0.028 Å, 0.038 Å, and 0.054 Å in Al-, Ga-, and In(dpp)$_3$ respectively. The extent of delocalization is clearly seen by comparing bond lengths with the related dihydroxy ligands, the catechols. The average C-O distance (calculated from a number of different metal complexes) is 1.36(1) Å for the catecholate anion and 1.29(1) Å for the delocalized semiquinone radical anion.[32] For the dpp anions in our metal complexes, the O(1)-C(3) bonds are signifcantly shorter (mean = 1.337(8) Å) than the catecholate bond and the O(2)-C(4) bonds are the same (mean = 1.297(8) Å) as the semiquinone bond (within the esd).

The only significant variations in ligand bond angles occur in the carbon atoms (C(3) and C(4)) that are part of the chelate ring. Chelation causes a compression in the interior angles of the chelate ring: compared to the free ligand values, the O(1)-C(3)-C(4) and O(2)-C(4)-C(3) bond angles are decreased in the Al and Ga complexes and are the same in the In complex. The smaller the metal the greater the compression. Further evidence of this is seen in $(C_6H_5)_2B(dpp)$ where these angles for the dpp$^-$ anion are further compressed to 111.8(4)° and 113.6(3)° respectively.[113]

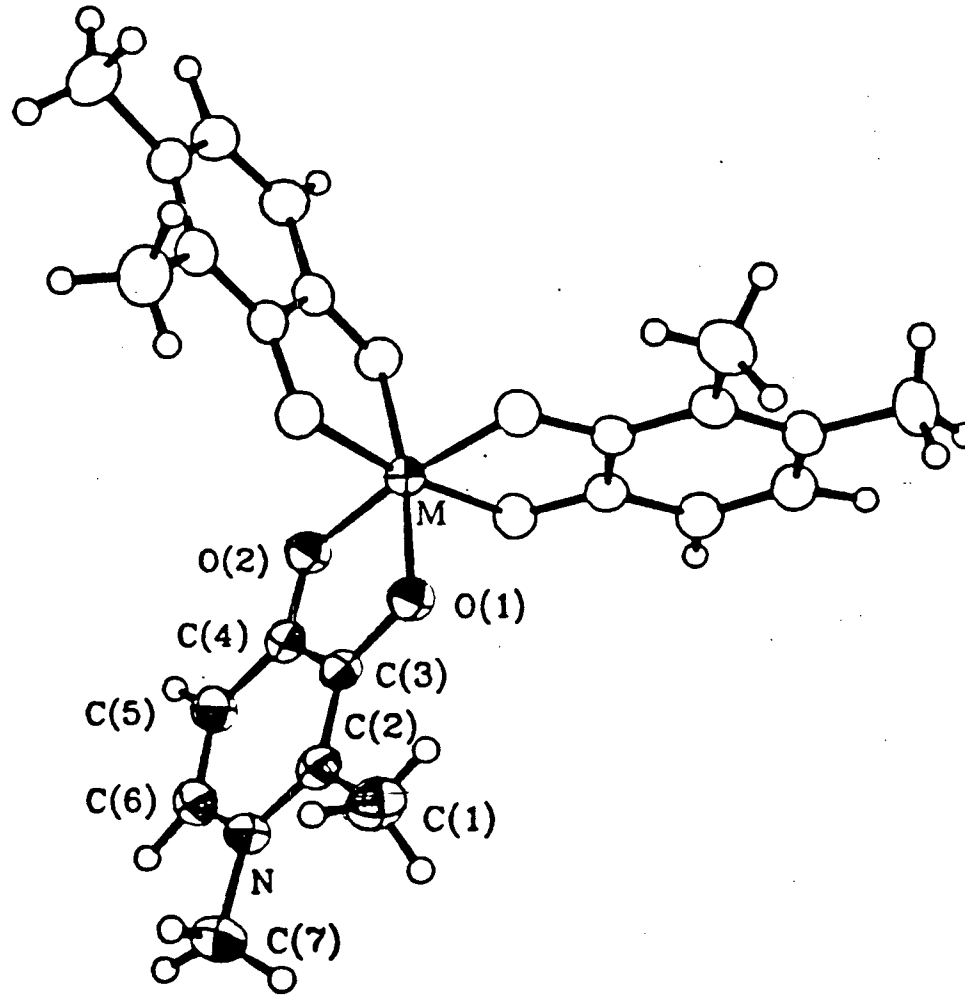

Figure 3.11. ORTEP view of the tris(ligand) portion of the $M(dpp)_3$ complexes (M = Al, Ga, and In).

Table 3.4. Bonding parameters for the $M(dpp)_3 \cdot 12H_2O$ complexes. The bond lengths (Å) are in the upper portion and the bond angles (deg) are in the lower portion of the table. For comparison, the parameters for the Hdpp ligand have been included in the last column.

Atoms	$M(dpp)_3$			
	M = Al	Ga	In	Hdpp
O(1) - C(3)	1.327 (3)	1.342 (5)	1.343 (3)	1.360 (3)
O(2) - C(4)	1.299 (3)	1.304 (5)	1.289 (3)	1.272 (3)
N - C(2)	1.369 (3)	1.372 (5)	1.355 (3)	1.369 (4)
C(2) - C(3)	1.385 (3)	1.382 (6)	1.393 (3)	1.376 (4)
C(3) - C(4)	1.423 (3)	1.409 (6)	1.403 (3)	1.430 (4)
C(4) - C(5)	1.398 (3)	1.403 (6)	1.410 (3)	1.407 (4)
C(5) - C(6)	1.360 (3)	1.359 (6)	1.344 (4)	1.364 (4)
C(6) - N	1.360 (3)	1.349 (5)	1.371 (3)	1.352 (4)
C(2) - C(1)	1.493 (3)	1.486 (7)	1.487 (4)	1.489 (4)
N - C(7)	1.476 (3)	1.470 (6)	1.463 (3)	1.482 (4)
O(1) - C(3) - C(2)	124.5 (2)	122.4 (4)	120.1 (2)	118.2 (3)
O(1) - C(3) - C(4)	115.3 (2)	116.9 (4)	119.1 (2)	119.2 (2)
O(2) - C(4) - C(3)	116.0 (2)	117.9 (4)	120.0 (2)	120.5 (3)
O(2) - C(4) - C(5)	125.7 (2)	124.2 (4)	123.0 (2)	124.3 (3)
C(6) - N - C(2)	121.2 (2)	121.1 (4)	120.2 (2)	120.8 (2)
N - C(2) - C(3)	119.0 (2)	118.9 (4)	119.7 (2)	118.6 (3)
C(2) - C(3) - C(4)	120.2 (2)	120.7 (4)	120.8 (2)	122.5 (3)
C(3) - C(4) - C(5)	118.4 (2)	117.9 (4)	116.9 (2)	115.2 (3)
C(4) - C(5) - C(6)	119.5 (2)	119.7 (4)	120.8 (2)	121.1 (3)
C(5) - C(6) - N	121.7 (2)	121.7 (4)	121.6 (2)	121.7 (3)
C(6) - N - C(7)	117.7 (2)	117.7 (4)	117.0 (2)	118.4 (3)
C(2) - N - C(7)	121.1 (2)	121.1 (4)	122.8 (2)	120.7 (3)
N - C(2) - C(1)	119.2 (2)	119.4 (4)	118.8 (2)	119.0 (3)
C(1) - C(2) - C(3)	121.9 (2)	121.7 (4)	121.4 (2)	122.3 (3)

Table 3.5. Intra-annular torsion angles of the chelate rings in the $M(dpp)_3$ complexes (deg).

Atoms	M = Al	Ga	In
O(2)-M-O(1)-C(3)	- 5.05 (14)	- 5.4 (3)	7.47 (14)
M-O(1)-C(3)-C(4)	4.7 (2)	5.0 (4)	- 7.2 (2)
O(1)-C(3)-C(4)-O(2)	- 1.0 (3)	- 0.8 (6)	0.8 (3)
M-O(2)-C(4)-C(3)	- 3.1 (2)	- 3.8 (5)	6.0 (3)
O(1)-M-O(2)-C(4)	4.50 (15)	5.0 (3)	- 7.21 (15)

The increasing size of the metal ion is accompanied by a reduction in ligand strain as evinced by compression of the O-C-C bond angles. By this criterion, In best fits the dpp^- anion since it caused the least deviation from the bond angles in the free ligand. This is a tentative conclusion as the changes are small and crystal packing forces could be a factor in the observed variations. The planarity of the chelate rings (Table 3.5) varies in the opposite direction. The metal ion is shifted out of the plane and the deviation from planarity is the greatest for $In(dpp)_3$. There is a compression of the $M(dpp)_3$ units from ideality along the C_3 axis leading to a decrease in the O(1)-M-O(2) angles and an increase in the exocyclic O(1)-M-O(2') angles in all the structures (Table 3.6). The exocyclic O(1)-M-O(1') and O(2)-M-O(2') angles are 90°(±1°) in the Al and Ga complexes, but they increase to 93.58 and 92.40 Å respectively in the In complex

The buckling of the chelate ring and the compression along the C_3 axis increase directly with the ionic radius of the metal center. An examination of the packing arrangement (see Figs. 3.8 and 3.10) shows that along the *c* axis (parallel to C_3) the

distance between *fac*-M(dpp)$_3$ units is governed largely by a single bridging O(3) water. The length of the H-bonds from O(3) to the ligand oxygens does not vary significantly among the three structures. If the rigid water network will not expand, an increase in the size of the metal center must result in compression along the C_3 axis and a twisting of the chelate plane.

Table 3.6. Bond angles (deg) for the metal-ligand interactions in M(dpp)$_3$ complexes.

Atoms	M = Al	Ga	In
O(1) - M - O(2)	84.23 (6)	83.22 (12)	77.87 (6)
O(1) - M - O(1)'	90.81 (8)	90.90 (12)	93.58 (6)
O(1) - M - O(2)'	95.71 (7)	96.65 (12)	97.74 (7)
O(2) - M - O(1)'$_{trans}$	171.85 (7)	170.48 (12)	166.18 (6)
O(2) - M - O(2)'	89.83 (8)	90.01 (12)	92.40 (6)
M - O(1) - C(3)	112.20 (13)	110.7 (2)	110.82 (13)
M - O(2) - C(4)	112.00 (14)	110.9 (3)	111.39 (14)

The M-O bond lengths are listed in Table 3.7; the differences in the M-O bond lengths and the differences in metal ionic radii are included in italics. Comparison of the differences shows that the M-O bond lengths are reasonably close to the values predicted by the differences in the size of the metal. The Al-O(2) bond shows the most deviation and this slight increase from the predicted length suggests the metal-oxygen bonding is weakest for Al(dpp)$_3$. The strength of the Ga-O bonds is seen by comparison to the 1.986(6) Å average Ga-O distance in K$_3$[tris(catecholato)Ga(III)].[34] The dative bond (Ga-O(2)) is the same length as the catecholate bond (within esds) and Ga-O(1) is significantly shorter. The

relative shortness of Ga-O(2) is further evidence of a significant contribution from the pyridinium resonance forms with a partial negative charge on O(2). The length of the Ga-O bonds also compares well to the bonding in tris(3-hydroxy-1-butyl-2-pyridinonato)iron (III);[107] when adjusted for the differences in metal ionic radii (a difference of 0.025 Å), the M-O distances are 2.024 and 1.955 Å.

Table 3.7. Metal ionic radii[30] and M-O bond lengths[a] in $M(dpp)_3$ complexes (Å).

	M = Al		Ga		In
Ionic Radius	0.535	*0.085*	0.620	*0.180*	0.800
M - O(1)	1.893 (2)	*0.074*	1.967 (3)	*0.167*	2.134 (2)
M - O(2)	1.923 (2)	*0.067*	1.990 (3)	*0.175*	2.165 (2)

[a] Going along a row, the differences between entries in adjoining columns are in italics.

The structural differences between the free and the complexed ligand are minor and the changes are indicative of increased double bond delocalization in the metal-ligand complexes. The *fac*-$M(dpp)_3$ units are isostructural and the variations between the structures are readily rationalized by consideration of the metal ionic radii and the rigidity of the packing arrangement. The metal-oxygen interactions are strong and compare favorably to those of other oxygen containing bidentate ligands known to be good chelators of trivalent metals.

3.4.2 The Hydrogen Bonded Water Network

The water molecules form a three dimensional array: half ($H_2O(3)$ and $H_2O(6)$) form a bridge from the *fac*-M(dpp)$_3$ units to the hexagonal channels formed by the other half of the water molecules ($H_2O(4)$ and $H_2O(5)$) in the corners of the unit cell (see Figure 3.10 for numbering). According to the classification of Falk and Knop,[114] in which waters are designated by the number and type of hydrogen bonding water neighbors (*a* is a proton acceptor and *d* is a proton donor), $H_2O(3)$ is *a*, $H_2O(6)$ *dda*, and the waters in the hexagonal channels ($H_2O(4)$ and $H_2O(5)$) are *ddaa*.

Table 3.8. H-bond distances (Å) and angles for M(dpp)$_3$•12H_2O.

Interaction	H···O		O·····O		O-H···O (deg)	
	M = Al	Ga	Al	Ga	Al	Ga
O(3)-H(a)···O(1)	1.95(6)	1.98(9)	2.861(3)	2.859(5)	161(4)	165(8)
O(3)-H(b)···O(2)	2.08(4)	2.19(6)	2.849(3)	2.842(6)	164(4)	159(7)
O(4)-H(a)···O(6)	2.12(5)	2.19(6)	2.772(3)	2.765(6)	159(5)	164(10)
O(4)-H(b)···O(4)	1.62(8)	1.58(12)	2.747(3)	2.746(5)	168(5)	154(8)
O(5)-H(a)···O(4)	2.06(10)	2.44(12)	2.802(4)	2.807(7)	150(9)	145(22)
O(5)-H(c)··O(5)[a]	1.50(13)	1.53(24)	2.793(4)	2.779(7)	174(6)	160(10)
O(5)-H(d)···O(5)	2.17(13)		2.793(4)		149(12)	
O(6)-H(a)···O(3)	1.72(4)	1.99(8)	2.729(4)	2.734(7)	174(3)	167(8)
O(6)-H(b)···O(5)	2.00(4)	1.91(7)	2.791(4)	2.778(7)	174(3)	171(6)

[a] This interaction involves H(O5b) for the Ga compound.

The H-bonds* (Table 3.8) between the ligand O atoms (O(1) and O(2)) and $H_2O(3)$ are relatively strong considering these oxygen atoms are chelating the metal atoms. All six of the chelating O atoms are hydrogen bonded to O(3) water molecules; the latter form an infinite chain down the *c* axis bridging from the hydroxy O(1) in one ligand to the keto O(2) of a ligand rotated by 120° and translated by one unit cell. (This is why Figure 3.8 shows the contents of two unit cells). The O···H and O···O distances for the chelating oxygens vary from 1.95(6) to 2.19(6) Å and from 2.842(6) to 2.861(3) Å respectively. Not surprisingly, the chelating hydroxy O forms shorter O···H bonds than the chelating keto O.

The hexagonal channels of water molecules in the corners of the unit cell are the most unique feature in these structures. (The water O(5) was found to be twofold disordered in the Al complex and is shown with four half protons bound to it in Figure 3.10.) Each of the water rings has crystallographically imposed $\bar{3}$ or S_6 symmetry and the rings essentially adopt the structure of ice[115] in its stable low pressure form, ice–I_h. (Refer to Fig.3.9 for a comparison of the water rings and the structure ice.) Every water molecule in the ring is hydrogen bonded to four nearest neighbors with the added distinction that the overall structure is predominantly proton-ordered, unlike ice–I_h which is completely disordered. The O···O distances in the channels (those involving O(4), O(5), and O(6)) vary from 2.75 to 2.81 Å compared with the average value of 2.75 Å for O···O in ice–I_h at 100 K.[116]

Within each water ring the hydrogen bonding is homodromic[117-119] because of the unidirectional circular bonding pattern. All the O-H···O bonds run in a counterclockwise direction when viewed down the hexagonal axis (see Figure 3.9). The arrangement is crystallographically imposed by the space group ($P\bar{3}$), however, and does not occur

* There were no significant differences in the H-bond parameters for $In(dpp)_3$ so they have been placed in the Appendix as Table A.5

independent of symmetry constraints as do the water networks in the structures of some nucleosides[120] and β-cyclodextrins.[121,122] Homodromic hydrogen bonding arrangements are favored (and more frequently observed despite symmetry constraints) over heterodromic or antidromic arrays because of an inherent lower dipole moment.[118] There is a considerable cooperative effect which results in increased hydrogen bonding activity for a hydroxyl group when it is already the donor or acceptor in a hydrogen bond. Quantum mechanical calculations have confirmed that chain structures (particularly cyclic) of hydrogen bonds are energetically favored over individual interactions.[123]

This is the first example where this arrangement of water rings occurs in hydrates containing (relatively) large metal complexes; there has recently been reported a tris(2-pyridinonato) iron complex that contains hexagonal water rings, but the rings are discrete and there is no three-dimensional water network.[107] Water rings are, however, well known in the crystal structures of ice[115,116] and the clathrate hydrates[124,125] The clathrate hydrates are crystalline compounds which consist of a hydrogen bonded water host network (often a $H_{40}O_{20}$ pentagonal dodecahedron) within which a guest is held by an interaction which varies from weakly hydrogen bonding, to ionically bonding where one or more ion is associated with, or incorporated in, the water framework.[126] We note similarities here with hexamethylenetetramine hexahydrate ($(CH_2)_6N_4 \cdot 6H_2O$), an unusual hydrate in which the host lattice is not based on a regular polyhedron, so there are no well defined polyhedral cavities.[127] It shares with the structures reported herein the hexagonal water rings; however, the water rings are staggered around the cage-like amine molecules in a spiral (instead of a linear chain) to which the latter are bound.

The above observations suggest that the $M(dpp)_3$ complexes present (when crystallized from water) appropriate conditions for the formation of the water channels in what is a previously unobserved, but energetically favored, hydrogen bonding arrangement. This probably results by virtue of both the complex size and the hydrophobic

core of the unit cell formed by the pairs of methyl groups on the ligands from the two *fac*-M(dpp)$_3$ units. There is a clear alternation of hydrophilic and hydrophobic regions along the *ab* diagonals of the unit cell; no doubt this feature also contributes to the unique hydrogen bonding arrangement. It may be that a driving force for the formation of the dodecahydrates is a variation on hydrophobic clathration[124,125] as well as the cooperativity[109] of H-bonding networks.

C. M(mepp)$_3$ Crystal Structures

3.5 Introduction

The importance of the H-bonded water network to the M(dpp)$_3$ structure was stressed in the preceding sections; because of the constraints inherent in such a rigid structure, it was felt that even a small variation in the ligand might be sufficient to alter the nature of the water network or to preclude its formation altogether. In the packing arrangement of tris(3-hydroxy-1-butyl-2-pyridinonato)iron(III) there are hexagonal water rings H-bonded to the chelating oxygens.[107] There are no bridging waters and no water channels: one water ring is sandwiched between two metal complexes (forming discrete units) and alternate waters in the ring are H-bonded to the chelating hydroxyl oxygens (the carbonyl oxygens do not act as H-bond acceptors) of one of the metal complexes. As soon as the first M(dpp)$_3$ structure was determined, we wondered if the water network was

unique to the Hdpp ligand; this very interesting Fe structure piqued our curiosity as to the water arrangements that might be possible with the other 3-hydroxy-4-pyridinone ligands.

Efforts to grow more crystals culminated in the determination of the structures of Al- and Ga(mepp)$_3$. The crystal growing attempts with the other metal complexes had met with little success and the M(mepp)$_3$ complexes were synthesized specifically for this structural study. The crystals were grown by slow evaporation (over a period of weeks) from dilute water solutions. Crystal growth was much slower than with the M(dpp)$_3$ complexes and the single crystals were considerably smaller. The replacing of a methyl with an ethyl group is, of course, a very minor structural change; however, this small change was sufficient to alter significantly the packing arrangement of the free ligands and it was thought a similar outcome might be possible with the tris-ligand metal complexes.

When the Al(mepp)$_3$ crystals analyzed as a decahydrate (the analytical sample was prepared analogously to the previously mentioned Al(dpp)$_3$ sample), we suspected we were dealing with a similar structure. The determination of the crystal structure proved that the water network was able to accommodate the N-ethyl group: the empirical formula was Al(mepp)$_3$•12H$_2$O, the space group* was trigonal $P\bar{3}$, and the water network was unchanged.** The Ga(mepp)$_3$ crystal structure showed that a change in metal ionic radii in concert with N-ethyl substitution was also insufficient to alter the water network. The Al and Ga complexes were essentially isostructural; the modifier "essentially" was necessitated by the same crystallographic inequality that distinguished the In(dpp)$_3$ complex from its Al and Ga analogues. For this reason, the In(dpp)$_3$ packing arrangement was not addressed previously and the nature of the inequality will be examined by a comparison of the unit cell packing in the Al- and Ga(mepp)$_3$ complexes.

---

* The crystallographic data for the M(mepp)$_3$ complexes are in the Appendix as Table A.4.

** Because there was no significant differences from the water network in the M(dpp)$_3$ structures, the M(mepp)$_3$ H-bond parameters are in the Appendix as Table A.6.

3.6 Results and Discussion

The *fac*-M(mepp)$_3$ units of the Al and Ga complexes are isostructural (Fig. 3.12), as is readily apparent by a comparison of the bond lengths and angles in Table 3.9. The C(5)-C(6) bond is significantly longer in the Al complex (by 0.02 Å) and that is the only difference in ring bond lengths. There appears to be an increase in delocalization compared to the free ligand but this is primarily due to change in only one bond, C(5)-C(6), that was the shortest for any of the structures solved (free ligands and metal complexes) in Hmepp and was the longest in Al(mepp)$_3$-- 1.350 vs. 1.380 Å. There is more delocalization in the C-O bonds than in either Hmepp or the M(dpp)$_3$ complexes. The difference between the two C-O bonds is 0.099 Å in Hmepp, and 0.020 and 0.024 Å in Al- and Ga(mepp)$_3$ respectively. This leads to the same conclusion as was reached with the M(dpp)$_3$ complexes; i.e., an increase in double bond delocalization occurs upon chelation.

Aside from the obvious difference in the N-alkyl groups, the *fac*-M(dpp)$_3$ and *fac*-M(mepp)$_3$ units are isostructural . The ligand bond lengths and angles are virtually the same (compare Tables 3.4 and 3.9). The chelate ring angles show a similar compression along the C_3 axis and the M-O bond lengths are comparable. In the water network, some of the H-bonds are slightly longer but, as was the case with the increased size of the metal ion, there is no evidence from the H-bond parameters that the water network is significantly affected by the additional methylene group in the M(mepp)$_3$ complexes.

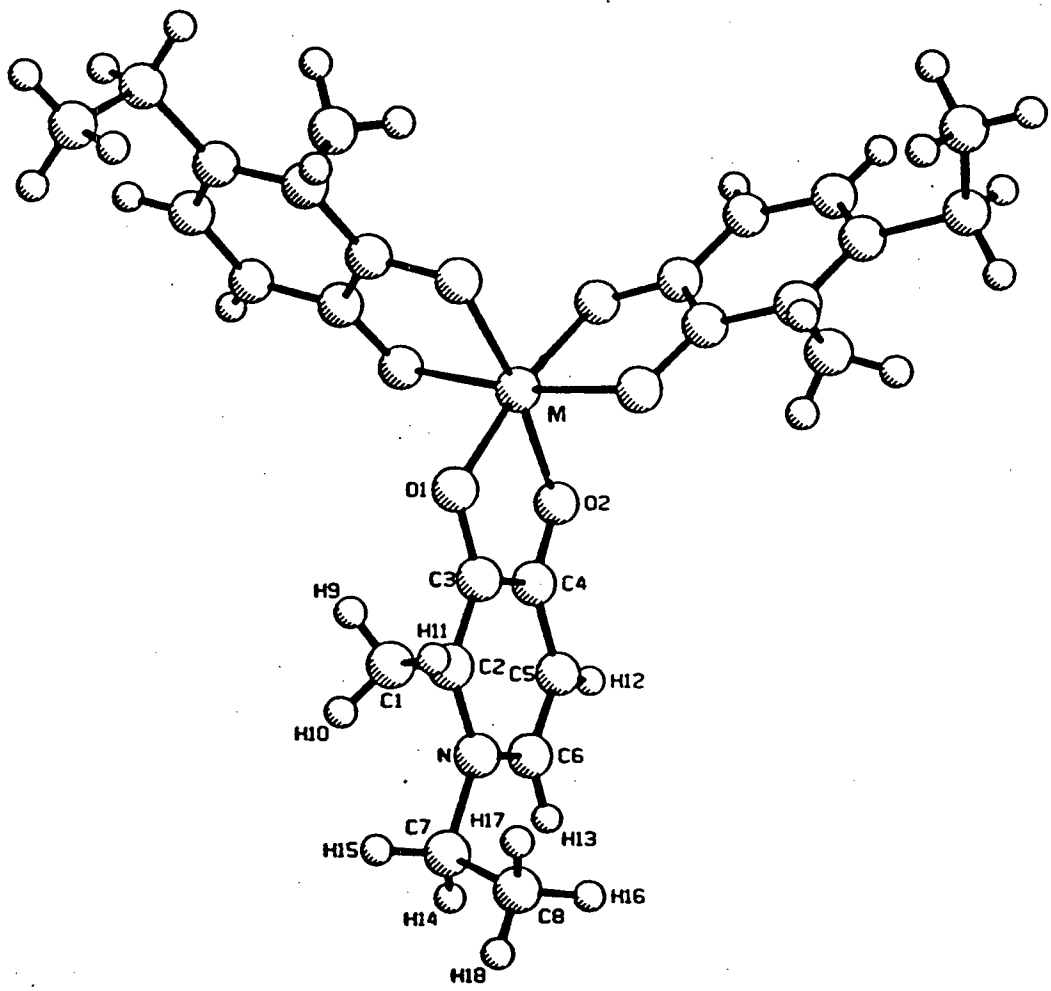

Figure 3.12. ORTEP view of the tris(ligand) portion of the $M(mepp)_3$ complexes.

Table 3.9. Bond parameters for $M(mepp)_3 \cdot 12H_2O$ complexes. The bond lengths (Å) are in the upper portion and bond angles (deg) are in the lower portion. For comparison, the parameters for the Hmepp ligand are in the last column.

Atoms	M = Al	Ga	Hmepp
M - O(1)	1.894 (1)	1.962 (1)	
M - O(2)	1.930 (1)	2.00 (1)	
O(1) - C(3)	1.317 (2)	1.327 (2)	1.357 (3)
O(2) - C(4)	1.297 (2)	1.303 (2)	1.258 (3)
N - C(2)	1.373 (2)	1.376 (3)	1.378 (3)
C(2) - C(3)	1.388 (2)	1.387 (3)	1.370 (3)
C(3) - C(4)	1.424 (2)	1.422 (3)	1.433 (3)
C(4) - C(5)	1.399 (2)	1.396 (3)	1.410 (3)
C(5) - C(6)	1.380 (3)	1.360 (3)	1.350 (4)
C(6) - N	1.342 (3)	1.349 (3)	1.351 (3)
C(2) - C(1)	1.494 (2)	1.485 (3)	1.490 (4)
N - C(7)	1.485 (2)	1.488 (3)	1.485 (3)
C(7) - C(8)	1.504 (3)	1.500 (4)	1.484 (4)
O(1) - M - O(2)	84.23 (5)	83.03 (6)	
O(1) - M - O(1)'	90.46 (6)	90. 52 (6)	
O(1) - M - O(2)'	94.87 (5)	95.29 (6)	
$O(2) - M - O(1)_{trans}$	172.50 (5)	171.34 (5)	
O(2) - M - O(2)'	90.93 (6)	91.79 (6)	
M - O(1) - C(3)	112.1 (1)	111.2 (1)	
M - O(2) - C(4)	111.3 (1)	110.7 (1)	
O(1) - C(3) - C(2)	124.0 (2)	122.4 (2)	118.3 (2)
O(1) - C(3) - C(4)	115.5 (1)	117.0 (2)	118.8 (2)
O(2) - C(4) - C(3)	116.2 (1)	117.5 (2)	121.3 (2)
O(2) - C(4) - C(5)	125.6 (1)	124.9 (2)	124.3 (2)
C(6) - N - C(2)	121.6 (1)	120.9 (2)	120.5 (2)
N - C(2) - C(3)	118.8 (2)	118.8 (2)	118.6 (2)
C(2) - C(3) - C(4)	120.5 (1)	120.6 (2)	122.9 (2)
C(3) - C(4) - C(5)	118.1 (1)	117.6 (2)	114.3 (2)
C(4) - C(5) - C(6)	119.2 (2)	120.1 (2)	121.9 (2)
C(5) - C(6) - N	121.8 (2)	122.0 (2)	121.8 (2)
N - C(2) - C(1)	120.5 (2)	120.2 (2)	120.0 (2)
C(1) - C(2) - C(3)	120.7 (2)	121.0 (2)	121.5 (2)
C(6) - N - C(7)	117.4 (2)	118.0 (2)	117.3 (2)
C(2) - N - C(7)	121.0 (2)	121.1 (2)	122.0 (2)
N - C(7) - C(8)	112.6 (2)	112.5 (2)	111.8 (2)

Table 3.10. Unit cell dimensions for $M(dpp)_3$ and $M(mepp)_3$ complexes.

Dimension	$M(dpp)_3$			$M(mepp)_3$	
	M = Al	Ga	In	Al	Ga
a (Å)	16.600 (2)	16.6549 (6)	16.842 (1)	17.1734 (8)	17.247 (1)
c (Å)	6.877 (1)	6.8691 (4)	6.8078 (7)	6.827 (1)	6.830 (2)
Volume ($Å^3$)	1641.3 (3)	1650.1 (1)	1672.3 (2)	1743.7 (3)	1759.4 (1)
D_c@ (g/cm^3)	1.33	1.47	1.48	1.33	1.40

@ D_c = calculated density.

There are some differences in the unit cell dimensions (Table 3.10) of the structures that were determined. (In the trigonal space group $P\bar{3}$, $a = b \neq c$, $\alpha = \beta = 90°$ and $\gamma = 120°$.) The rigidity of the water network that was responsible for the compression of the M-O-C bond angles along the C_3 axis (parallel to the *c*- axis) can be seen in the length of *c*. For the $M(dpp)_3$ complexes, this dimension decreases (slightly as the metal radius increases) to a minimum for In; the increase in the size of the N-alkyl substituent likewise causes a decrease in this parameter, e.g. 0.050 Å between $Al(dpp)_3$ and $Al(mepp)_3$. It is along the *ab* diagonal that the changes in the metal and ligand are accommodated by the water network. The result is an increase in *a*:, e.g., a 0.242 Å increase for In- vs. $Al(dpp)_3$, and a 0.573 Å increase for $Al(mepp)_3$ vs. $Al(dpp)_3$.

The packing diagram of $Al(mepp)_3$ (Fig. 3.13) shows how the N-ethyl group fits into the hydrophobic core that is made up of one ligand from each of the two *fac*-$M(mepp)_3$ units in the cell. The flexibility of the structure in the *ab* diagonal is due to the large ring that encircles the core and consists of bridging waters, one side of the hexagonal water

channels, and the M-O bonds in the *fac*-M(mepp)$_3$ units (the oxygen atoms have been darkened to highlight this ring). The ligands in the core are separated by 3.5±1 Å; i.e., normal van der Waal's contacts. The points where the ligand carbon atoms approach the water rings, C(8)-O(5) and C(6)-O(6), are likewise separated by ~3.5 Å. To maintain this distance from the water network, the N-ethyl group must twist out of the ligand plane. The length of *c* (> 6.8 Å) is considerably greater than van der Waal's contact distances so there is room to accommodate the N-ethyl group without an increase in *c* and, therefore, without an increase in the length of the H-bonds that determine this dimension.

Focussing on this inner core and its encircling ring, it is possible to see why the increase in metal radius did not disrupt the water network. Increasing the length of the O-M-O portion of the inner ring pushes the water channels away from each other (increases *a*) but no strain is put on the water channels because they are connected via the *fac*-M(mepp)$_3$ unit rather than directly connected by H-bonds. The structure can be thought of as four rigid water columns held together by the more flexible *fac*-M(mepp)$_3$ units. An increase in the size of the metal simply pushes the water columns apart in the *a* and *b* directions, and in the one direction where direct strain could be placed on water H-bonds, the octahedral metal complexes are compressed before the H-bonds are stretched.

The crystallographic inequality that distinguishes In(dpp)$_3$ from its Al and Ga analogues also separates the M(mepp)$_3$ complexes from each other. A comparison of the packing diagrams of Al- and Ga(mepp)$_3$ clearly indicates that the unit cells are not equivalent. There is a rotation of the *fac*-M(mepp)$_3$ units by ca. 60° about the C_3 axis with respect to the water network. Each unit cell contains one Λ and one Δ stereoisomer; this was necessary for the ligands in the hydrophobic core to lie parallel to each other and, therefore, to define the dimensions of the core. In order for the ligands to be as close as possible, the rings are staggered so the C(1) methyl groups point away from each other. In the unit cell of Al(mepp)$_3$ (see Fig. 3.13), the Λ isomer is in the upper left of the cell and

the methyl groups project into the plane of the paper; the Δ isomer is in the lower right and the methyl groups are toward the viewer. Figure 3.14 shows the packing in the unit cell of $Ga(mepp)_3$ and here the position of the stereoisomers is reversed. This was referred to as a crystallographic inequality simply because it only involves the unit cells and does not alter the *fac*-$M(mepp)_3$ units or the interaction of the water rings with these units. It is possible this alteration of the packing arrangement is caused by the size of the metal as for both ligands, the change occurs in the tris-ligand complex with the largest metal; i.e., $In(dpp)_3$ and $Ga(mepp)_3$. However, it is not readily apparent why this rotation of the ligand orientation occurs and it must be considered simply a crystallographic oddity.

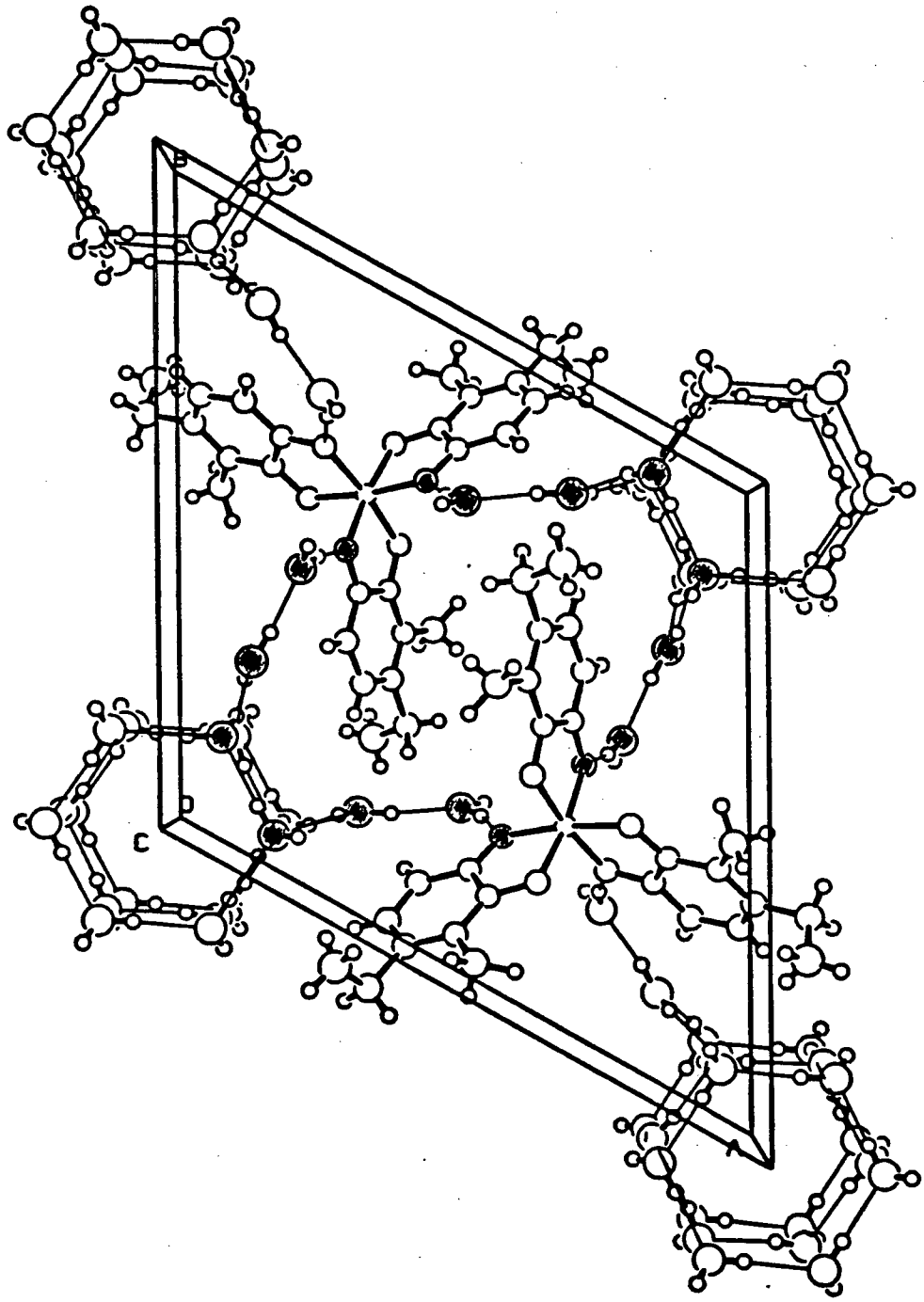

Figure 3.13. ORTEP view down the *c* axis of the unit cell packing of Al(mepp)$_3$.

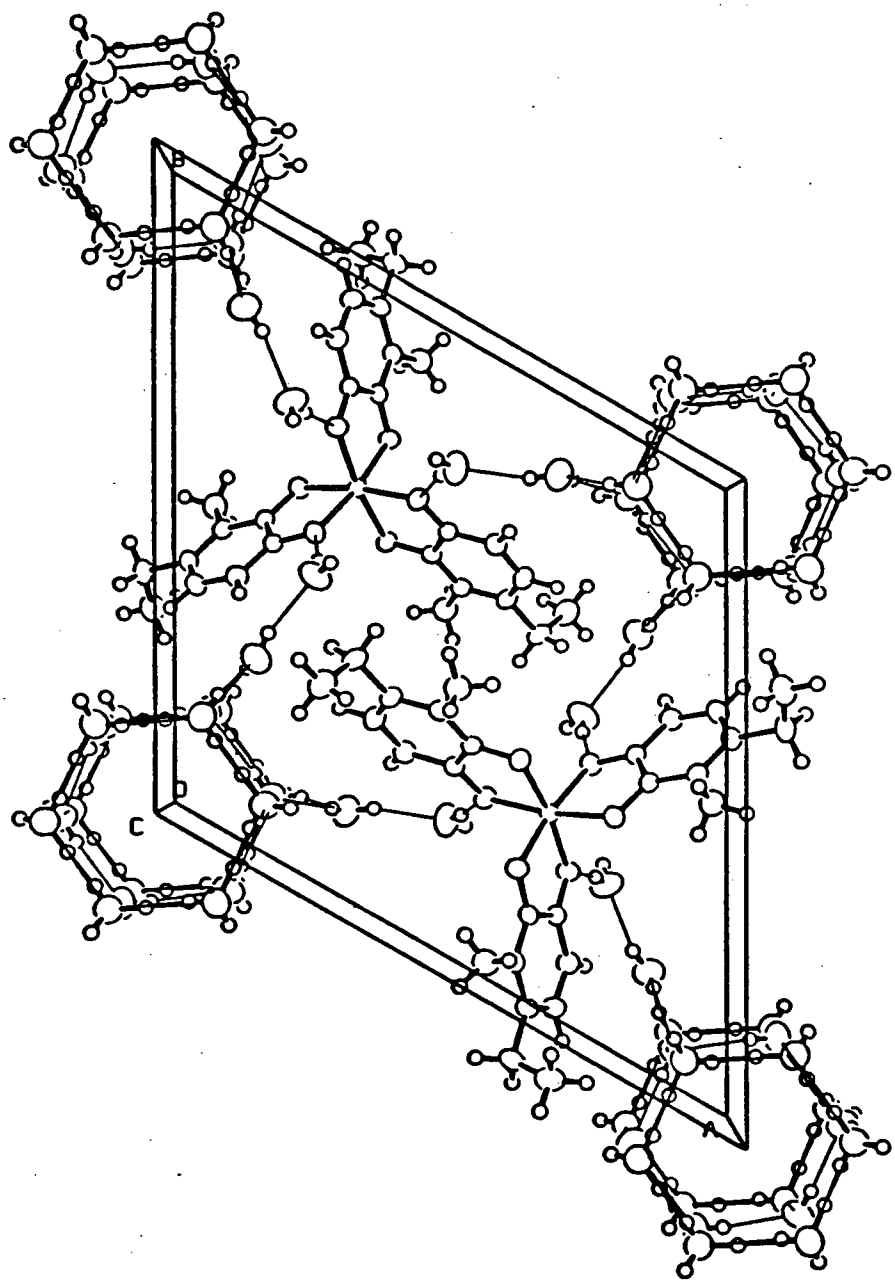

Figure 3.14. ORTEP view down the *c* axis of the unit cell packing of $Ga(mepp)_3$.

Chapter IV NMR Studies

A. Aluminum-27 NMR Spectroscopy

4.1 Introduction

The ^{27}Al nucleus has a nuclear spin of 5/2 and, therefore, it has a nuclear quadrupolar moment (Q). When a quadrupolar nucleus is placed in a magnetic field, the NMR energy levels are perturbed by quadrupolar effects. This quadrupolar interaction is affected by the direction of the electric field gradient that is fixed by the molecular framework. Thus the quadrupolar energy can be modulated by the Brownian motion of the molecule and if this occurs at the proper rate, spin-lattice relaxation (T_1) will be induced. Because the molecular motion is random, it has random phase and this leads to the loss of phase coherence between nuclei, i.e., spin-spin relaxation (T_2). The result is an efficient magnetic relaxation mechanism dominated by nuclear quadrupole relaxation.[128,129]

The electric field gradients are generated by ligand field asymmetry so there is a direct connection between the line width of the ^{27}Al NMR signal and the geometry of the coordinated ligands or coordinated solvent molecules. Octahedrally solvated Al^{3+}, tetrahedral AlX_4^-, and Al_2X_6 dimers exhibit high symmetry and have relatively narrow line widths. For trigonal species, the line widths (measured as peak widths at half height, $W_{1/2}$) become much larger. The overall range of line widths is from 3 Hz (for $[Al(H_2O)_6]^{3+}$) to over 6000 Hz.[130] There have been a number of studies using ^{27}Al NMR line widths as a probe to determine the coordination number of organoaluminum complexes

in organic solvents.[131] A far lesser amount of data has been collected in aqueous solution for Al complexes with biologically active ligands.[132-134]

The ^{27}Al isotope is 100% naturally abundant and has a relative receptivity one-fifth that of the proton. Comparison with the 1.11% natural abundance and 0.016 relative receptivity of ^{13}C indicates why ^{27}Al NMR does not require the instrument time typical of ^{13}C NMR. The practicality of ^{27}Al NMR can best be illustrated by comparing its nuclear properties to those of its congener Ga and of two other quadrupolar nuclei, ^{17}O and ^{15}N, that are used as NMR nuclei. The data in the last two columns of Table 4.1 were calculated from the following equation for nuclear spin quadrupolar relaxation (T_Q) that is valid in the limit of fast motion.[128]

$$\frac{1}{T_Q} = \frac{1}{T_1} = \frac{1}{T_2} = \frac{3}{40} \frac{2I + 3}{I^2 (2I - 1)} \left(\frac{eQ}{\hbar}\right)^2 \left(\frac{d^2v}{dz^2}\right)^2 \tau_c$$

I is the nuclear spin quantum number, eQ is the electric quadrupole moment, $\hbar$ is Planck's constant divided by 2π, $\frac{d^2v}{dz^2}$ is the maximum electric field gradient at the nucleus, and τ_c is the correlation time for Brownian motion. The line width factor, defined as

$$\frac{(2I + 3)\, Q^2}{I^2 (2I-1)}$$

can be used to compare the line widths of quadrupolar nuclei. Normalized to the value for ^{27}Al, the relative line widths of the Ga isotopes are the largest and the other two quadrupolar nuclei have peaks < 10% that of ^{27}Al. However, when the differences in abundance and receptivity are used to determine the relative peak heights, defined as

$$\left(\frac{\text{abundance} * \text{ receptivity}}{\text{line width factor}}\right)$$

^{27}Al NMR has a hypothetical sensitivity an order of magnitude (or more) greater than the other quadrupolar nuclei in Table 4.1. As a result of this, high resolution ^{27}Al NMR has been used to quantify Al^{3+} to 1 ppm (37 μM).[135]

Table 4.1. The NMR properties of several quadrupolar nuclei (refs. 128 and 129-Appendix 2)

Isotope	I	Isotopic abundance (%)	NMR frequency (MHz)	Relative[1] receptivity	Quadrupole moment ($10^{-28}m^2$)	Relative[2] line width	Relative[3] peak height
^{27}Al	5/2	100	26.08	0.206	0.149	1.00	54.6
^{69}Ga	3/2	60.4	24.04	0.042	0.19	6.7	1.00
^{71}Ga	3/2	39.6	30.55	0.057	0.12	2.6	2.24
^{17}O	5/2	0.037	13.56	0.00011	-0.026	0.03	0.003
^{14}N	1	99.63	7.23	0.001	0.01	0.07	3.8
^{1}H	1/2	99.98	100.0	1	--	--	--

1 Relative (to ^{1}H) receptivity at a constant field with equal numbers of nuclei.

2 Relative (to ^{27}Al) line width.

3 Relative (to ^{69}Ga) peak height.

We did attempt some studies with ^{71}Ga NMR, but its lack of sensitivity (see Table 4.1) coupled with the low solubility of our Ga complexes made it impossible to detect any signals in a practical time span. ^{27}Al NMR served as a characterization technique and it was also used to readily determine the success of our tris-ligand Al complex preparations. The constraints on instrument access unfortunately restricted this latter application. Our primary utilization of this NMR technique was the determination of the hydrolytic stability of the tris(3-hydroxy-4-pyridinonato) Al complexes.

^{27}Al NMR has been used extensively to examine the pH dependent speciation of Al,[136] and the chemical shifts and narrow line widths of the predominant Al species at pH < 4, $[Al(H_2O)_6]^{3+}$, and at pH > 9, $[Al(OH)_4]^-$, are quite different from those of the tris-ligand complexes in this study. When a solution of an Al complex was sampled at a

series of pH values from < 2 to > 10, the ^{27}Al NMR spectra readily indicated the pH region where the hydrolysis products first appeared. The broad peaks of our complexes made it difficult to quantify by this technique, but it did paint a clear picture of what we referred to as the "window" of hydrolytic stability for $Al(ma)_3$.[37] Similar Al hydrolysis experiments using ^{27}Al NMR have been carried out with the tris-ligand Al complexes of acetylhydroxamate,[137] oxalate,[138] lactate,[139] and a number of hydroxycarboxylate ligands.[134] The closest comparison to the spectra of the tris(3-hydroxy-4-pyridinonato) Al complexes were the spectra of $Al(ma)_3$.

4.2 Materials and Methods

The ^{27}Al NMR spectra were recorded at ambient probe temperature (ca. 18 °C) on a Varian XL-300 NMR spectrometer at 78.16 MHz and a pulse width of 15 μs. The first experiments used a sweep width of 20 KHz and an acquisition time (T_{aq}) of 0.20 s. 6500 Transients were needed to achieve a reasonable signal to noise ratio (S/N) and the recording of one spectrum required 22 minutes. Because of the broad lines, we felt the resolution could be reduced in order to complete one variable-pH experiment (involving ten or more samples) in the two hour time blocks available on this instrument. Combinations of sweep width (20 to 60 KHz) and T_{aq} (0.05 to 0.40 s) were tried before settling on 50 KHz and 0.12 s. These acquisition parameters allowed the resolution of both the narrow signals from the hydrolysis products and the broad signals from the Al-ligand complexes. If the sample concentrations were > 10 mM, 3500 transients gave a good S/N and the 7 minute run time per sample was compatible with the limitations on instrument availability. The spectra were referenced to the $[Al(H_2O)_6]^{3+}$ signal (set as zero) from 0.20M $Al(ClO_4)_3$ in

0.10M $HClO_4$. D_2O was added for locking and downfield chemical shifts were positive. The spectra were recorded by the author.

Purified compounds, distilled and deionized water, and a Fisher Accumet model 805 pH meter (calibrated with pH 4 and 10 buffer solutions) were used in the variable-pH experiments. Solutions of the Al complexes were made in 15 mL H_2O and 2 mL D_2O (for a lock signal) and the initial pH was adjusted to < 2 by the addition of 8 M HCl. The pH was raised by the addition of 8 M NaOH and the solution was equilibrated between pH changes for ≥ 10 minutes. Aliquots were withdrawn and filtered through glass fibers into the NMR tube. The sampling was initiated at the lowest pH and was repeated at approximately one pH unit intervals up to pH > 10. The hydrolysis was completely reversible within the 2-3 hour time frame of the experiment.

4.3 Results and Discussion

The chemical shift range of the ^{27}Al nucleus is approximately 450 ppm and, like the line widths, the shift is characteristic of the ligand symmetry about the Al atom. The signals for hexacoordinate Al nuclei are quoted as occurring from 20 to -46 ppm and AlO_6 species usually appear close to 0 ppm.[130] There are exceptions to this rule: the tris(hydroxamato) Al complexes and the alumichrome trihydroxamato peptides resonate at 36-42 ppm[137] and a dimeric acetate species gives a signal at 38 ppm.[136] These exceptions have led to the proposal that downfield shifts near 38 ppm could be characteristic of chelation by small-ring-forming bidentate ligands.[136] The tris(3-hydroxy-4-pyronato) Al complexes have chemical shifts of ca. 39 ppm and the tris(3-hydroxy-4-pyridinonato) Al complexes resonate at essentially the same frequency. The downfield shifts are due to the

inequivalence of the chelating hydroxy and carbonyl oxygen atoms. The Al nuclei are not subject to a rigorously octahedral field and this is also reflected in the relatively broad peaks of these tris-ligand Al complexes.

The chemical shifts and the $W_{1/2}$ values of the tris(3-hydroxy-4-pyridinonato) Al complexes are listed in Table 4.2; the data are from the variable-pH experiment spectra of the pH 7-8 samples. $Al(mhpp)_3$ is not sufficiently water soluble for the variable-pH experiment and its spectrum was recorded in CD_3OD. The values for $Al(ma)_3$ are included for comparison and to put these data in perspective, $Al(acac)_3$ (D_3 point group) resonates at 0 ppm with $W_{1/2} \cong 100$ Hz.[130]

Table 4.2. ^{27}Al NMR data for the tris(3-hydroxy-4-pyridinonato) Al complexes.

	$Al(ma)_3$	$Al(mpp)_3$	$Al(dpp)_3$	$Al(mepp)_3$	$Al(mimo)_3$	$Al(mhpp)_3$
ppm	38	38	37	37	37	38
$W_{1/2}$ (Hz)	900	600	700	780	1600	1400

Our other data (spectroscopic and crystallographic) indicate the AlO_6 coordination sphere is very similar for all the 3-hydroxy-4-pyridinone ligands; it is not likely that differences in ligand symmetry would account for the variations in line widths that were observed. NMR line widths are also affected by temperature, solvent viscosity, exchange processes, and the mass of the solute.[129] The proton NMR indicate an exchange process is occurring at room temperature in the Al complexes and this could contribute to the variations in line widths. In comparison to $Al(mpp)_3$, the larger R groups in $Al(mimo)_3$ and $Al(mhpp)_3$ may be decreasing the molecular tumbling rate; this would increase the τ_c for Brownian motion and, as indicated in the above equation, the relaxation rate (and therefore the $W_{1/2}$) for the larger tris-ligand Al complexes would increase.

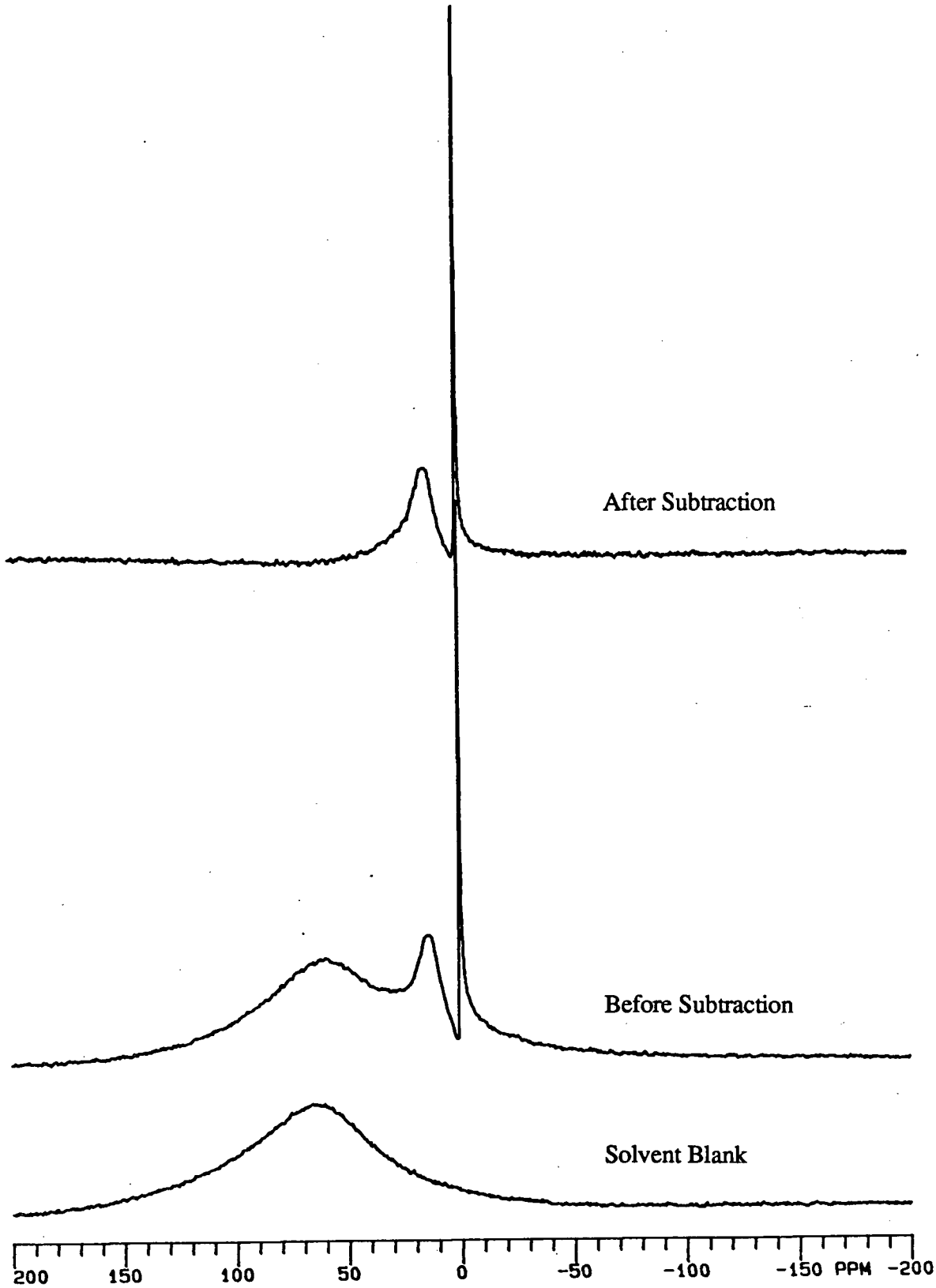

Figure 4.1. ^{27}Al NMR spectra of $Al(mpp)_3$ at pH 1.8 showing the background correction.

The minimum concentration for the variable-pH studies was 10 mM; this cutoff point is not due to the sensitivity of the technique but rather is due to the background signal from the Al in the ceramics of the NMR probe. This is a well documented phenomenon[140,141] and the probe Al has a broad (~6000 Hz) signal centered at ca. 60 ppm. The background signal from the probe overlaps the signals from the tris-ligand Al complexes (near 40 ppm). The probe signal is also out of phase with the signals from the solution Al nuclei which makes it difficult to properly phase the spectrum. It is possible to do a background correction by subtracting the free induction decay (FID) of a solvent blank from the sample FID and Fourier transforming the resulting signal. Figure 4.1 depicts the before and after spectra of a pH 1.8 $Al(mpp)_3$ sample with an initial Al concentration of 15 mM. (The sharp signal at 0 is from $[Al(H_2O)_6]^{3+}$ and the smaller broad peak at 17 ppm is from $[Al(dpp)(H_2O)_4]^{2+}$.) This background correction works well but the experimental procedure presented an additional complication. As the pH was raised, the composition of the solution changed due to the addition of base and this was hard to duplicate in the solvent blank. If the conductivity of the solvent blank was sufficiently different from that of the sample, it effectively detuned the probe so the phase shifts were altered and the subtraction did not work. This problem was handled by making several solvent blanks and using the one that gave the best results for a particular sample.

The interference from the background signal can be avoided by using Al concentrations > 20 mM. For $Al(mepp)_3$ and $Al(mimo)_3$, 40 mM solutions were used; $Al(mpp)_3$ is soluble to 16 mM and background subtraction was necessary in a number of the spectra. $Al(dpp)_3$ is only soluble to 1.2 mM at neutral pH, but we were able to make a supersaturated solution with an initial Al concentration of 30 mM at pH 1.8. The insolubility of the tris-ligand Al complex is due to the incorporation of water molecules (see Chapter III) and this is not an instantaneous process. There was no appreciable precipitation in the base solution over the two to three hours required for the variable-pH experiment. The NMR spectra were recorded immediately after sampling to avoid precipitation in the NMR tube. (Crystals did form in the tubes

overnight and it was this experiment that first indicated X-ray diffraction grade crystals of this compound could be grown from water.) The aqueous solubility of $Al(mhpp)_3$ is similar to that of $Al(dpp)_3$ and a concentrated solution can be made in acidic solution. However, its low solubility is due to the lipophilic N-hexyl groups and the variable-pH experiment was not feasible because a pervasive precipitate formed at ca. pH 2.5. (A detailed summary of the solubility properties of these complexes is in Chapter V.)

The variable-pH ^{27}Al NMR spectra for $Al(mpp)_3$ are shown as Figure 4.2. The acidic hydrolysis is evinced by a shoulder at pH 3.4 on the upfield side of the $Al(mpp)_3$ peak at 37 ppm. This results from the partial protonation of ligands in the coordination sphere of the Al and their replacement with waters. At pH 3.1 this shoulder is resolved into two shoulders resulting from the $[Al(mpp)_2(H_2O)_2]^+$ (28 ppm) and $[Al(mpp)(H_2O)_4]^{2+}$ (17 ppm) species. When the solution is acidified further, the completely hydrated species $[Al(H_2O)_6]^{3+}$ is observed at 0 ppm. As the pH drops the signals from the hydrolysed species gain in intensity at the expense of the $Al(mpp)_3$ peak. Even at the lowest pH of 1.8, there is still a signal from the monoligand species although most of the Al is in $[Al(H_2O)_6]^{3+}$. When the pH is raised, the ligands are replaced by the hydroxide ion to form ultimately $[Al(OH)_4]^-$ at pH 11 (80 ppm, $W_{1/2} \cong 60$ Hz). The basic hydrolysis of Al^{3+} is time dependent and this explains why no intermediate species analogous to those formed at acidic pH were found in the time frame of the experiment.

The $Al(mpp)_3$ pH 8.9 sample was left (in an NMR tube) at room temperature for two weeks and the spectrum recorded at that time is contrasted to the initial spectrum in Figure 4.3. After two weeks, the intensity of the $Al(mpp)_3$ signal is reduced by one-third and the broad peak at 61 ppm is probably due to four coordinate mixed aquo/hydroxo/mpp Al complexes. In the basic hydrolysis of tris(lactato)aluminum(III), mixed hydroxo/lactato complexes are ascribed to a broad peak at 60 ppm.[139]

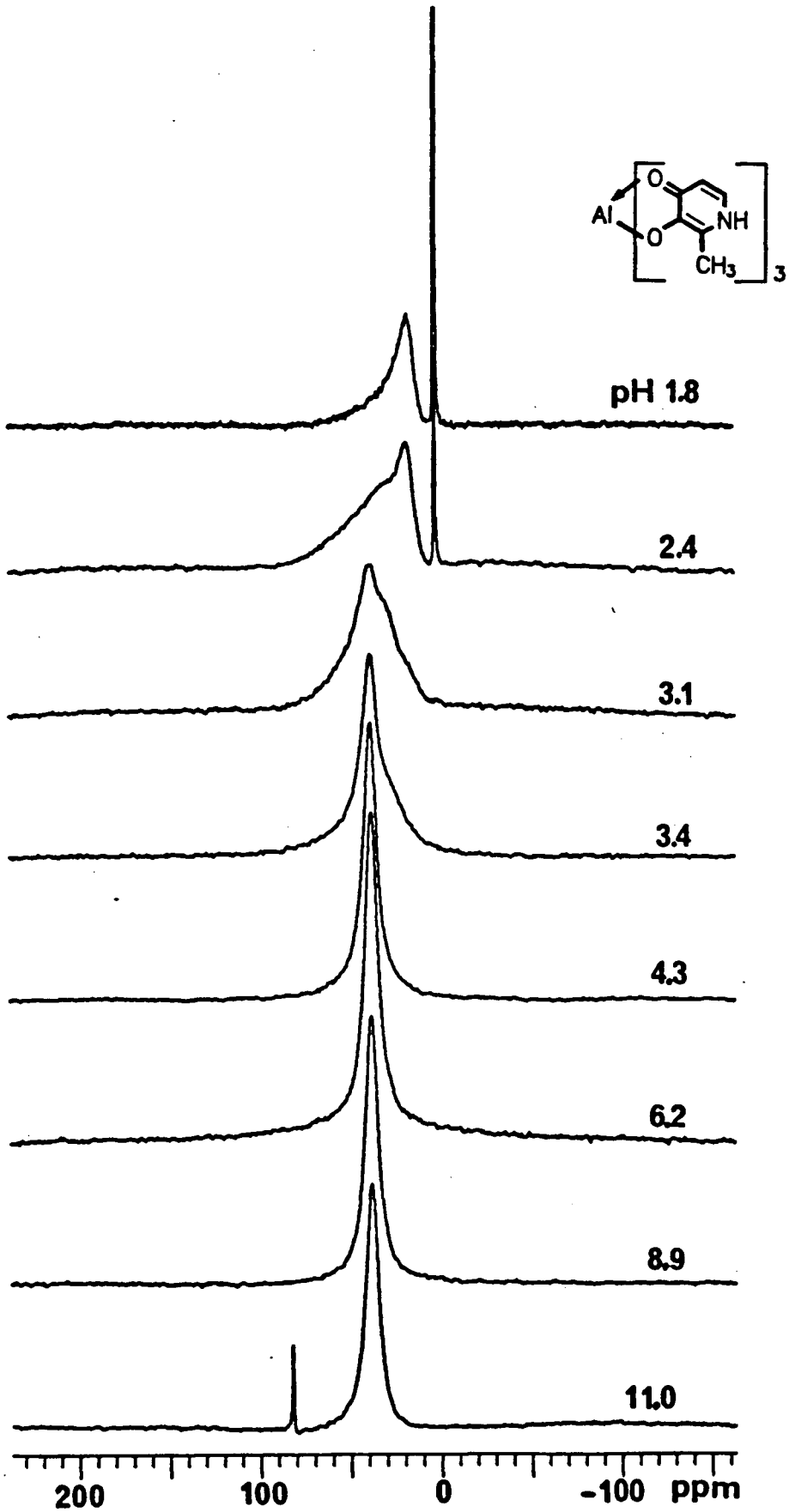

Figure 4.2. The variable-pH ^{27}Al NMR spectra of $Al(mpp)_3$.

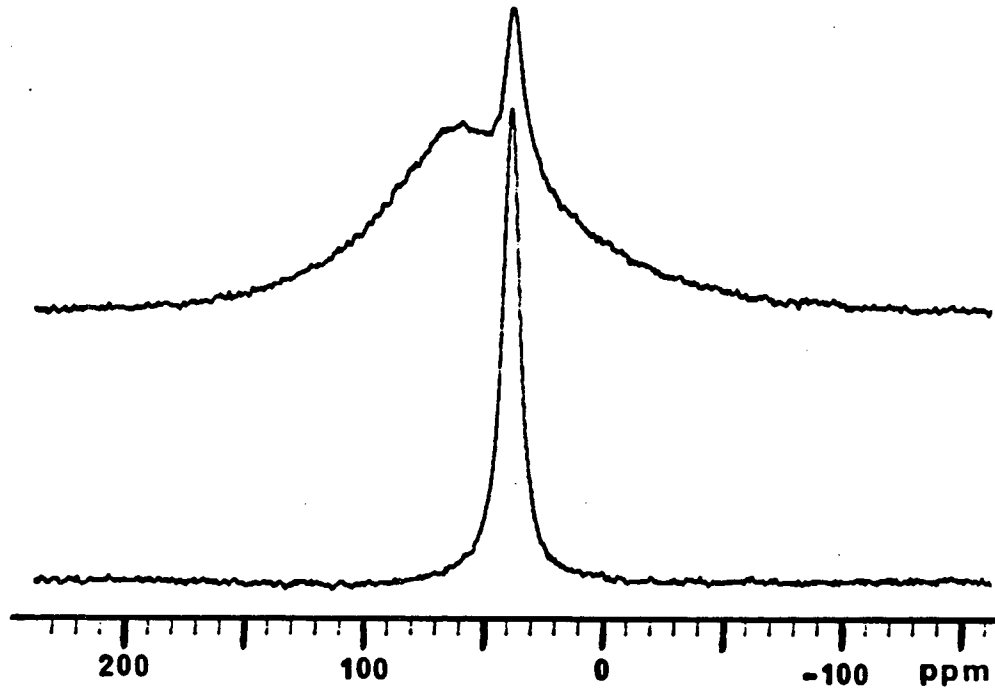

Figure 4.3. ^{27}Al NMR spectra of $Al(mpp)_3$ at pH 8.9. The bottom spectrum is 2 hours after sampling and the top spectrum is the same NMR sample 2 weeks later.

A comparison of the variable-pH spectra of $Al(mpp)_3$ with those for $Al(ma)_3$ indicates that the tris(3-hydroxy-4-pyridinone) complex is more stable to both acidic and basic hydrolysis. In the spectra of $Al(ma)_3$, the signal from $[Al(H_2O)_6]^{3+}$ first appears at pH 3.2 and $Al(OH)_4^-$ is evident at pH 9; the spectra of $Al(mpp)_3$ show no signals from either of these species at similar pH values. The difference is particularly evident at higher pH where the $[Al(OH)_4]^-$ signal does not occur until pH 10.8 in $Al(mpp)_3$.

The $Al(dpp)_3$ spectra (Fig. 4.4) are similar to those of $Al(mpp)_3$: the intermediate species occur at 26 ppm ($[Al(dpp)_2(H_2O)_2]^+$) and at 14 ppm ($[Al(dpp)(H_2O)_4]^{2+}$). At pH 2.3 there appears to be significantly more of the bisligand species as the two peaks at 26 and 14 ppm are resolvable, unlike in the $Al(mpp)_3$ spectra. The only significant change in

the $Al(mimo)_3$ spectra (aside from broader peaks) is a shift in the window of hydrolytic stability toward lower pH (Fig. 4.5). It must be stated that it is somewhat unfair to compare the spectra of the Al complexes in this study. We are observing a competition for the Al ion among water, hydroxide ions, and the 3-hydroxy-4-pyridinone ligands; the concentrations of the first two are fixed at any given pH but the ligand concentrations were different for each complex studied. It is possible to conclude that the tris(3-hydroxy-4-pyridinonato) Al complexes are more stable to hydrolysis than $Al(ma)_3$ on the basis of this experiment, however, since the initial $Al(ma)_3$ concentration was larger (50 mM) than any Al concentration used in this study.

The first variable-pH experiment with $Al(mepp)_3$ (Fig. 4.6) gave spectra that showed a second hydrolysis product at pH > 9.0 (62 ppm, $W_{1/2} \cong 50$ Hz). This narrow peak was likely due to the polymeric $[AlO_4Al_{12}(OH)_{24}(H_2O)_{12}]^{7+}$ (commonly referred to as "Al_{13}") species whose symmetric tetrahedral AlO_4 core resonates at 62.5 ppm.[131] Al_{13} is the principal ^{27}Al NMR detectable base hydrolysis product that is formed when solutions containing only $[Al(H_2O)_6]^{3+}$ are neutralized by the addition of 2.5 equivalents of base. The polymer is unstable at the acidic pH where it forms and it can undergo slow transformations to give other less symmetric species that have much broader signals. The appearance of the spectrum is very different depending on the speed of the hydrolysis and this added to the difficulty in determining the precise nature of the Al hydrolysis reactions.[136]

Given the similarity of the 3-hydroxy-4-pyridinone ligands, it seemed unlikely that $Al(mepp)_3$ was undergoing hydrolysis in a significantly different fashion from the other complexes where no Al_{13} signals were observed. In the other variable-pH experiments, the isolated tris-ligand Al complexes were used as the starting material, but in this experiment $Al(NO_3)_3$ and the free ligand (in stoichiometric ratio) were used. It appears there was a slight excess of Al that was hydrolysed to the Al_{13} polymer, as the length of the

experiment was short enough to ensure this would be the preferred hydrolysis product. This was confirmed by repeating the experiment with purified $Al(mepp)_3$ as the starting material: there was no Al_{13} signal in the spectra at pH 9.6 and the addition of $Al(NO_3)_3$ resulted in the appearance of the 62 ppm peak that subsequently disappeared when an excess of the free ligand was introduced.

The pH region where the Al_{13} signal was found is not as readily explained. The Al_{13} species forms at ca. pH 4 and at pH > 8 it should disappear as, in the absence of other ligands, $[Al(OH)_4]^-$ is the dominant Al hydrolysis product at higher pH.[136] The lack of a signal at lower pH could be ascribed to an exchange with the $Al(mepp)_3$ complex, but the persistence of the signal (there was no significant change in the spectrum after one hour) at higher pH is something of a mystery. The Al_{13} species was seen in hydrolysis experiments with tris(lactato)aluminum; there was a weak signal at 62 ppm that appeared at pH 7 and was completely gone by pH 10 where only $[Al(OH)_4]^-$ was present.[139] No signal due to Al_{13} was found in a pH controlled study of a series of hydroxy carboxylic acids even at 1:1 ligand to Al ratios.[134]

The robustness of these Al complexes is evident from their wide window of hydrolytic stability, from pH < 4 to > 9. They appear to be more stable to hydrolysis than $Al(ma)_3$ and this is corroborated by the formation constants (see Chapter V) as the log β_3 for the tris(3-hydroxy-4-pyridinonato) Al complexes is ~32 compared to a log β_3 of 22.5 for $Al(ma)_3$.[59] The variable-pH experiment with $Al(mepp)_3$ directly illustrates the ability of the 3-hydroxy-4-pyridinones to compete with the hydroxide ion. The results of this variable-pH ^{27}Al NMR study indicate the tris(3-hydroxy-4-pyridinonato) Al complexes should resist in vivo hydrolysis except in the highly acidic conditions of the stomach.

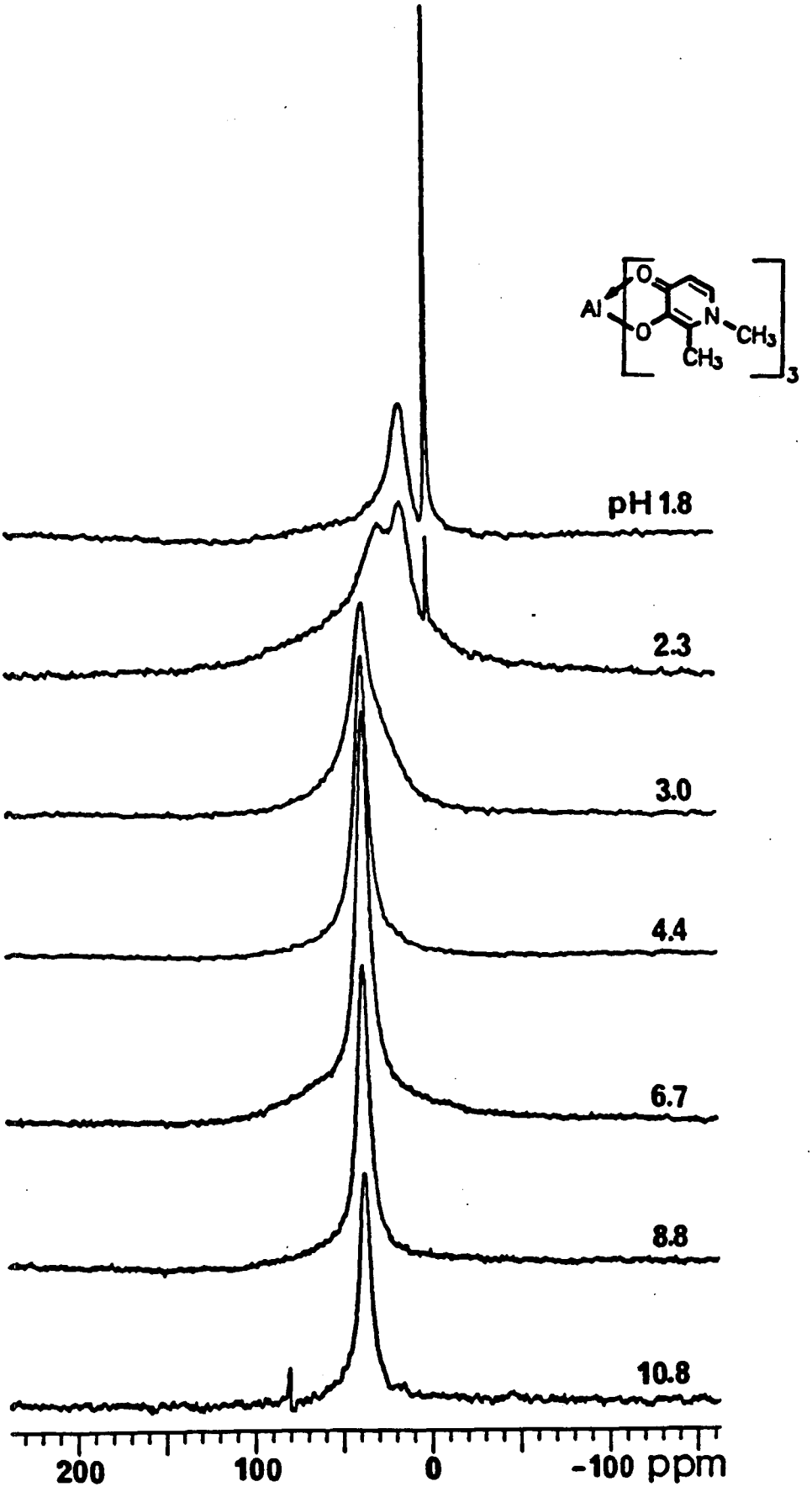

Figure 4.4. The variable-pH ^{27}Al NMR spectra of $Al(dpp)_3$.

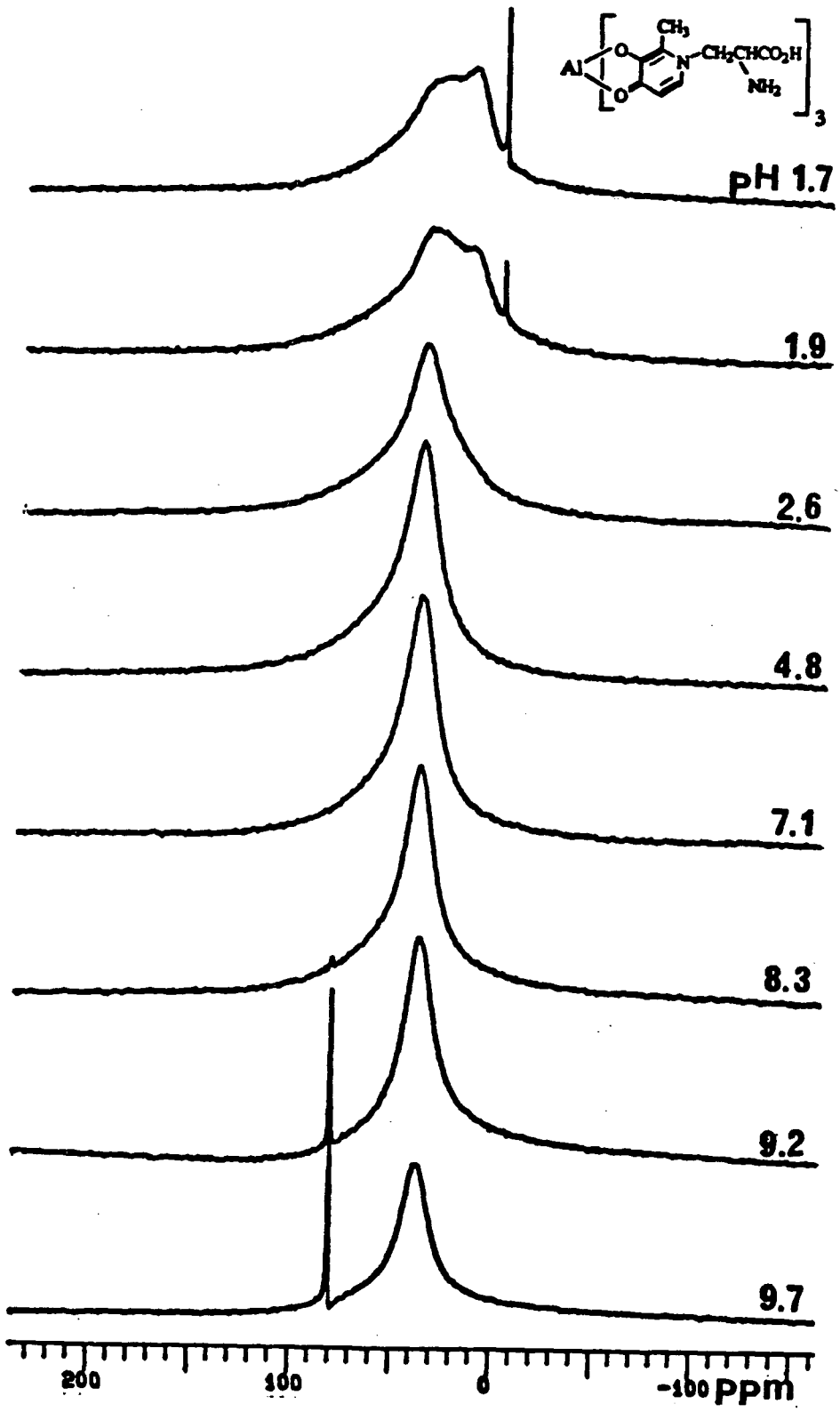

Figure 4.5. The variable-pH ^{27}Al NMR spectra of $Al(mimo)_3$.

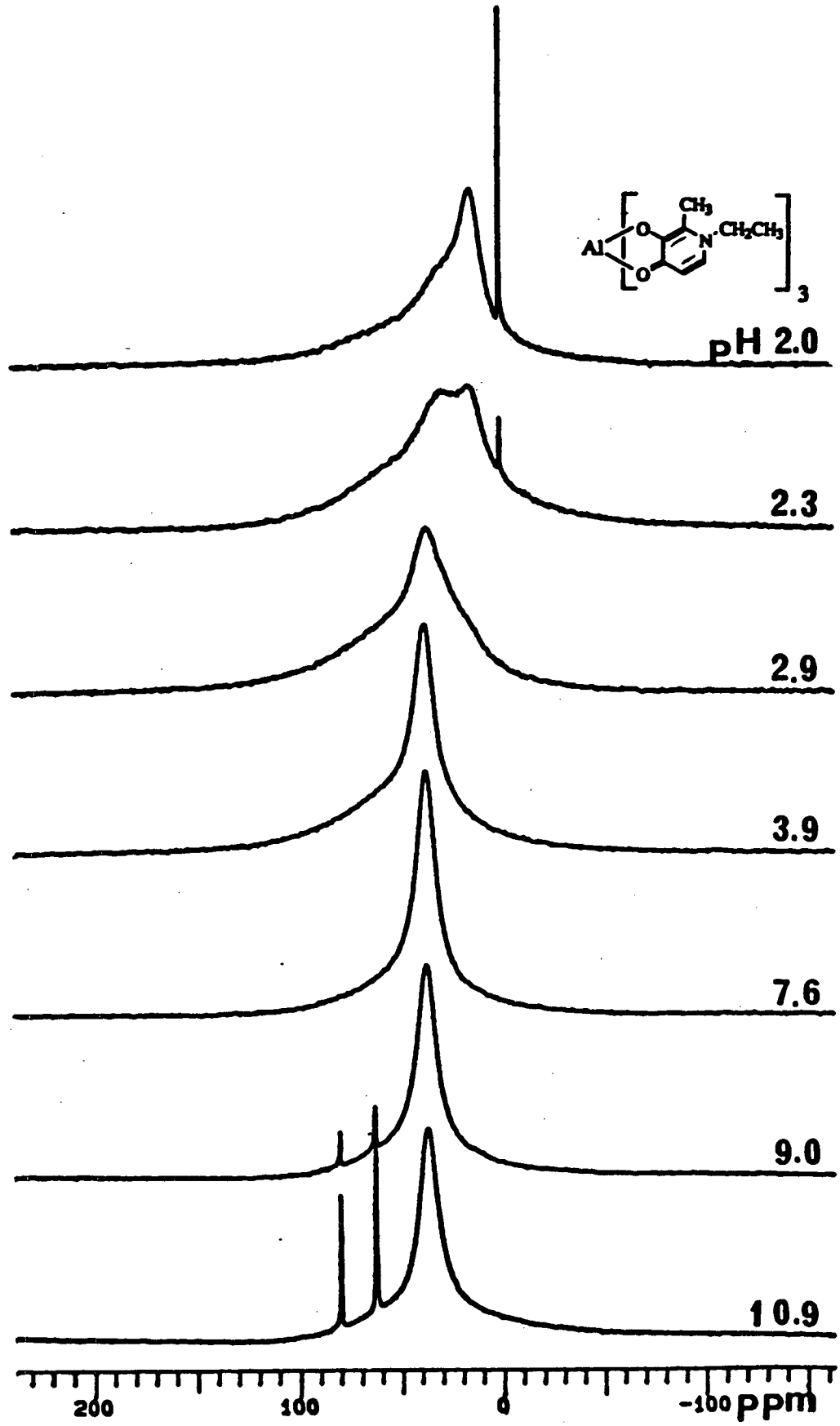

Figure 4.6. Variable-pH ^{27}Al NMR spectra of a 3:1 Hmepp to $Al(NO_3)_3$ mixture.

B. Variable-Temperature Proton NMR Spectroscopy

4.4 Introduction

In tris-ligand metal complexes, asymmetric bidentate ligands may assume a facial (*fac*) or a meridional (*mer*) geometry. The *fac* and *mer* geometric isomers* are each enantiomeric pairs of Δ and Λ stereoisomers. (Figure 4.7 is a generalized diagram illustrating the four isomers.) The rearrangement reactions are geometric isomerization and racemization; these reactions can occur separately or simultaneously depending on the mechanism of the rearrangement. Three types of mechanisms have been proposed: (1) the complete dissociation of one ligand to give a four-coordinate intermediate, (2) the rupture of one metal-ligand bond to give a five-coordinate intermediate, and (3) twisting processes (Bailar or Rây-Dutt twists) that do not require the cleavage of any metal-ligand bonds.[142] The majority of research on the rearrangement reactions of tris-ligand metal complexes has been directed towards differentiating between the two intramolecular mechanisms.

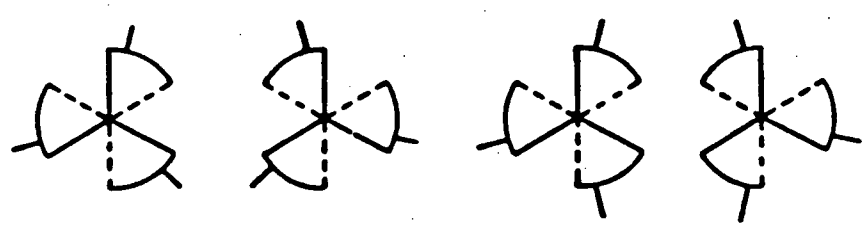

Figure 4.7. Isomers of tris-ligand metal complexes with asymmetric bidentate ligands.

*They are frequently referred to as cis and trans isomers respectively.

Gordon and Holm[143] define two limiting types of tris-ligand systems based on the rates of the rearrangement reactions. The kinetically "slow" systems are those in which the geometric isomers can be completely separated and partially resolved. The reaction rates[144] are $\lesssim 10^{-2}\ s^{-1}$ and complexes containing inert metal ions such as Cr^{3+} and Co^{3+} are in this category. The second type is designated "fast"; this means that the intramolecular rearrangements are rapid enough to prevent separation or resolution of the isomers, but they are not so rapid as to disallow isomer detection by NMR spectroscopy or other techniques such as low temperature HPLC.[145] Tris-ligand Al and Ga complexes fall into the fast category.

NMR is particularily suited to the examination of the rearrangement reactions because the *fac* isomer has a threefold symmetry axis and the *mer* isomer is asymmetric; the three ligands of the *fac* isomer are magnetically equivalent and the chemical shifts of the nuclei on these ligands will be different from that of their inequivalent counterparts in the *mer* isomer. If the chemical shift differences are large enough, the isomers may be identified and it is possible to measure the rates of isomerization and racemization. In the early 1960's, Fay and Piper used variable temperature ^{19}F NMR to examine the fluxional behavior of tris(trifluroacetylacetonate) (tfac) complexes with a variety of metals including Al, Ga, and In.[146] This classic work established the utility of variable-temperature NMR for the study of stereochemically nonrigid inorganic complexes. Proton NMR has been used extensively to study the rearrangement reactions of tris(β-diketonato) metal complexes and the group 13 metals have figured prominently in this work.[144,147] The fluxionality of tris-ligand Al and Ga complexes with other ligands such as EDTA[148] and α-substituted tropolonates (α–RT)[149,150] has also been examined by NMR techniques. The tropolone complexes are of particular interest as these bidentate ligands chelate the metal center with the same binding group (the α-hydroxyketone moiety) as the 3-hydroxy-4-pyridinones.

The tris(3-hydroxy-4-pyridinonato) Al complexes exhibit complex proton NMR spectra at the ambient probe temperature of the 300 MHz NMR instrument. Under the same conditions, the Ga analogues give the expected first order spectra. The spectra of the Al complexes can be rationalized on the basis of *fac-mer* isomerization that is slow enough to result in overlapped signals from the geometric isomers. A variable-temperature NMR study of the $M(dpp)_3$ complexes was conducted to verify that ligand rearrangement is the source of the difference between spectra of the analogous tris-ligand Al and Ga complexes. The results of this study indicate that two exchange processes are occurring and the coalescence temperature (T_c) for the higher temperature process is near room temperature for $Al(dpp)_3$ and is at -9 °C for $Ga(dpp)_3$.

The solubility properties of the $M(dpp)_3$ complexes necessitate the use of protic solvents. The majority of this work was done in CD_3OD due to the solubility of the $M(dpp)_3$ complexes and the large temperature range available with this solvent. $Ga(dpp)_3$ is too insoluble in D_2O to allow the acquisition of a spectrum in a reasonable length of time. $Ga(dpp)_3$ is quite soluble in $(CD_3)_2SO$ but it does not reach the region of slow exchange above the freezing point (18.5 °C) of this solvent. Therefore, the difference in lability between the two metals was examined by variable-temperature NMR in CD_3OD. Because of the importance of water interactions to the solid state structure of the $M(dpp)_3$ complexes, we were also interested in determining if the rate of the rearrangement reaction for $Al(dpp)_3$ is significantly different in water. The exchange process for $Al(dpp)_3$ was examined in D_2O, $(CD_3)_2SO$, and CD_3OD; because of the low water solubility of $Al(dpp)_3$, the fluxionality of the more water soluble $Al(mpp)_3$ was also investigated in D_2O.

4.5 Materials and Methods

The spectra were recorded on a Varian XL-300 NMR spectrometer equipped with a variable temperature probe. The thermocouple was calibrated using a methanol calibration standard and was accurate within ± 1 ° over a range of -70 to 60 °C. The spectra in CD_3OD and $(CD_3)_2SO$ were referenced to the solvent peak and those in D_2O were referenced internally to $(CD_3)_2CO$. The spectra were recorded by the author. Al- and $Ga(dpp)_3$ and $Al(mpp)_3$ were prepared and purified as reported herein (Section 2.6). $In(dpp)_3$ and $Al(ma)_3$ were synthesized by others in this laboratory (C. Matsuba and M. Finnegan) and were purified by recrystallization. The equilibrium distribution of the $Al(dpp)_3$ geometric isomers in the absence of exchange was determined by computer simulation using the NMR line-shape program DNMR3.[151]

4.6 Results and Discussion

The spectra of Ga- and $Al(dpp)_3$ in CD_3OD at 18 °C clearly show the differences that prompted this variable-temperature NMR study (Figs. 4.8 and 4.9--the spectral regions without signals have been omitted for clarity). The singlet for the CH_{3c} group has a $W_{1/2}$ of 1.6 Hz in $Ga(dpp)_3$ compared to an exchange broadened 7.0 Hz in $Al(dpp)_3$. The downfield doublets in the $Al(dpp)_3$ spectrum are also broadened and a second signal is just starting to appear as shoulders on the H_b doublet. The $Al(dpp)_3$ spectra in $(CD_3)_2SO$ (Fig. 4.10) and D_2O (Fig. 4.11), also at 18 °C, afford better resolution of the signals from the *fac* and *mer* isomers due to the slightly larger chemical shift difference and the higher coalescence temperature in these solvents. In both spectra, there are four distinct signals from the three inequivalent CH_{3c} groups of the *mer* isomer and the one unique methyl of the *fac* isomer.

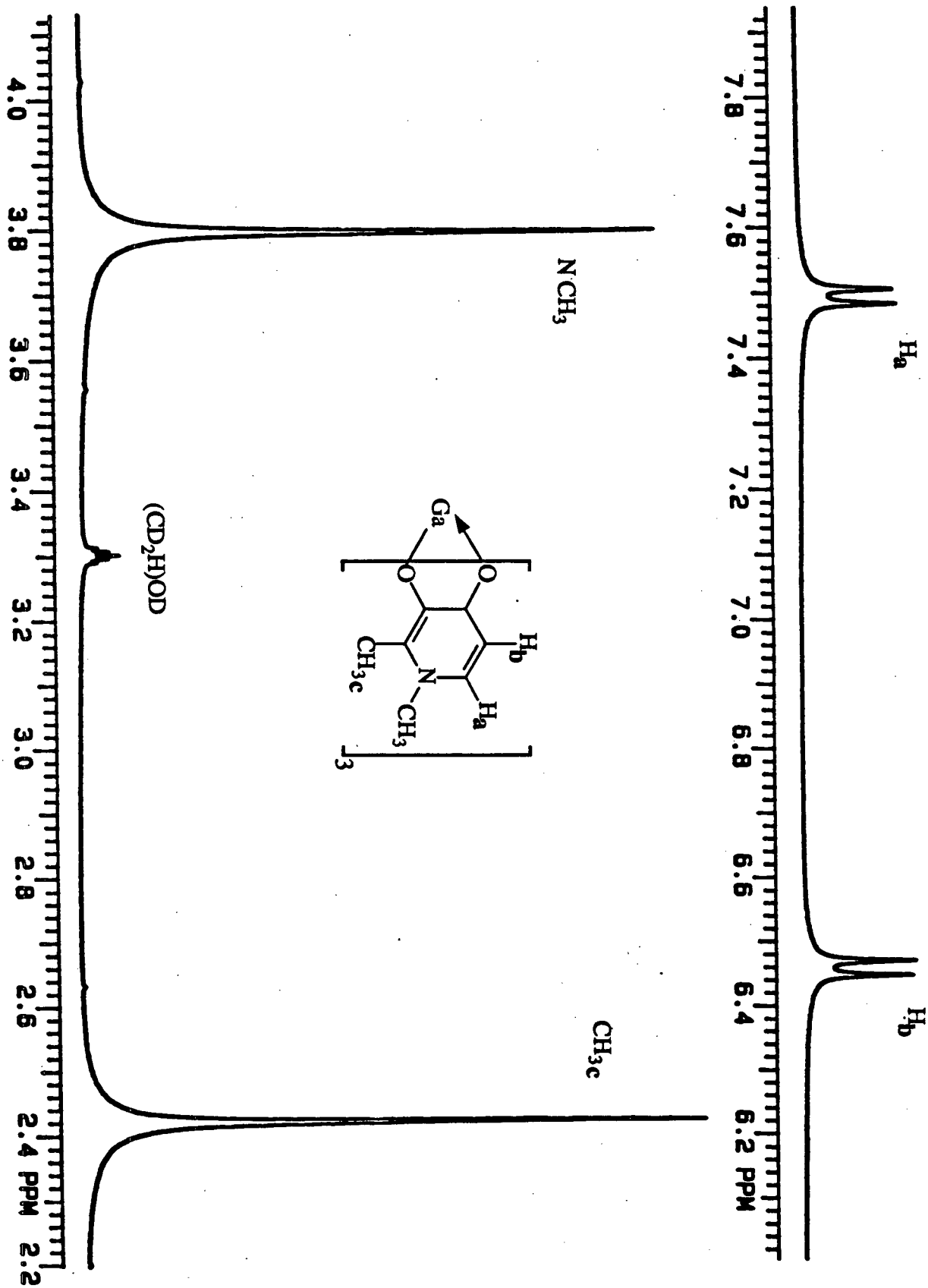

Figure 4.8. 300 MHz proton NMR spectrum of $Ga(dpp)_3$ in CD_3OD at 18 °C.

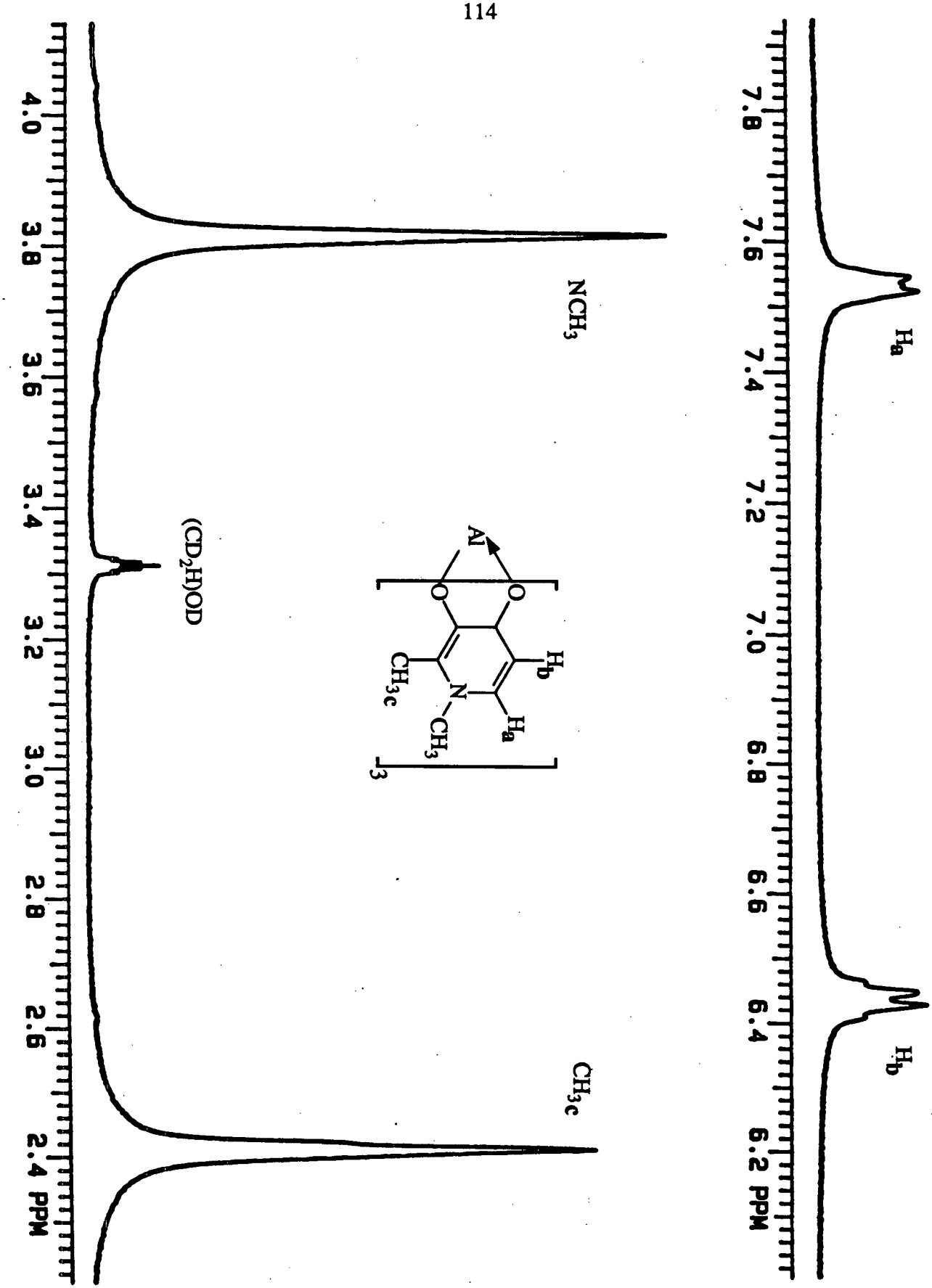

Figure 4.9. 300 MHz proton NMR spectrum of $Al(dpp)_3$ in CD_3OD at 18 °C.

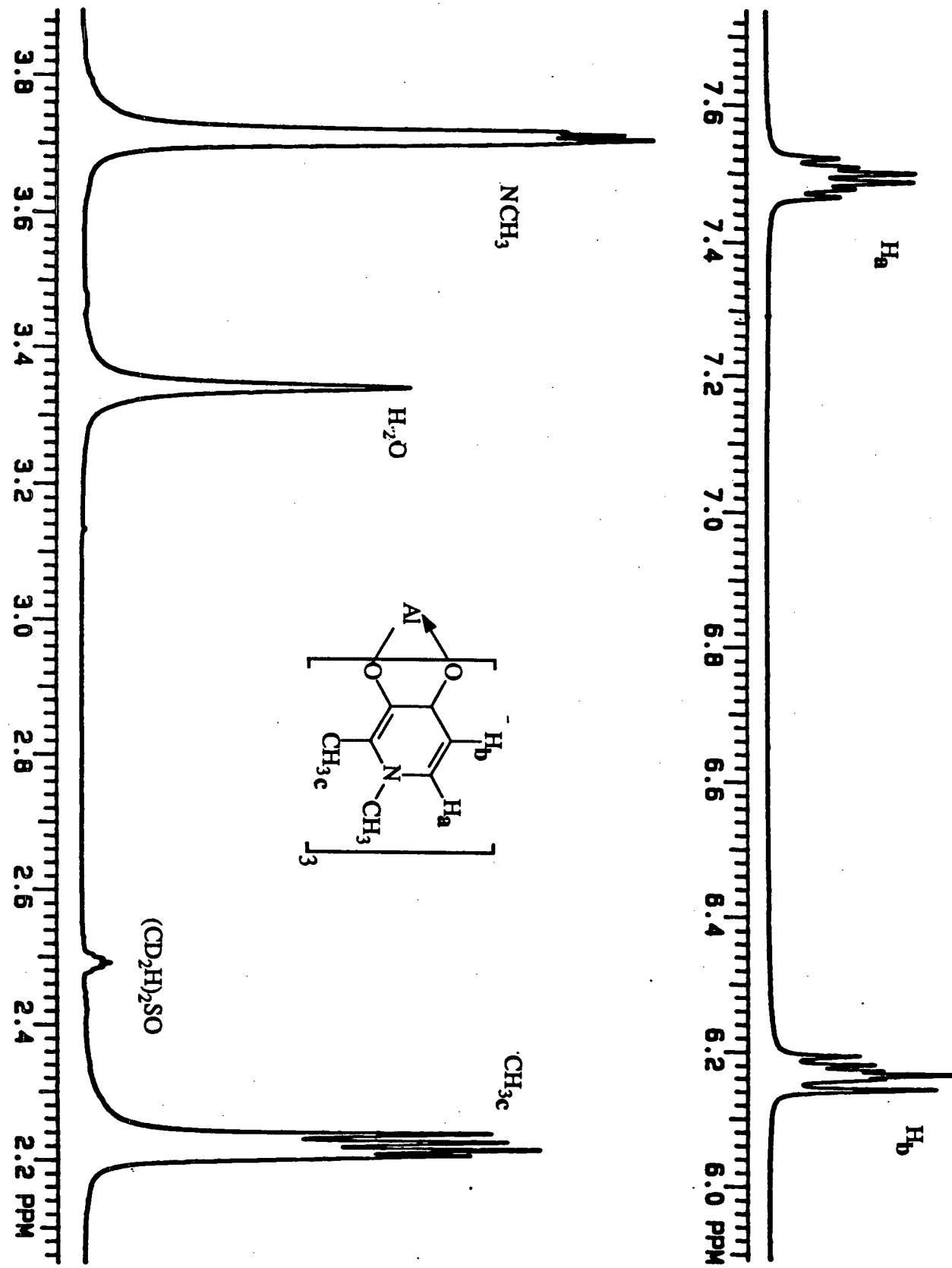

Figure 4.10. 300 MHz proton NMR spectrum of $Al(dpp)_3$ in $(CD_3)_2SO$ at 18 °C.

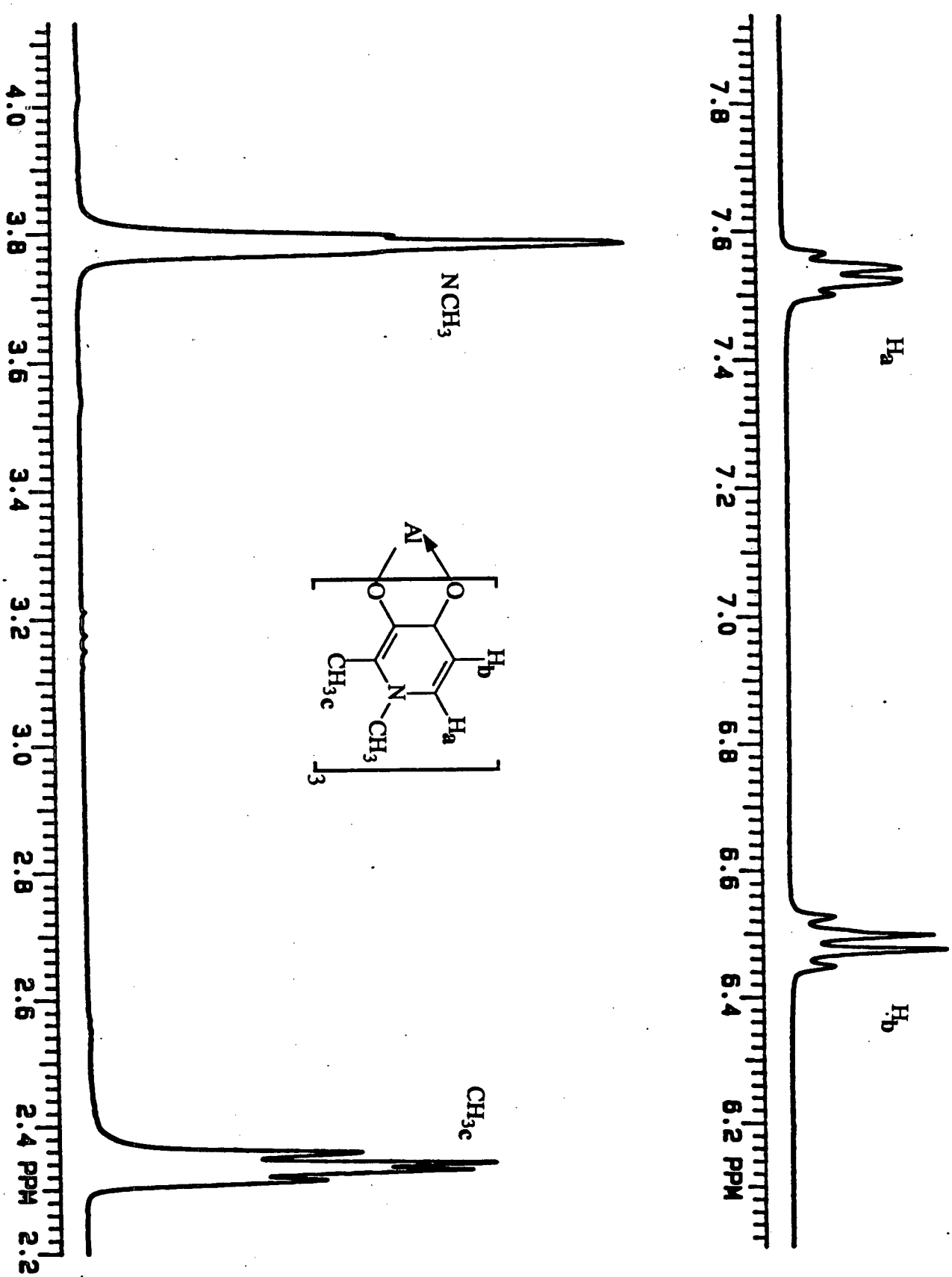

Figure 4.11. 300 MHz proton NMR spectrum of $Al(dpp)_3$ in D_2O at 18 °C.

The chemical shift differences in the downfield doublets are quite small so the H_a and H_b ring protons are of limited utility for identifying the geometric isomers in any of the solvents. The same is true of the N-CH_3 signal. For this reason, the kinetic parameters were determined from the temperature-dependent CH_{3c} spectra. Among the four signals, the one that was different in intensity was assigned to the *fac*-isomer; this assignment rationale was used by Piper and Fay for the fluorine resonances in the M(tfac)$_3$ complexes.[146] Figure 4.12 shows the CH_{3c} signals for Al- and Ga(dpp)$_3$ in the absence of exchange (-30 °C) and the signal assigned to the *fac* isomer is marked with an asterisk. (The scale in Hertz indicates the magnitude of the peak separation and not the chemical shift.) Two of the *mer* isomer signals in Ga(dpp)$_3$ appear as shoulders, but the assignment of the peak with the odd intensity to the *fac* isomer has been made with other tris-ligand metal complexes where only two of the four peaks are resolvable.[149]

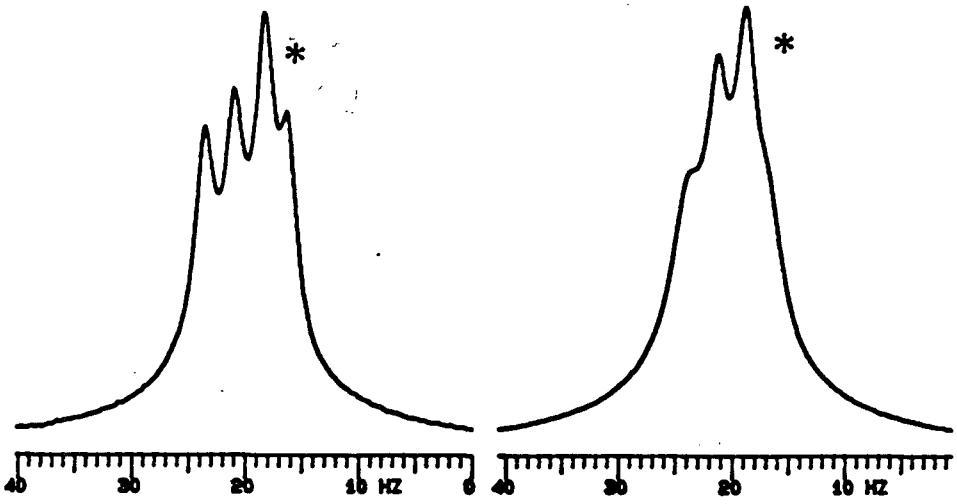

Figure 4.12. CH_{3c} spectra for Al(dpp)$_3$ (left) and Ga(dpp)$_3$ (right) in CD_3OD at -30 °C..

A statistical distribution of the geometric isomers would give four peaks of equal intensity, i.e., the *fac* isomer would be 25% of the total concentration. It has been stated that the *mer* isomer is the more stable isomer due to its lower dipole moment and this was

used to explain the smaller than statistical (18%) equilibrium distribution for the kinetically fast $Al(tfac)_3$ complex.[146] Gordon and Holm maintained that unless the complexes were sterically constrained, a statistical or nearly statistical distribution of isomers would usually be formed in solution.[143] The Al- and $Ga(\alpha\text{-RT})_3$ complexes had a slight excess of the *fac*-isomer at equilibrium[150] and this was also the situation for $Al(dpp)_3$. DNMR3 was used to simulate the equilibrium spectrum of $Al(dpp)_3$ in the absence of exchange and the best fit (Fig. 4.13) was obtained with a 32% distribution for the *fac*-isomer. The enhanced stability of the *fac* isomer was interesting when considered in concert with the solid state structures (see Chapter III). It was thought that the water networks imposed a *facial* geometry on the $M(dpp)_3 \cdot 12H_2O$ complexes, but these NMR results in methanol suggest that the *fac* isomer enjoys at least a small thermodynamic advantage independent of the H-bonded water network. The close match of the computer simulation also supports the assignment of the larger signal to the *fac*-isomer.

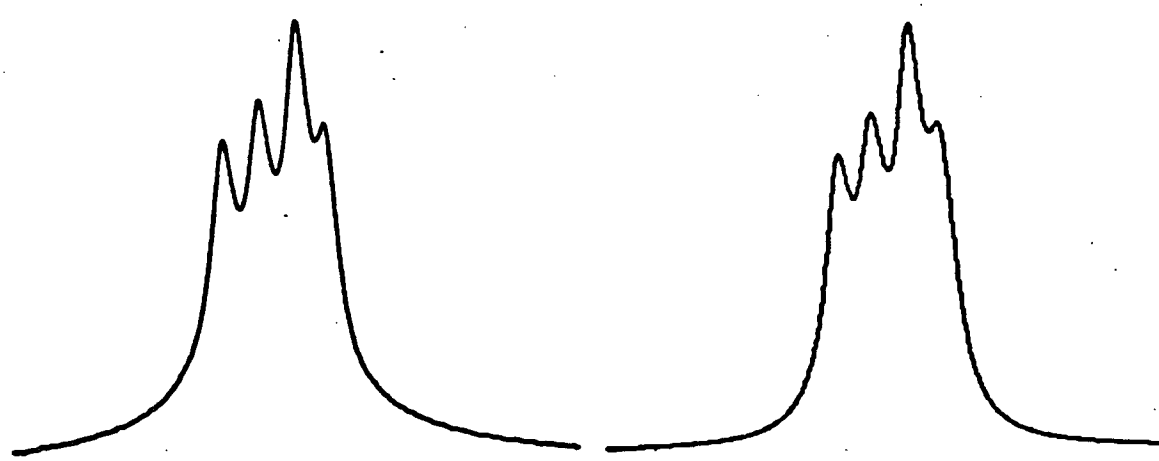

Figure 4.13. Experimental (left) and simulated (right) $Al(dpp)_3$ CH_{3c} spectra in CD_3OD (-30 °C).

For the exchange of nuclei between two inequivalent sites, the rate of exchange at the temperature of coalescence (k_{Tc}) is given by: $k_{Tc} = \frac{\pi \Delta\nu}{\sqrt{2}}$ where $\Delta\nu$ is the frequency separation (in Hertz) between the resonance components in the absence of exchange.[152]

For the CH_{3c} spectra, $\Delta\nu_e$ (the experimentally observed frequency separation) was taken as the difference between the signal for the *fac*-isomer and the furthest downfield signal from the *mer*-isomer. A source of error in using this equation is the temperature dependence of the chemical shifts that is presumably due to solvent-solute interactions.[153] To correct for this temperature dependence, the $\Delta\nu_e$ was plotted against temperature at several points in the region of slow exchange, and the line was extrapolated to the region of fast exchange. Then $\Delta\nu$ was read from the extrapolated line at the T_c. In our systems, the values of $\Delta\nu_e$ were small (5-8 Hz) and the variations due to temperature dependence were barely within the resolution error of the instrument; therefore, the required adjustments in $\Delta\nu$ were minor. The value of the free energy of activation ($\Delta G^{\ddagger}_{Tc}$) was calculated from the Eyring equation[154] (assuming the transmission coefficient to be unity): $k_{Tc} = \frac{K_B}{h} T_c\, e^{-\Delta G^{\ddagger}/RTc}$

where h is Planck's constant, K_B is Boltzman's constant, and R is the gas constant.

The simplified Gutowsky-Holm equation[152] is used to calculate the rate constants for an exchange process from the peak separations in the slow exchange region; the rate constants can then be used to determine the E_a, $\Delta H^{\ddagger}$, and $\Delta S^{\ddagger}$ for the exchange reaction. The size of the error in using this approximation is related to the length of T_2 and the magnitude of $\Delta\nu$. When $\Delta\nu$ is small and T_2 is short, the errors become comparable to the calculated rate constants and the peak separation method should not be used.[155] A value of less than 0.33 for the ratio of T_2 (expressed as $W_{1/2}$) to $\Delta\nu$ was cited as the minimum requirement for using the simplified equation.[156] For the CH_{3c} spectrum in $Al(dpp)_3$, the T_2 determined by computer simulation is 0.135 s ($W_{1/2}$ = 2.36 Hz) and the $\Delta\nu$ is 5.1 Hz. The ratio of $W_{1/2}$ to $\Delta\nu$ is 0.46 and the simplified equation could not be used for this complex, or for $Ga(dpp)_3$ either as the CH_{3c} signal from the Ga complex is even more poorly resolved.

The preferred method for estimating rate constants is line-shape simulation. The DNMR3 computer program allows mutual and non-mutual exchange (referred to in the program documentation as "otherwise"). The non-mutual exchange routine has multiple chemical configurations that can have unequal populations and it is possible to simulate the equilibrium spectrum of $Al(dpp)_3$ in the absence of exchange with this routine; however, the non-mutual routine cannot directly accommodate exchange between chemical configurations of different symmetry. With the mutual exchange routine, the population difference between the *fac*- and *mer*-isomers cannot be incorporated so the larger peak due to the *fac* isomer is not modelled. Because of these limitations, the DNMR3 simulated spectra did not correspond well enough to the experimental spectra to merit inclusion in this thesis.

Qualitatively, the $M(dpp)_3$ complexes appear to undergo two exchange processes in a fashion similar to that of the $M(\alpha\text{-RT})_3$ complexes.[149,150] This is illustrated by the CH_{3c} spectra for $Al(dpp)_3$ over a temperature range of -90 to 38 °C which are included as Figure 4.14. The spectra for $Ga(dpp)_3$ are similar and Figure 4.15 is a view of the exchange process for all of the protons in the complex (the spectral regions without signals have been omitted in this reproduction). In both $M(dpp)_3$ complexes there is a low temperature exchange process (LTP) with a T_c near the -98 °C low temperature limit of our CD_3OD study. There is a second exchange process with a T_c of 21 and -9 °C in Al- and $Ga(dpp)_3$, respectively. The kinetic parameters at the T_c for this higher temperature process (HTP) are listed in Table 4.3. The LTP for the $M(\alpha\text{-RT})_3$ complexes was identified as racemization by means of a trigonal twist and the HTP was *fac-mer* isomerization. By comparison to the spectra of the $M(\alpha\text{-RT})_3$ complexes, the variable-temperature NMR spectra of the $M(dpp)_3$ complexes support the conclusion that the exchange process near ambient temperature is due to *fac-mer* isomerization.

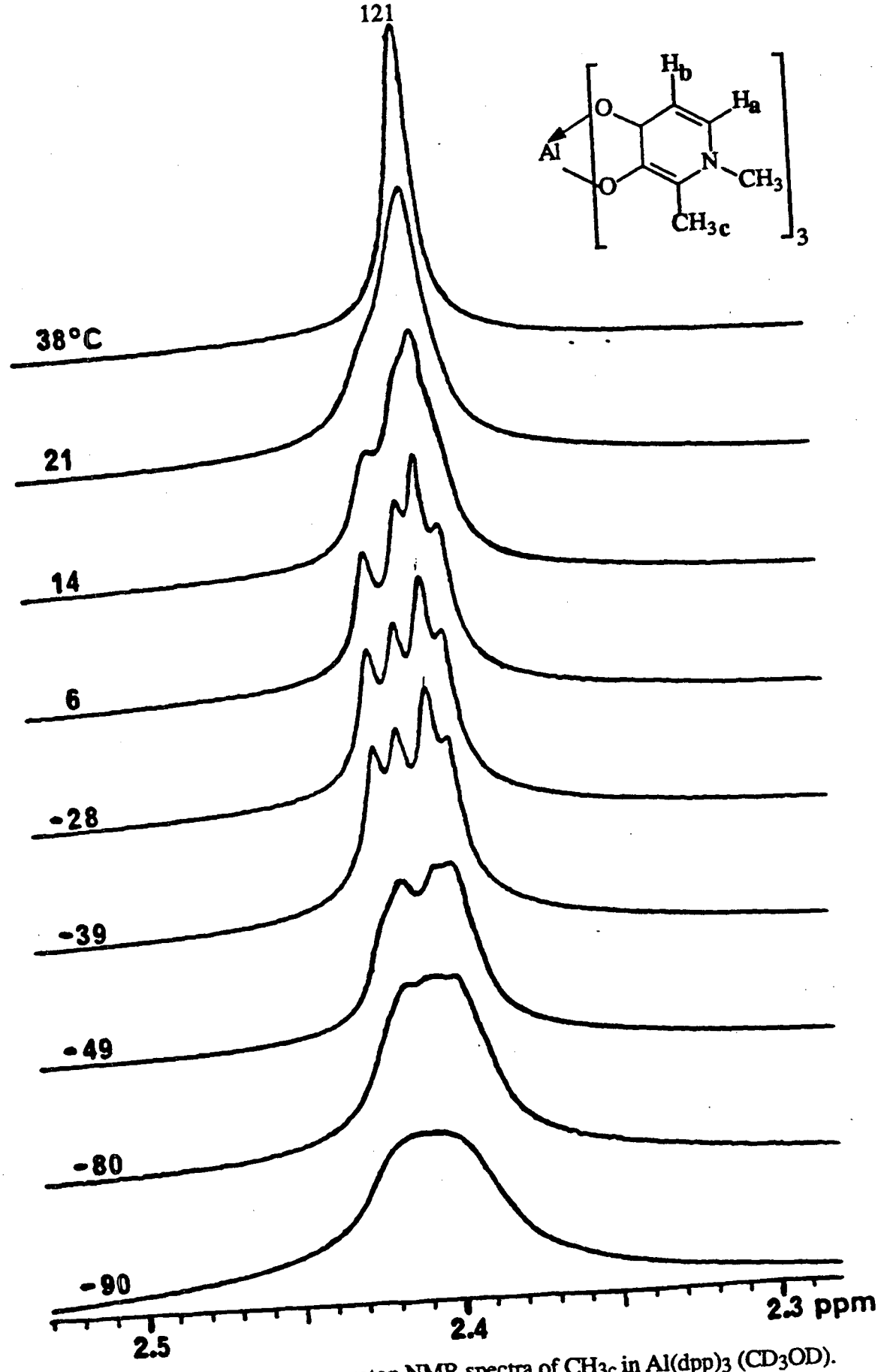

Figure 4.14. Variable-temperature proton NMR spectra of CH_{3c} in Al(dpp)$_3$ (CD_3OD).

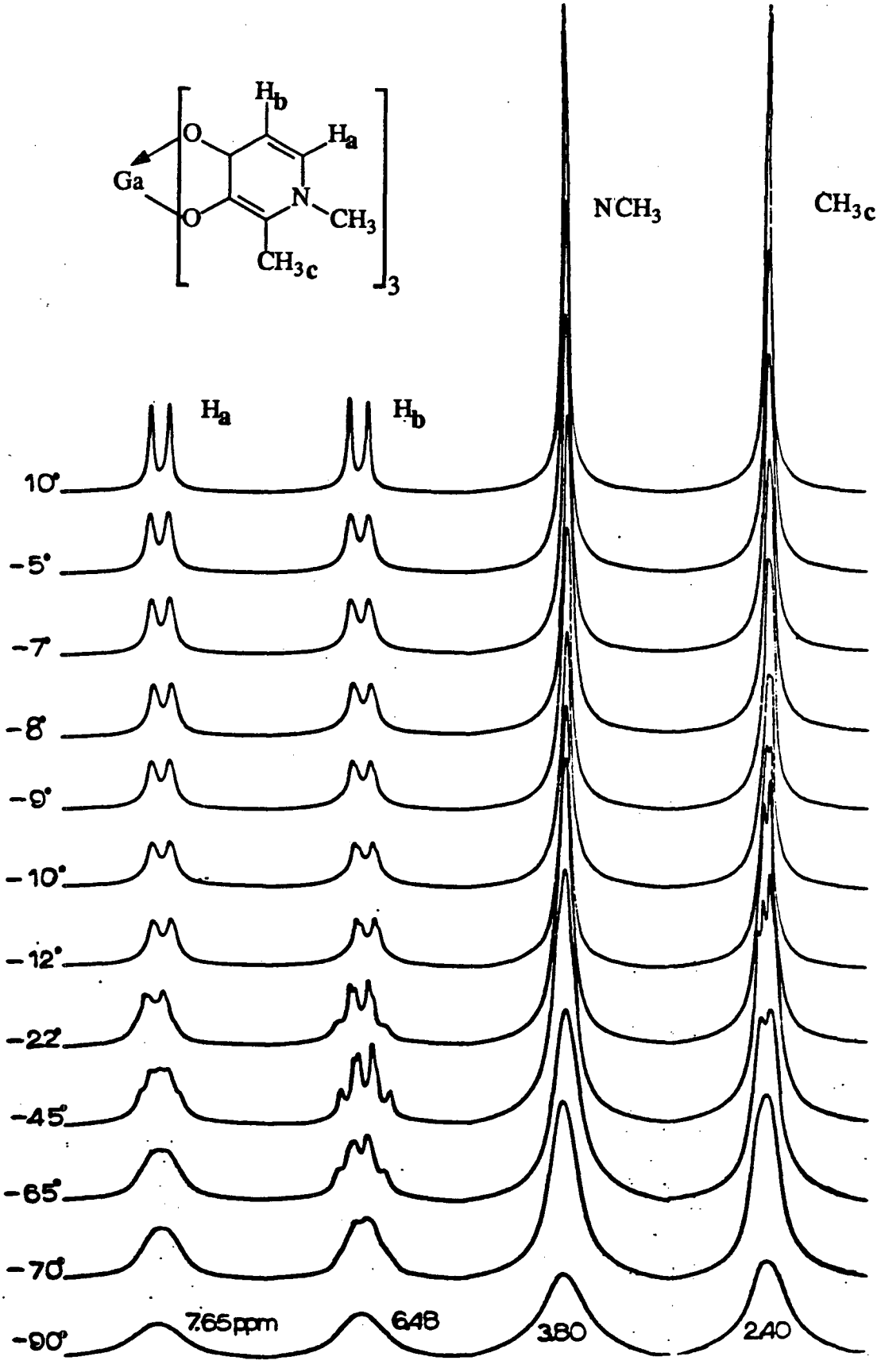

Figure 4.15. Variable-temperature proton NMR spectra of $Ga(dpp)_3$ in CD_3OD.

Table 4.3. Kinetic data for tris(3-hydroxy-4-pyridinonato) metal complexes at the T_c.

Complex	Solvent [ε^c]	$\Delta\nu$ (Hz)	T_c (°C)[a]	k_{Tc} (s^{-1})	$\Delta G^{\ddagger}_{Tc}$ (kcal/mol)[b]
$Ga(dpp)_3$	CD_3OD	4.8	-9	10.7	14.2 ± 1.2
$Al(dpp)_3$	CD_3OD [32.7]	5.1	21	11.3	15.7 ± 1.3
	$(CD_3)_2SO$ [40.7]	7.2	38	16.0	16.5 ± 1.4
	D_2O [78.5]	8.0	34	17.8	16.0 ± 1.4
$Al(mpp)_3$	D_2O	6.0	36	13.3	16.5 ± 1.4

[a] Errors were estimated to be ± 2 °.

[b] Errors were estimated assuming an order of magnitude error in the rate constants.

[c] Dielectric constants at 25 °C.

The $M(dpp)_3$ complexes are more labile than Al- and $Ga(tfac)_3$ that have a $\Delta G^{\ddagger}_{Tc}$ of 21.4 and 18.7 kcal/mol respectively (in $CDCl_3$).[157] Since the rate-accelerating influence of the CF_3 groups is well documented,[158] it would appear that the 3-hydroxy-4-pyridinones constitute a relatively labile tris-ligand metal system. This is only speculation, however, as the contribution from solvent effects has not been taken into account. The rearrangement rates for d^0 and d^{10} metals are dependent on the ionic radius of the metal[144] and the $M(dpp)_3$ complexes exhibit the predicted kinetic order (Al < Ga < In). $Ga(dpp)_3$ has a lower $\Delta G^{\ddagger}_{Tc}$ than $Al(dpp)_3$ and the In analogue gives only an averaged spectrum down to -80 °C in CD_3OD.

For a series of aprotic solvents, it was found that the T_c and $\Delta G^{\ddagger}_{Tc}$ of $Al(tfac)_3$ decreased as the dielectric constant of the solvent increased.[159] There was no indication of a similar trend in this study and the kinetic parameters for the $Al(dpp)_3$ exchange process were essentially the same in the three solvents that were used (see Table 4.3). The kinetic

data for Ni(phenanthroline)$_3^{2+}$ showed no simple correlation between the racemization rate and the dielectric constant of the solvent (this study included water and methanol).[158] The results for Al(dpp)$_3$ are in agreement with this conclusion.

In order to obtain mechanistic information on the rearrangement reaction, it is necessary to ascertain that one is dealing with an intramolecular process. This can be accomplished by examining the NMR spectrum of a mixture of the tris-ligand metal complex of interest and another tris-ligand metal complex. If it takes an appreciable amount of time to form the mixed-ligand species, it can be concluded that ligand exchange is slower than the rearrangement reaction, e.g., no NMR signals attributable to mixed-ligand species were detected in one hour at room temperature for a mixture of Al(acac)$_3$ and tris(1-phenyl-5-methylhexane-2,4-dionato)aluminum(III).[160] When ligand exchange is completed in a shorter period of time (in minutes at room temperature), the NMR spectrum at a temperature above the T_c for the rearrangement reaction can be used to determine the relative rates of the two processes. If multiple signals assignable to the mixed-ligand species are observed at a temperature where the rearrangement process gives an averaged spectrum, it can again be concluded that the intermolecular process of ligand exchange occurs at a slower rate. This is considered sufficient proof that the rearrangement reaction is an intramolecular process.

Our interest in the possibility of solvent effects on the exchange process made it worthwhile to qualitatively compare the rates of ligand exchange and ligand rearrangement for Al(dpp)$_3$ in CD_3OD. The other tris-ligand aluminum complex used in the ligand exchange experiment was Al(ma)$_3$. The Al-maltol complex was chosen because, unlike the tris(3-hydroxy-4-pyridinonato) Al complexes used in this study, the chemical shift of the ring protons was sufficiently removed from that of Al(dpp)$_3$ to permit easy differentiation of the signals from the two ligands.

The ratio of the NMR sample was 3:1 $Al(ma)_3$ to $Al(dpp)_3$ and Figure 4.16 shows the proton NMR spectrum fifteen minutes after mixing (at a probe temperature of 18 °C). It is evident that mixed-ligand species have already formed and the 2:1 ratio of the signals from the N-methyl group of the dpp^- ligand (at 3.82 ppm) suggests the formation of $Al(dpp)_2ma$ and $Al(ma)_2dpp$ species. Figure 4.17 highlights the spectra of the H_a and H_b ring protons: in the 3:1 mixture, the signals from the maltol in the mixed-ligand species are shifted slightly upfield from those of $Al(ma)_3$ and the signals at the chemical shift of $Al(dpp)_3$ indicate that all of the dpp^- ligands are on mixed-ligand species.

The T_c for $Al(dpp)_3$ in CD_3OD is 21 °C and as the top spectrum in Figure 4.17 illustrates, the ligand rearrangement rate is slow at 18 °C. However, the signals from the mixed-ligand species are sharp and well resolved at this temperature. This is evidence that the ligand exchange rate is comparable to the rate of ligand rearrangement. To verify this, the 3:1 mixture was cooled (in 10° increments) to -50 °C and the variable-temperature NMR spectra of the H_b proton on the dpp^- ligand are reproduced as Figure 4.18. The sharp overlapped doublets of the 18 °C spectrum are significantly broadened at -10 °C (a similar effect is observed for the other signals in the spectrum). At -20 °C the ligand exchange rate is slow enough to permit the observation of signals from the inequivalent dpp ligands on the $Al(dpp)_{3-n}(ma)_n$ species. The ligand exchange rate is slower at -30 °C and this can be considered the spectrum in the absence of ligand exchange as it is unchanged at -40 and -50 °C. It is apparent that ligand exchange is occurring at a rate somewhat faster than that of the rearrangement reaction. It is necessary to cool the sample to a temperature comparable to the T_c of the more labile $Ga(dpp)_3$ (-9 °C) in order to slow the ligand exchange process enough to observe the signals from all of the mixed-ligand species.

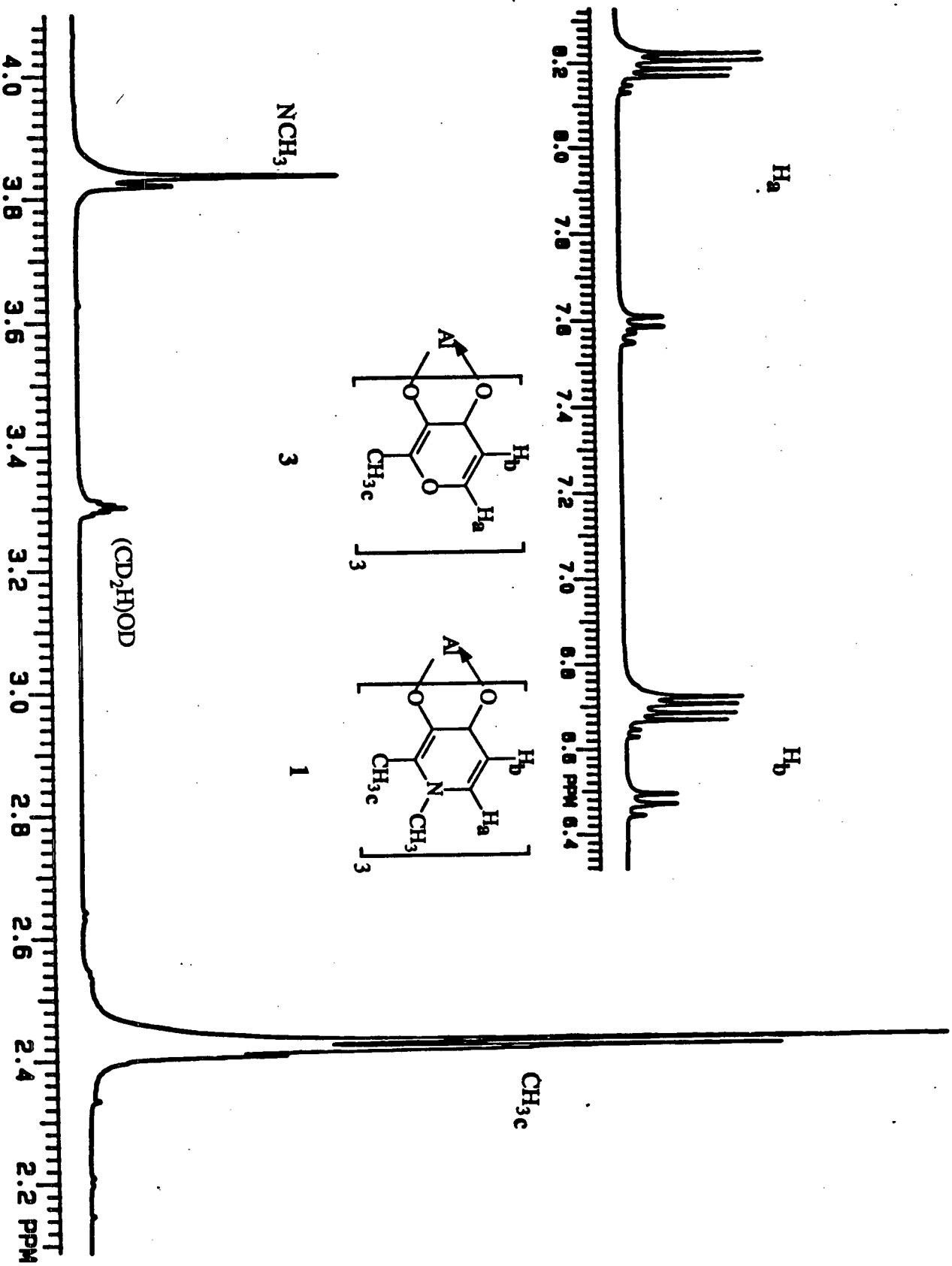

Figure 4.16. Proton NMR spectrum of 3:1 $Al(ma)_3$ to $Al(dpp)_3$ in CD_3OD at 18 °C.

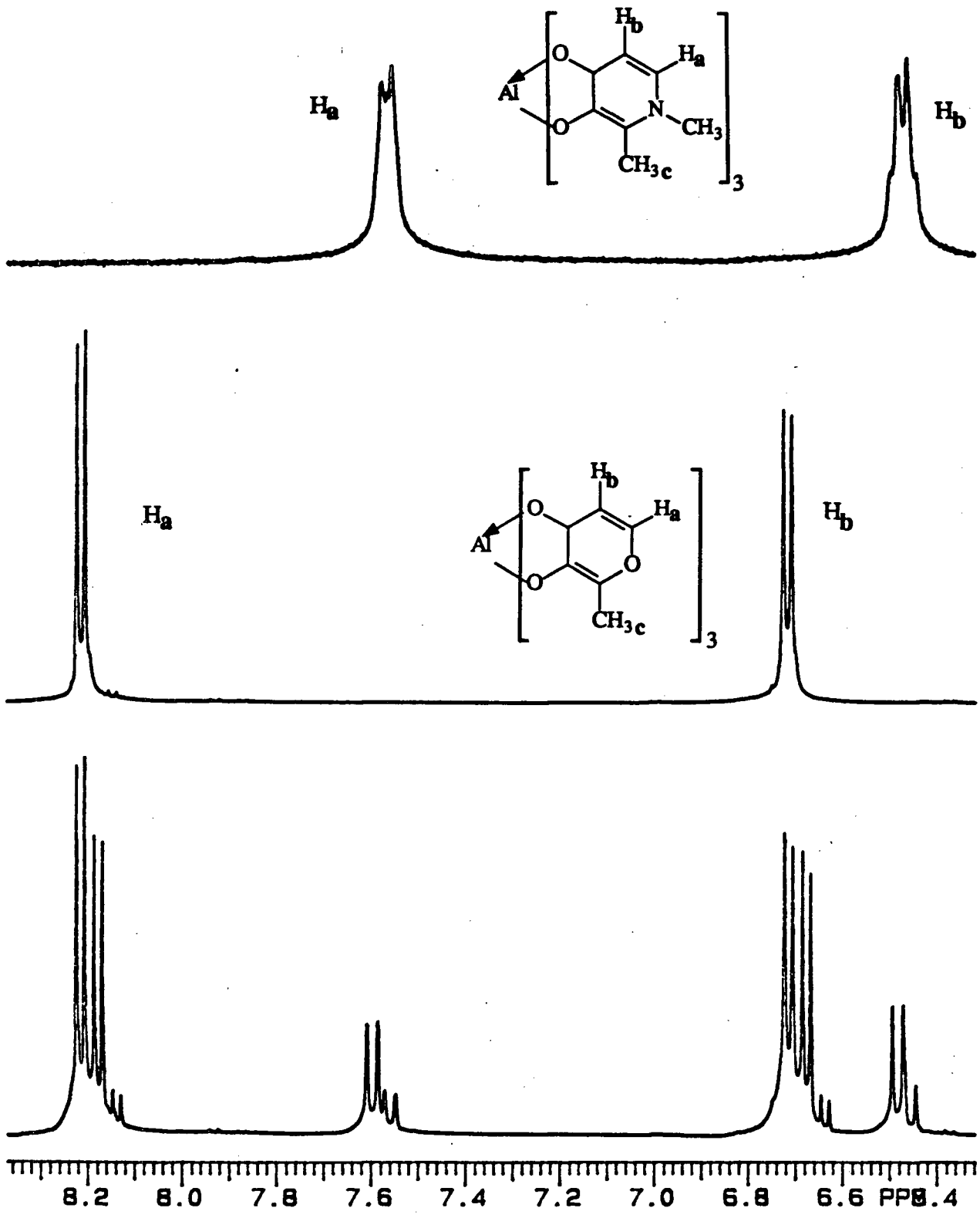

Figure 4.17. Proton NMR spectra of H_a and H_b in $Al(dpp)_3$ (top), $Al(ma)_3$ (middle) and the 3:1 $Al(ma)_3$ to $Al(dpp)_3$ mixture (bottom). All spectra in CD_3OD at 18 °C.

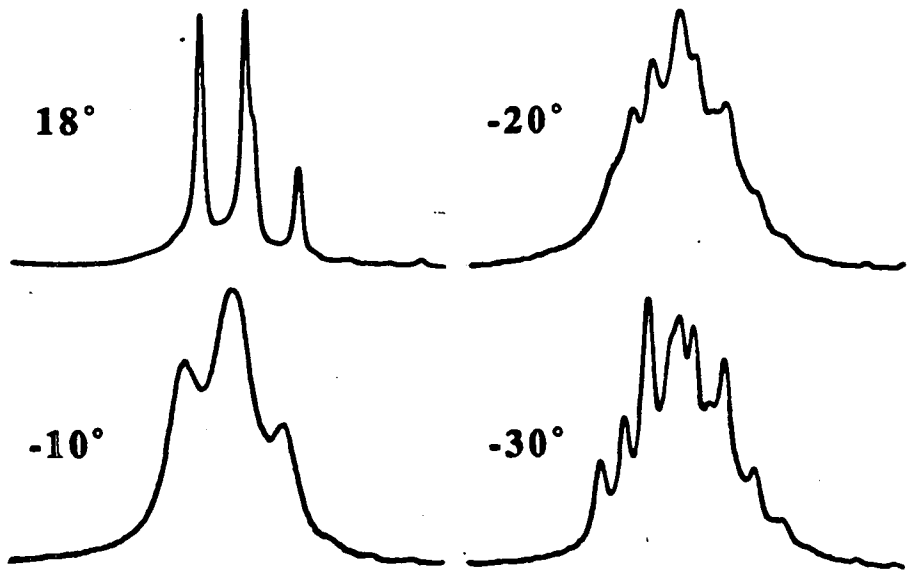

Figure 4.18. Variable-temperature proton NMR spectra of H_b in the dpp$^-$ ligand on the mixed-ligand species (in CD_3OD and temperatures are °C).

The ligand exchange experiment indicates the rearrangement reaction for $Al(dpp)_3$ in CD_3OD is an intermolecular process. The racemization of $Ni(phenanthroline)_3^{2+}$ in water proceeds through a dissociative mechanism and the similarity of the activation energies for the process in methanol (and a number of other solvents) is used to support the proposition that the same mechanism is occurring in all of the solvents studied.[158] By analogy, the similarity of $\Delta G^{\ddagger}_{Tc}$ in D_2O and $(CD_3)_2SO$ to the value in CD_3OD suggests there is an intermolecular exchange occurring in all of these solvents.

It can be concluded on the basis of the variable-temperature NMR experiments that *fac-mer* isomerization is the reason for the fluxional NMR spectra of the tris(3-hydroxy-4-pyridinonato) Al and Ga complexes . It appears the exchange process is intermolecular and, therefore, the isomerization mechanism likely involves ligand dissociation. In addition, the solubility properties of these Al and Ga complexes make it very unlikely that the mechanistic details of their ligand rearrangement processes could be determined.

Chapter V Solution Studies

A. Aqueous Solubility

5.1 Introduction

During the synthesis of the ligands and the tris-ligand metal complexes, their interesting and at times unexpected aqueous solubilities were duly noted. This led to solid state studies on single crystals of several compounds grown from, and in the case of the metal complexes grown with, water. The crystal packing arrangements were dictated by H-bonding and we wanted to discover if this form of molecular association also affected the solution behavior of these compounds. The accurate measurement of aqueous solubility was one method used to establish the correlation between the solid state and solution properties. Accurate knowledge of the aqueous solubility was also of practical value as regards synthetic and biological applications.

The unusual aqueous solubility properties of nitrogen heterocycles were noted as early as 1899 when it was found that the insertion of hydroxyl groups progressively decreased the water solubility of purine. This unexpected result was also observed for π-deficient N-heterocycles as exemplified by 4-hydroxy-2-pyridinone which is 160 times less water soluble than either 2- or 4-pyridinone. To explain this, Albert suggested that intermolecular H-bonding from the ring nitrogen to the exocyclic oxygen atom was preferred over H-bonding to water molecules.[104] The reduced aqueous solubility of the 3-hydroxy-4-pyridinones can be attributed to strong intermolecular H-bonds, but with the exception of Hmpp, the ring nitrogen was not directly involved. In comparison to the free

ligands, the interesting feature of the metal-ligand complexes was that their solubilities were governed by solvent rather than intermolecular H-bonding and still the result was a lowered aqueous solubility.

The solubility was determined at 25 °C and in an attempt to gauge the relative strength of the H-bonds, the change in solubility upon heating to 37 °C was also measured for several compounds. In keeping with our interest in biological applicability, the measurements were done in isotonic pH 7.4 buffer. The 3-hydroxy-4-pyridinones have a $\pi \rightarrow \pi^*$ transition (~280 nm) and the solute concentrations were measured by monitoring this band. Since it was employed primarily as an analytical technique (it was also used in the determination of the *n*-octanol/water partition coefficients), ultraviolet (UV) spectroscopy was included in this chapter rather than with the other spectroscopic techniques in Chapter II.

5.2 Materials and Methods

Water was deionized with Barnstead D8902 and D8904 cartridges and distilled in a Corning MP-1 Megapure still. Trizma-7.4 HCl (tris(hydroxymethyl)aminomethane) is available from Sigma. The isotonic buffer solution was 0.15 M NaCl and 0.05 M Trizma which gives pH 7.42 (±0.05) at 25°C. Solution temperatures (±0.1°C) were maintained with water-jacketed beakers and a Julabo circulating waterbath. Samples were centrifuged at 3300 rpm in a Centrific Centrifuge model 228. All aliquots were withdrawn with Eppendorf digital pipettes, either 10-100 μL or 100-1000 μL (1-1.5% error). The electronic spectra were measured from 370 to 210 nm with a Perkin Elmer Coleman 124 UV-Vis spectrophotometer (1 cm cell). Trizma absorbs in the UV near the 210 nm instrument cut-off point so it was necessary to use buffer as the reference solution.

L-Mimosine was recrystallized from water; the other ligands and metal complexes were prepared and purified as previously described in Chapter II. All samples were rigorously dried prior to weighing.

5.2.1 Procedure for the Determination of Molar Absorptivity (ε)

By comparison to other 3-hydroxy-4-pyridinones,[161] a reasonable estimate of ε for the free ligands was 12,000 L $mol^{-1}cm^{-1}$ for the selected band (λ_{max}). Based on this, 1 mM stock solutions (in 100 mL volumetric flasks) were made from accurately weighed compound. Five 10 mL standard solutions were made (5 to 80 μM for the free ligands, 3 to 40 μM for the metal complexes) that covered an absorbance range of 0.070 to 1.200. Plots of concentration (c) versus absorbance (A) were made and all the compounds obeyed Beer's Law ($A = \varepsilon bc$ with $b = 1$ cm) over these concentration ranges. Each plot had at least five points and in some cases a second set of measurements was made and all the points were included in the graph. The values of ε were calculated by linear regression analysis (correlation coefficients ≥ 0.999). The ε values in Tables 5.1 and 5.2 have an estimated error of ± 500 L $mol^{-1}cm^{-1}$; this is consistent with the propagation of dilution and instrument errors and is ≤ the standard deviations (σ) calculated from several of the Beer's Law plots. The instrument error in λ_{max} is ± 1 nm.

5.2.2 Procedure for the Determination of Aqueous Solubility at 25 and 37 °C

Suspensions of each compound in buffer were placed in the 25 °C waterbath, stirred for 30 minutes, and equilibrated for an additional hour to allow the finely suspended

solids to settle. Aliquots were withdrawn from the saturated solutions, filtered through glass wool into centrifuge tubes, and centrifuged for five minutes. This step was necessary because of the large dilutions required to obtain concentrations suitable for spectroscopy; any solids in the final aliquot were redissolved upon dilution and resulted in errors in the calculated solubility. Accurate aliquots were withdrawn from the centrifuged samples and diluted with buffer to the concentrations necessary to give absorbances between 0.500 and 1.500 (the dilution factors ranged from 10 for $Ga(mhpp)_3$ to 16,667 for Hmepp). Four measurements were made for each solution and the average absorbance (A_{25}) and the previously determined ε values were used to calculate the concentrations.

Propagation of the weighing, dilution, and instrument errors would allow the reporting of concentrations to three significant figures. The additional systematic errors inherent in solubility studies (such as the effects of small amounts of impurities) and in this procedure (such as the lack of temperature control once the samples were removed from the waterbath) limited our confidence so the concentrations were reported with two significant figures. In Tables 5.3 and 5.4, the concentrations have an estimated error of ±5 in the second digit. The concentrations of $M(mpp)_3$, $M(dpp)_3$, and $M(mepp)_3$ were measured on three separate occasions and the reported values for σ (r=3) supported this estimated error.

For the absorbance measurements at 37 °C, the suspensions were equilibrated at the higher temperature for 30 minutes and treated as above. The absorbances (A_{37}) were corrected for changes in the dilution factor and the percent change on heating was calculated as $\left(\frac{A_{37}}{A_{25}} - 1\right) \times 100$.

5.3 Results and Discussion

5.3.1 Ultraviolet Spectroscopy

The ultraviolet spectra of pyridine and its derivatives are similar to that of benzene; they have an E (ethylinic) and a B (benzenoid) band above 210 nm that originate from $\pi \rightarrow \pi^*$ transitions.[162] Due to the lone pair of electrons on the nitrogen, there is a weak $n \rightarrow \pi^*$ transition (R-band) that is generally only observable in the vapor phase. The B-band in pyridine is at 257 nm (in water with $\varepsilon = 2750$ L mol^{-1}cm^{-1}); conjugated and/or electron-donating substituents cause this band to shift to lower energy.[162,163] OH and CH_3 groups cause bathochromic shifts of 18 and 5 nm respectively.[104] In good agreement with this, the B-band in the N-substituted ligands is at 280 ± 2 nm and is at a slightly shorter wavelength in Hmpp (Table 5.1). Compared to their respective ligands, the B-band in the metal-ligand complexes show a small bathochromic shift (9-16 nm) and the Ga complexes are consistently at the longest wavelength (Table 5.2).

Table 5.1. λ_{max} (nm) and ε x 10^{-3} (L mol^{-1}cm^{-1}) for the B-band in the free ligands.

	Hmpp	Hdpp	Hmepp	Hmhpp	Mimosine	H_2exn
λ_{max}	273	278	279	279	282	278
ε	12.4	13.6	14.2	12.4	15.0	26.1

Table 5.2. λ_{max} (nm) and ε x 10^{-3} (L $mol^{-1}cm^{-1}$) for the B-band in the metal-ligand complexes.

	$M(mpp)_3$		$M(dpp)_3$		$M(mepp)_3$		$M(mhpp)_3$		$M(mimo)_3$	
	Al	Ga	Al	Ga	Al	Ga	Al	Ga	Al	Ga
λ	285	286	290	291	292	293	293	294	291	294
ε	26.4	27.1	28.4	29.4	30.7	30.8	28.8	30.0	30.2	30.5

For pyridine derivatives, the intensity of the B-band can be greatly enhanced by auxochromic substituents (saturated groups with nonbonded electrons).[163] This enhancement accounts for the large increase in the ε between the 3-hydroxy-4-pyridinones and pyridine. Increasing solvent polarity also has a marked hyperchromic effect on the B-band attributable to solvent H-bonding with the nitrogen lone pair of electrons and this increase in intensity is at a maximum for pyridinium salts.[162] The smaller ε values for Hmpp and the $M(mpp)_3$ complexes may be due to a decreased electron density on the ring nitrogen when compared to the N-substituted compounds. This could result in somewhat weaker solvent H-bonds and, therefore, a reduced hyperchromic effect. The differences are small (from 1200 to 4300 L $mol^{-1}cm^{1}$) but consistent; the one exception is Hmhpp and it is possible that the hydrophobic N-hexyl group could disrupt the H-bonding sufficiently to account for the lower ε of this ligand.

5.3.2 Aqueous Solubility at 25 and 37 °C

At 25 °C, Hmpp is less than half as water soluble as Hdpp (Table 5.3). The replacement of a hydrophilic amino with a hydrophobic methyl group increases water solubility and intermolecular H-bonding is the likely explanation for this unusual behavior. The evidence from IR spectroscopy and the crystal structure indicated that the O-H···O hydrogen bonds in Hmpp were weaker than in Hdpp so the decrease in water solubility must be due to the N-H···O=C hydrogen bonds. The strength of the Hmpp H-bonds in solution was shown by the proton NMR experiment in which the intermolecular interactions persisted in $(CD_3)_2SO$, a good H-bond acceptor solvent.

It is interesting to compare these compounds to 4-pyridinone and 4-hydroxy-2-pyridinone whose water solubility (at 20 °C) is 105 and 0.65 mM respectively.[104] Despite the presence of two methyl groups, Hdpp has a solubility comparable to 4-pyridinone. This could be due to the relative position of the H-bonding sites and, therefore, the extent of the H-bonded network. When the H-bond sites are ortho, as in Hdpp, it is possible to form dimeric units. When they are para, as in 4-pyridinone, the most likely interaction would be the formation of H-bonded chains that could reduce the relative water solubility. The addition of a second H-bond donor in 4-hydroxy-2-pyridinone presents the possibility of a three-dimensional H-bonded structure, and as with Hmpp, the result is a further reduction in water solubility.

The situation is not so straightforward when Hmepp is compared to Hdpp; the substitution of an ethyl for a methyl group increases the water solubility almost sixfold. The increased volume of the unit cell and the appreciably lower melting point for Hmepp compared to that of Hdpp led us to expect the water solubility to be greater, but the magnitude of the difference is surprising. The compounds both form dimeric units and on

the basis of IR stretching frequencies, the H-bonds are of similar strength. The large increase in solubility must be due to a weaker crystal lattice in Hmepp; although intermolecular H-bonds are important, they are by no means the only factor in determining aqueous solubility.

Table 5.3. Water solubility (mM) at 25 °C.

	Hmpp	Hdpp	Hmepp	Hmhpp	Mimosine	H_2exn
Solubility	38	95	570	5.6	19	0.56

Hmhpp is minimally water soluble and, unlike the other 3-hydroxy-4-pyridinones studied, Hmhpp is soluble in a number of aprotic solvents (including diethyl ether, CH_2Cl_2, and acetonitrile). It is apparent that the N-hexyl group, and not the potential for H-bonding, is the deciding factor in the solubility properties of Hmhpp. The results for H_2exn indicate why this compound was difficult to characterize and support the conclusion that the lower water solubility is due to H-bonded polymerization. The low water solubility of L-mimosine, a compound with four H-bonding sites, strongly suggests that intermolecular H-bonding is forming a crystal lattice capable of resisting solvation by water molecules (or by any other solvents short of dilute acids and bases).

The increased size of the tris-ligand metal complexes should result in a decrease in water solubility compared to that of the free ligand. However, the water solubility of the free ligands is strongly influenced by their ability to form intermolecular H-bonds via the α-hydroxy ketone moiety and formation of the metal complexes removes this H-bonding site. It is possible that diminished intermolecular association could offset the increase in

size and result in greater not lesser aqueous solubility for the metal complexes. This appears to be the case with mimosine as $Al(mimo)_3$ is five times as soluble as the free ligand (Table 5.4). The substituent zwitterion becomes the dominant factor in determining the water solubility and, given the acidity of the ammonio proton (pKa of 7 in the free ligand[97]), one would predict appreciable water solubility. $Ga(mimo)_3$ is approximately one-half as soluble as its Al analogue and the other ligands show a similar contrast between their Al and Ga complexes. The reduction in solubility is consistent with the larger size of the metal center, but the magnitude of the difference is not easily rationalized considering that in no instance does the metal account for more than 16% of the mass of the tris-ligand metal complex.

Table 5.4. Water solubility (mM) at 25 °C and % change $\left(\frac{[\text{metal complex}]}{[\text{ligand}]} \times 100\right)$

	$M(mpp)_3$		$M(dpp)_3$		$M(mepp)_3$		$M(mhpp)_3$		$M(mimo)_3$	
	Al	Ga	Al	Ga	Al	Ga	Al	Ga	Al	Ga
Sol.	16(1)	7.5(5)	1.2(1)	0.70(2)	19(1)	11(1)	0.69	0.20	95	55
%	42	20	1.2	0.74	3.3	1.9	12	3.6	500	289

The $M(mimo)_3$ complexes are the exception rather than the rule and the rest of the tris-ligand metal complexes have a much lower water solubility than that of the free ligand. The $M(dpp)_3$ complexes have the maximum change as the solubility of $Ga(dpp)_3$ is < 1% that of Hdpp (see bottom row in Table 5.4). The decrease is not as large in the $M(mpp)_3$ complexes (e.g., 42% for $Al(mpp)_3$); this is probably due to the lower solubility of the free ligand and the availability of the NH group for solvent H-bonding in the metal-ligand complexes. That the $M(mhpp)_3$ complexes are less soluble than Hmhpp is not surprising

since there are three lipophilic hexyl groups per molecule instead of one. The large decrease in solubility for the $M(dpp)_3$ complexes results in solubilities on the order of those for the hydrophobic $M(mhpp)_3$ complexes and this is rather surprising. The solid state packing arrangement presents a possible explanation for the low water solubility of the $M(dpp)_3$ complexes.

Solid water consists of hexagonal water rings interconnected in a honeycomb arrangement to give a rigid quasi-infinite network (refer to Fig. 3.9). On melting, some of the H-bonds are disrupted and the network of water molecules becomes irregular and less open than in the ice structure. It is generally accepted that there would still be an infinite network linking together many finite discrete networks of varying sizes but the exact structure of the finite units is still very much open to debate.[164] In the solid state, the $M(dpp)_3$ complexes are able to fit into and in a sense hold together separate water structures. A similar situation could be occurring in aqueous solution; rather than being pulled apart by the solvent molecules, the metal-ligand complexes could be incorporated into the disordered fabric of liquid water to form insoluble polymers of the inorganic complexes and the water columns.

The $M(dpp)_3$ and $M(mepp)_3$ complexes have the same solid state packing arrangement and both show similar large decreases in water solubility when compared to the free ligands. But the $M(mepp)_3$ complexes are ca.16 times as soluble as the $M(dpp)_3$ complexes and they are even more water soluble than the $M(mpp)_3$ complexes despite the obvious difference in hydrophilicity between the N-ethyl and N-H groups. Hmepp is substantially more water soluble than Hdpp for reasons that are not readily apparent and the $M(mepp)_3$ complexes could be forming water polymers that are simply more soluble than their $M(dpp)_3$ analogues.

The difference between the $M(dpp)_3$ and $M(mepp)_3$ complexes is further shown by the change in absorbance found on heating to 37 °C. The experiment was motivated by the large aqueous solubility temperature coefficient that was observed in the synthesis of the $M(dpp)_3$ complexes and was exploited in crystal growing to make the supersaturated solutions from which the single crystals were obtained. Neither the $M(mpp)_3$ nor the $M(mepp)_3$ complexes appear to exhibit this property and the results of the quantitative study confirm the experimental observations. On heating to 37 °C, the absorbance of the $M(dpp)_3$ solutions increases by nearly 200% while the $M(mpp)_3$ and $M(mepp)_3$ solutions show no significant change (A_{37} is within ± 10% of A_{25}). (For perspective, the absorbance of all the free ligands increased by ca. 30%.) This simple experiment serves to illustrate the unique aqueous solution behavior of the $M(dpp)_3$ complexes.

The 3-hydroxy-4-pyridinone ligands synthesized in this study varied comparatively little in size or electronic configuration yet they exhibited a considerable range of water solubilities. The order of water solubility expected for the free ligands was Hmhpp < Hmepp < Hdpp < Hmpp and the order found was Hmhpp < Hmpp < Hdpp << Hmepp. This illustrates the interesting, albeit somewhat unexpected, results that can be obtained by simple N-alkyl substitution. The determination of the aqueous solubilities also made it possible to correlate the spectroscopic and crystallographic studies directly to a property of concern to our goal of developing biologically relevant ligands.

B. Octanol/Water Partition Coefficients

5.4 Introduction

The distribution of a solute between two immiscible phases in which it is soluble has long been a subject of investigation. The early workers established that the concentrations of the solute in the two phases was constant and independent of the relative solution volumes.[165] While the physical chemists strove to develop a theoretical description of the partition phenomena, applications for this physicochemical property developed from the discovery (near the turn of the century) that the relative narcotic activities of drugs was often directly related to their oil/water partition coefficient.[166] In the late 1960's, Hansch and co-workers proposed that the *n*-octanol/water system was a good model for the lipoidal biophase in living organisms and, therefore, could be useful in studying the distribution of solutes between blood and lipid in living organisms.[167] In pharmacological research, the *n*-octanol/water partition coefficient (P)* has been accepted as the operational definition of lipophilicity and is now widely employed in the design and development of new bioactive compounds.

The measurement of log P for the Ga and In complexes was useful in establishing their potential as radiopharmaceutical imaging agents (In has two suitable radioisotopes). The increasing interest in Al chelators for the treatment of various neurological disorders

---

* This may be represented as $K_{octanol/water\ (ow)}$, P_{ow} or D_{ow}. Log P is used in the computational methods for the estimation of P and in the numerous quantitative structure-activity relationship (QSAR) studies involving this property; therefore, log P is the most frequently (but by no means exclusivley) encountered symbol for this property.

linked to aluminum[15,168] made it worthwhile to determine the log P values for the free ligands and the tris-ligand Al complexes. A log P of 2 has been proposed as ideal for the design of barbituates, but the complexity of brain uptake makes it impossible to set a lower log P limit in neurological drug design.[27] Levin reported a structure-activity relationship between the permeability of the blood-brain barrier, and the log P and molecular weight of a substance.[26] He found that drugs with log P values as low as -3.0 could penetrate the brain in detectable amounts. The following table is intended merely to give an idea of the range in lipophilicity found for small molecules that readily enter the brain.

Table 5.5. The log P values of some common drugs.[27]

ethanol	- 0.31	morphine	0.07
nicotine	0.45	cocaine	1.05
caffeine	0.08	phenobarbital	1.42
codeine	0.23	amphetamine	- 0.84

The log P can be measured by shaking a solute with the immiscible solvents and measuring the solute concentration in one or both of the phases. Conceptually simple, the consensus opinion is that the classic "shake-flask" method is experimentally difficult and very time consuming.[169,170] The difficulties in measuring the partition coefficient have at times caused wide variations in the reported log P values; in a recent study, an author went so far as to eliminate from consideration all log P values that were in conflict with those reported by Hansch and his co-workers.[171] (This reflects both the high regard that is afforded Hansch and the difficulties of measuring P.) This has led to the development of numerous alternative methods for determining log P values.[170,172,173] The most widely used alternative is reverse phase high performance liquid chromatography (HPLC) with

methanol-water as the eluent.[170,174] The HPLC retention times are converted to log P by means of a standard set of solutes for which the shake-flask log P values have been measured; however, this method has been criticized as being unreliable, especially for hydrophobic compounds that require high proportions of methanol (> 50%) in the eluent.[169]

The log P is an additive-constitutive property of a substance and as such it can be estimated using a substituent constant, π, defined in an analogous manner to the Hammet σ constant.[165] A manual algorithm was developed that has since given way to a computerized method of estimating log P: for a homologous series, the log P values are measured for the compounds with key structural features capable of mutual interaction and then estimated for the other members of the series. The computations are non-trivial (and expensive) and the estimated log P values are often quite different from the experimentally derived results. Despite the problems in its execution, the shake-flask method is considered the most accurate and reliable method for measuring log P values.[169]

5.5 Materials and Methods

Reagent grade *n*-octanol was distilled and the first and last quarters were discarded. The pH 7.4 isotonic buffer was prepared as described in Section 4.2. The two solvents were mutually saturated by stirring a 1:1 mixture overnight and the saturated solvents were used for all measurements. The ligands and metal-ligand complexes were purified by recrystallization or sublimation. The solute concentration in the aqueous phase was determined by monitoring the absorbance of the B-band; the spectra were recorded on the UV spectrophotometer used for the aqueous solubility study. Trial solutions made with

n-octanol saturated buffer indicated the small amount of *n*-octanol was not affecting the position or intensity of the B-band. The reference solution was *n*-octanol saturated buffer that had been centrifuged for the same length of time as the sample solutions. This was necessary because *n*-octanol absorbs near 210 nm and a small difference in its concentration between the reference and sample solutions was found to cause serious baseline drift.

The initial absorbance was kept between 0.5 and 1.0 which required concentrations of ~30 μM for the metal complexes and ~60 μM for the free ligands. 1 mM stock solutions were diluted (using graduated cylinders) to make 25 mL solutions at the desired initial concentrations. A 10 mL aliquot was withdrawn and placed in a 15 mL centrifuge tube labelled as the initial solution. Two 6 mL aliquots were withdrawn and placed in centrifuge tubes labelled as extraction tubes. 6 mL of *n*-octanol was added to the extraction tubes and they were inverted 100 times (>2 minutes contact time). After >15 minutes equilibration, the tubes were centrifuged until the two layers were visibly clear (typically at least 15 minutes). The *n*-octanol layer was removed with a pasteur pipette, and the aqueous layer was used to rinse the cuvettes and to make one absorbance reading per tube. The initial solution was also centrifuged and two absorbance readings were made. This was repeated three times per compound thus producing six measurements of the initial absorbance and six of the post-extraction value. The values of P were calculated from the absorbance of the aqueous phase as follows[175] and the mean log P ($r \geq 6$) and σ were reported.

$$\frac{\text{(initial absorbance)-(post-extraction absorbance)}}{\text{post-extraction absorbance}} \times \frac{\text{volume of buffer}}{\text{volume of } n\text{-octanol}}$$

From 0 to 25 °C, the log P can vary from 0.005 to 0.01 log units/degree;[165] this is within the error for the shake-flask method and no attempt was made to control the

partitioning temperature. Ideally, samples of both phases should be analyzed to check for material balance as a guard against unforeseen losses. This requires an analytical procedure for both phases which further increases the time required for the measurements. It has been shown that if care is taken to ensure that no special solute interactions are occurring, reliable results can be obtained by analyzing only one phase.[176]

5.6 Results and Discussion

Once we decided on using the shake-flask method, it remained to choose an analytical technique. One option was flame atomic absorption spectroscopy (FAAS) and this technique has been used to determine the log P for a variety of Hg complexes.[177] The viscosity of *n*-octanol did present problems for sample aspiration, but a procedure was developed and several Al and Ga complexes were studied (analyses done by T. Karpishin). The compound that was used to verify our FAAS procedure was $Al(ma)_3$. Shake-flask extraction with UV spectroscopy as the analytical technique gave a log P of -0.17 for 57 μM $Al(ma)_3$[37] (this value was reproduced by our collaborators at another laboratory[178]). Using the FAAS procedure, the $Al(ma)_3$ log P was -1.22 ± 0.10 for a 2.5 mM solute concentration and a similar large deviation from the value determined with UV spectroscopy was seen for $Ga(ma)_3$. The log P was also found to be concentration dependent as the $Al(ma)_3$ log P values ranged from -1.70 at 15 mM to -1.10 at 1.5 mM.

The partitioning should be done at the lowest solute concentrations possible since P is concentration dependent and only theoretically valid at infinite dilution; however, concentrations of 10^{-1} M are considered sufficiently dilute for neutral molecules that have little tendency to associate in solution.[176] The $Al(ma)_3$ log P is not constant at mM

concentrations and this suggests intermolecular association. The fact that the log P is an order of magnitude higher at 57 μM than at 2.5 mM certainly supports this conclusion. To avoid errors from solute association, the partition concentrations can be decreased until no further change in log P is found.[176] This is not possible with FAAS because of the detection limits for Al and Ga (the bottom end of the working range is 1.5 and 0.72 mM, respectively[179]).

We experimented with FAAS because of problems with the procedure we used to measure the log P values of tris(3-hydroxy-4-pyronato) Al and Ga complexes (analyses done by T.Lutz).[37] This procedure was prone to give large fluctuations in log P values and changing the analytical technique offered a possible improvement. FAAS did solve the problem of precision, but the large discrepancy from the "true" log P for $Al(ma)_3$ made the accuracy of the results suspect. The experiments with FAAS did alert us to the potential complication that intermolecular association presented. The large molar absorptivities of the 3-hydroxy-4-pyridinones made UV spectroscopy the analytical technique of choice for this study.(μM detection limits).

The problems with our first procedure for determining log P were not rectified by changing the analytical technique so adjustments were made to the extraction steps and the revised procedure is reported herein. $Ga(ma)_3$ was used to test the revised procedure and the log P (in brackets in Table 5.6) was in agreement with our previously published value. The error of ±0.03 log units was calculated on the basis of two separate experiments (r=12) and it was the same as the error considered acceptable for the shake-flask method.[176] The lower limit that can be measured with acceptable precision by this procedure is a log p of -1.75. For log P values lower than this, the difference between the initial and post-extraction absorbances (initial absorbance of 1 and 1:1 extraction) is ≤ three times the instrument error (± 0.005 absorbance units).

The accepted way to extend the log P range is to increase the ratio of *n*-octanol to buffer, thereby increasing the difference between the two absorbance readings (this also decreases the error in log P). However, extractions at these ratios formed emulsions that were very difficult to remove and the failure to get completely clear solutions is known to produce large errors in log P values.[176] We found that letting the solutions stand for > 24 hours did not remove the emulsions and even centrifuging for several hours did not always give clear solutions. Based on the log P values of the 3-hydroxy-4-pyrone metal complexes (Table 5.6), the lower limit on log P imposed by 1:1 extractions was acceptable as it was thought the 3-hydroxy-4-pyridinone metal complexes would have log P values within an order of magnitude of these results. We also felt that a log P of -1.75 made a reasonable cut-off point as compounds with values below this are quite hydrophilic and this would significantly limit their ability to cross cell membranes.

The log P values for a number of In complexes were determined using the revised procedure.[112] When the results for the In complexes of maltol and kojic acid are included with the log P values determined previously for the Al and Ga analogues (Table 5.6), a reasonable pattern emerges (for the structures of the 3-hydroxy-4-pyrones see Fig.2.2). With its additional hydroxyl group, kojic acid is considerably more hydrophilic than maltol. For both ligands, the metal complexes have smaller log P values than the free ligands, and the relative order of the lipophilicity of the metal-ligand complexes is the same; i.e. In > Al > Ga. The results for the tris-ligand metal complexes with pyromeconic acid and cholorokojic acid (5-hydroxy-2-(chloromethyl)-4-pyrone) were predictable: removing the ring methyl group from maltol (to give pyromeconic acid) produced a decrease in lipophilicity and replacing the methyl OH group in kojic acid with a Cl atom (to give chlorokojic acid) produced an increase in lipophilicity.

Table 5.6. Log P values for the 3-hydroxy-4-pyrone complexes (σ values are in parenthesis).

	Free Ligand[a]	ML_3 Al	ML_3 Ga	ML_3 In
Maltol	0.090	- 0.17	- 0.29 [- 0.22 (3)]	- 0.009 (8)
Pyromeconic acid		- 1.12	--	- 0.62 (6)
Kojic acid	- 0.64	- 1.06	- 1.10	- 0.82 (6)
Chlorokojic acid		--	--	- 0.31 (4)

[a] These values are from ref. 180 and were determined by the shake-flask method.

The log P values for the 3-hydroxy-4-pyrones are presented as an example of a well behaved metal-ligand system. The log P values are reasonable for metal complexes and changes in structure produce predictable changes in the log P. By comparison, the 3-hydroxy-4-pyridinones could be called a "truculent" metal-ligand system based on their log P values (Table 5.7). With the exception of Al- and Ga(mhpp)$_3$, the metal complexes have much lower than expected log P values. Instead of being similar to the values of the 3-hydroxy-4-pyrone metal complexes, they are at or near the lower log P limit for the shake-flask procedure employed in this study. Professor Hansch graciously agreed to measure the log P of a Ga(dpp)$_3$ sample and the result reported to us (italicized entry in Table 5.7) is in agreement with the value that was determined in our laboratory . The error in log P (±0.10 log units) is significantly larger than the ± 0.02 log units typical for what Hansch referred to as "well behaved compounds."[181] The tris(3-hydroxy-4-pyridinonato) metal complexes have log P values that are lower and more difficult to measure than was predicted on the basis of the results for the 3-hydroxy-4-pyrone system.

Table 5.7. Log P values for the 3-hydroxy-4-pyridinone complexes.

	Free Ligand	ML_3 Al	Ga	In
Hmpp	- 0.52 (8)	< - 1.75	- 1.51 (6)	< - 1.75
Hdpp	- 0.74 (8)	< - 1.75	- 1.55 (20) *-1.59 (10)*	< - 1.75
Hmepp	- 0.37 (3)	- 1.68 (6)	- 1.64 (20)	--
Hmhpp	0.95 (10)	1.32 (20)	1.38 (12)	--

It is possible that the interaction of water molecules with the tris(3-hydroxy-4-pyridinonato) metal complexes is affecting the partitioning process. The partitioning in this laboratory was done at 30 μM solute concentrations, and Hansch used $Ga(dpp)_3$ concentrations from 27 to 3 μM without observing any concentration dependence. This indicates that intermolecular association is not responsible for the low log P values. The solid state and the water solubility studies demonstrated the strength of the interaction between water molecules and the metal complexes. If the metal-ligand complexes are associating with liquid water in a fashion comparable to the $M(dpp)_3$ and $M(mepp)_3$ solid state structures, the reduced log P values would be reasonable as the most lipophilic portion of the complex would be shielded from the *n*-octanol molecules (see Chapter III). It is difficult to account for the effects of solvent-solute association on partitioning,[165] but water association comparable to that found in the solid state structures could explain both the lower water solubility and the lower log P values of these metal-ligand complexes.

The free ligands were certainly better behaved than the metal complexes, but the order of lipophilicity was unexpected; instead of Hmpp < Hdpp < Hmepp < Hmhpp as predicted on the basis of the N-substituents, Hmpp was more lipophilic than Hdpp. If one

equates lipophilicity to a lower water solubility, Hmpp was significantly more lipophilic than Hdpp and this was thought to be the result of intermolecular H-bonding (see Table 5.3). The log P of Hmpp was measured at 52 μM and H-bonded dimerization is not considered to be a significant factor in log P measurements at concentrations below the mM level.[165] Also, if there is intermolecular association , the log P should be smaller not larger than expected. Once again the physical properties of the homologous series of ligands did not follow the predicted order.

The $M(mhpp)_3$ complexes have log P values larger than that of Hmhpp; obviously the lipophilicity imparted by three hexyl groups dominates the partitioning process just as it governed the aqueous solubility. The $M(mpp)_3$, $M(dpp)_3$, and $M(mepp)_3$ complexes have smaller log P values than their respective ligands and this indicates they would have potential as therapeutic chelating agents. The ideal chelating agent would be a ligand that is lipophilic enough to be distributed to the sites of metal accumulation and that forms metal-ligand complexes more hydrophilic than the free ligand.[168] This would diminish redistribution of the metal to other tissues and would expedite the elimination of the metal from the body. Taking the removal of Al from the brain as a hypothetical clinical situation, the ligands--Hmpp, Hdpp, and Hmepp--are small enough and are sufficiently lipophilic to cross the blood-brain barrier (based on Levin's structure-activity relationship[26]). The tris-ligand Al complexes are at least an order of magnitude more hydrophilic than the free ligands and this fits the above criteria for a therapeutic chelating agent.

C. Potentiometric Equilibrium Measurements

5.7 Introduction

In the reaction of a trivalent metal with a bidentate ligand, a series of equilibria are established involving the metal, the ligand, and metal-ligand complexes. These equilibria are illustrated in Figure 5.1 along with the definitions of the stepwise (K_n) and overall (β_n) formation constants. The generalized formula for the overall formation constants is $\beta_n = \frac{[ML_n]}{[M]\,[L]^n}$.

$M + L \overset{K_1}{\rightleftharpoons} ML$	$K_1 = \frac{[ML]}{[M]\,[L]}$	$\beta_1 = K_1$
$ML + L \overset{K_2}{\rightleftharpoons} ML_2$	$K_2 = \frac{[ML_2]}{[ML]\,[L]}$	$\beta_2 = K_1K_2$
$ML_2 + L \overset{K_3}{\rightleftharpoons} ML_3$	$K_3 = \frac{[ML_3]}{[ML_2]\,[L]}$	$\beta_3 = K_1K_2K_3$

Figure 5.1. Equilibrium equations and constants for the reaction of a trivalent metal with bidentate ligands.

The above equations describe the equilibria for Al and Ga in aqueous solution (neglecting mixed hydroxo complexes). For the 3-hydroxy-4-pyridinone ligands, L is the conjugate base formed by the dissociation of the hydroxyl proton, and the neutral ML_3 complex was predicted to be the dominant metal-ligand species at physiological pH. Variable-pH ^{27}Al NMR experiments provided a qualitative picture of the pH-dependent

speciation of the Al complexes that clearly supported this prediction. To obtain a quantitative evaluation of the Al speciation, and to confirm our assumption of an analogous speciation for the Ga complexes, potentiometric titrations were performed to determine the formation constants.

The preparation and standardization for all the solutions and the potentiometric titration procedure are included in the Appendix as Procedure A.1. This procedure was developed by Dr. David Clevette of this laboratory and it has been reported previously.[182] The computational methods used to calculate the formation constants were developed elsewhere and are referenced as such in the procedure. The data for Hmpp, Hdpp, Hmepp, and Hmhpp (Table 5.8) were reported to the author by Dr. Clevette.

5.8 Results and Discussion

The 3-hydroxy-4-pyridinone ligands form Al and Ga complexes of great stability (Table 5.8); the overall stability constants β_3 are all > 10^{30} at 25 °C and an ionic strength of 0.15 M NaCl (isotonic). In the equilibrium calculations a hydrolysis model consisting of the species $[M(OH)_n]^{(3-n)+}$ (n = 1, 2, 3, 4) with formation constants according to ref. 25 was applied. The polynuclear species $[Al_2(OH)_2]^{4+}$ and $[Al_3(OH)_4]^{5+}$ were also included in the calculations. In conjunction with the studies in this laboratory, Professor Staffan Sjöberg examined the equilibrium reactions of Al with Hdpp and Hmpp. He found that effects due to possible mixed Al^{3+}- OH^- - L^- species were negligible at total ligand to aluminum ratios of 1, 2, 3, and 5;[183] therefore, a total ligand to metal ratio of just greater than three was used in all the potentiometric titrations performed in our laboratory.

Table 5.8. Log protonation constants (K) and log β_n for the equilibrium reactions of Al, Ga, and In with the 3-hydroxy-4-pyridinone ligands synthesized in this study (25 °C, 0.15 M NaCl).

Constant	Metal	Hmpp	Hdpp	Hmepp	Hmhpp[b]
log K_1		9.80 (1)	9.86 (3)	9.81 (2)	9.92 (2)
log K_2		3.65 (1)	3.70 (1)	3.64 (2)	3.59 (1)
log β_1	Al	11.87 (3)	11.91 (2)	11.75 (4)	11.51 (1)
	Ga	13.34 (3)	13.17 (15)	13.15 (9)	--
	[a]In	13.51 (1)	13.60 (2)	13.53 (1)	
log β_2	Al	22.54 (3)	22.83 (2)	22.52 (5)	22.49 (1)
	Ga	24.41 (1)	25.16 (15)	24.98 (11)	--
	[a]In	23.70 (1)	23.93 (3)	23.78 (1)	
log β_3	Al	32.05 (3)	32.25 (5)	32.17 (6)	31.71 (3)
	Ga	32.85 (6)	34.32 (14)	33.88 (13)	--
	[a]In	32.76 (2)	32.93 (3)	32.80 (1)	

[a] The In values were included in reference to Figure 5.7.

[b] Data for the Ga and In complexes were not available due to their low water solubility.

The affinity of the hydroxide ion for Al and Ga has been alluded to at several points in this thesis and one of the primary objectives of this research project was the synthesis of ligands that would prevent the formation of metal hydroxides at neutral pH. The competition between the ligands and the hydroxide ion can be represented graphically by using the data in Table 5.8 to produce plots of metal speciation as a function of solution pH. Since the variation in log β_n values among the four ligands is minor, the Al-Hdpp speciation diagrams are representative of the ligands studied. In Figure 5.2, the speciation diagram for 3 mM Hdpp (top figure) shows no hydrolysis at neutral pH and $[Al(OH)_4]^-$ does not occur in significant amounts (> 1% of the total Al) below pH 8.5. Even with a thousand-fold dilution in ligand concentration (bottom figure), the metal-ligand species still predominate from pH 4 to 8 and 60% of the initial Al is in $Al(dpp)_3$ at physiological pH. The qualitative observations of an absence of hydrolysis products in the synthesis of the tris(3-hydroxy-4-pyridinonato) Al complexes are verified by these quantitative results.

The pH 4 to 9 window of hydrolytic stability for the tris-ligand Al complexes that was determined by the variable-pH ^{27}Al NMR study (see Section 4.3) is confirmed by the potentiometric titration data. Using the same concentrations of Al and Hdpp as in the NMR experiment ([Al] = 35 mM and 3:1 Al to Hdpp) it is possible to "simulate" the ^{27}Al NMR spectral results in a qualitative fashion. In Figure 5.3, several spectra from the variable-pH ^{27}Al NMR study are shown next to bar graphs of the equilibrium speciation profile calculated at the same pH. The agreement between the two methods is very good and this comparison also serves as a verification of the assignment of the upfield ^{27}Al NMR signals to the mono- and bisligand Al species.

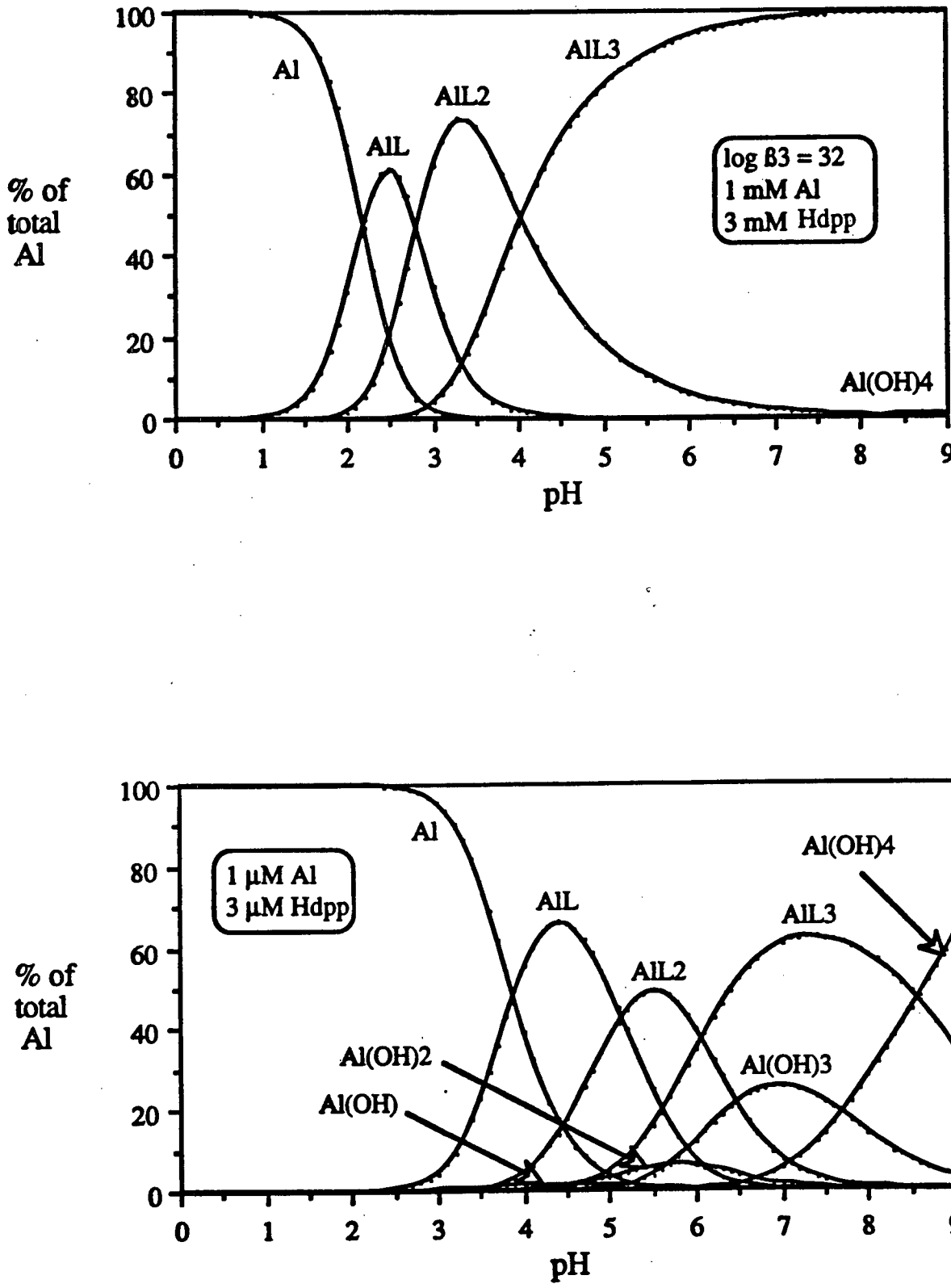

Figure 5.2. Speciation diagrams for 3:1 Hdpp to Al at 3 mM (top) and 3 µM (bottom) ligand concentrations (25 °C, 0.15 M NaCl).

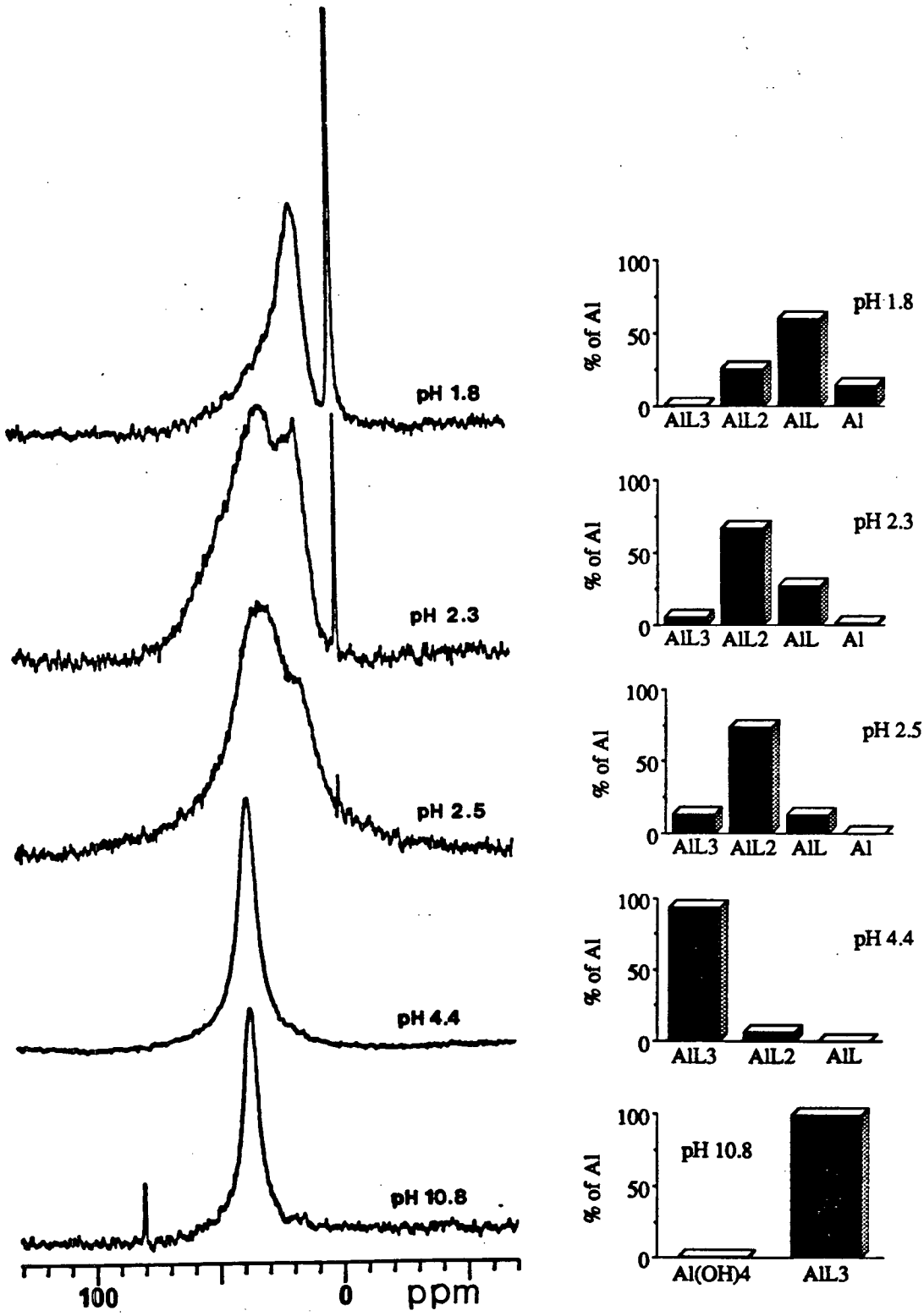

Figure 5.3. Left: variable-pH ^{27}Al NMR spectra for 0.035 M $Al(dpp)_3$. Chemical shifts (ppm) are: $[Al(OH)_4]^-$ (80), $[Al(dpp)_3]$ (38), $[Al(dpp)_2(H_2O)_2]^+$ (26), $[Al(dpp)(H_2O)_4]^{2+}$ (14), and $[Al(H_2O)_6]^{3+}$ (0).
Right: Al speciation profiles calculated for 0.035 M Al using data at 25 °C and 0.15 M NaCl (L = dpp).

It was not possible to perform variable-pH ^{71}Ga NMR experiments because of the low sensitivity of this quadrupolar nucleus and the low solubilities of the Ga complexes. Their hydrolytic stability could be inferred from the similarity of their synthesis, characterization, and physical studies data to that of the corresponding Al complexes. The determination of the formation constants establishes that the Ga-ligand complexes exhibit the same resistance to hydrolysis as their Al analogues and this is readily apparent from the speciation diagram for 3 mM Hdpp and 1 mM Ga (Fig. 5.4). The greater stability of the Ga-hydroxides and the larger log β_n values of the Ga-Hdpp complexes results in a slight shift in the region of hydrolytic stability towards lower pH. A comparison of the Al and Ga speciation diagrams shows that the cross-over point at which the $[M(H_2O)_6]^{3+}$ species is reduced to 50% of the total metal concentration is shifted from a pH of 2.2 to a pH of 1.4 and the $[M(OH)_4]^-$ species appears at a lower pH and in greater concentration in the Ga diagram.

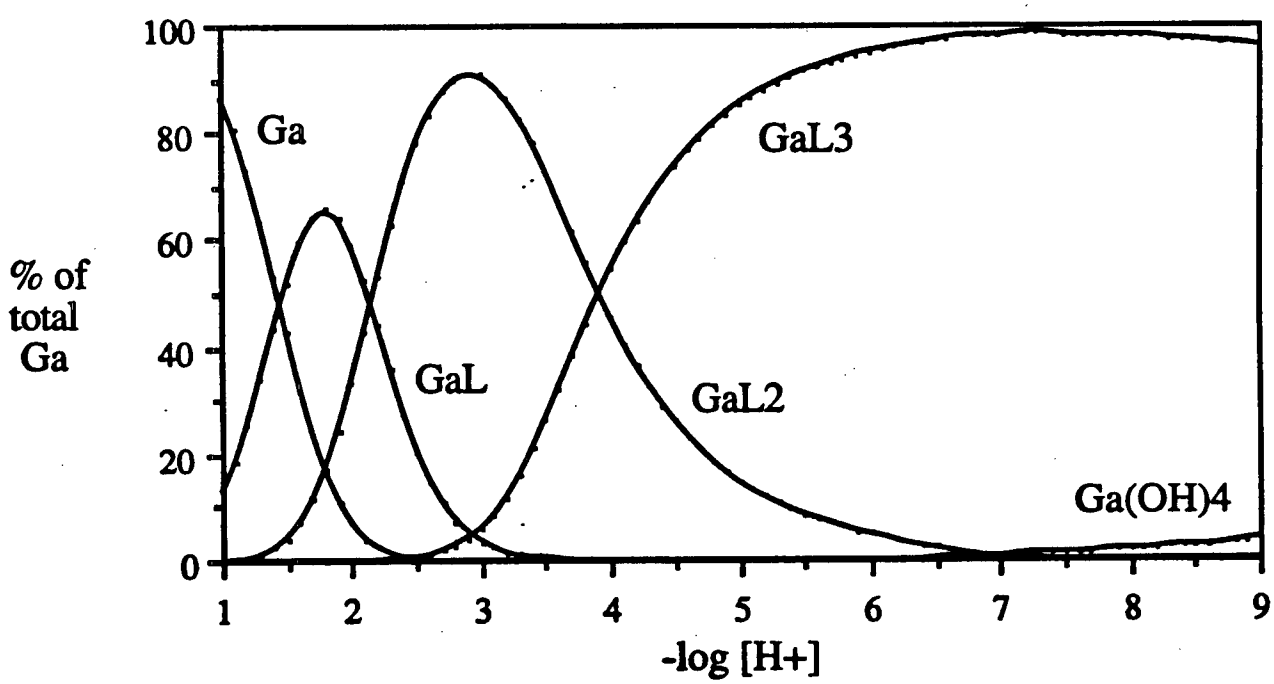

Figure 5.4. Speciation diagram for 3 mM Hdpp and 1 mM Ga at 25 °C and 0.15 M NaCl.

The 3-hydroxy-4-pyridinone ligands and their precursor maltol are amphoteric (Figure 5.5). The two stepwise protonation constants for the ligands (K_1 and K_2) are given in Table 5.8. At the conception of this research project, it was thought that the N-alkyl groups would enhance the ability of the ring nitrogen to stabilize a positive charge. This should have resulted in more ring double bond delocalization and larger K_2 values by increasing the stability of the pyridinium resonance hybrid and the pyridinium cation. The data from the solid state studies (refer to Section 3.2) and these protonation constants both show that this anticipated effect of N-alkylation did not occur. The log β_3 values for the metal complexes also indicate the metal binding efficacy of the 3-hydroxy-4-pyridinone ligands was not significantly affected by N-alkylation.

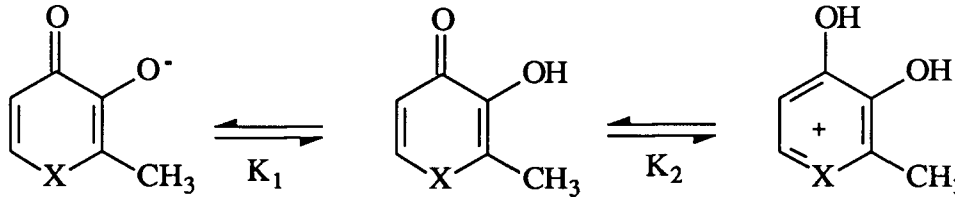

Figure 5.5. Protonation equations for 4-pyridinone ligands (X = N–R) and maltol (X = O)

Hmpp is the 4-pyridinone ligand closest in structure to maltol and comparison of the protonation constants shows that the 4-pyrones are stronger acids. (The data for maltol[59] were collected in 0.6 M NaCl; because the magnitude of the formation constants is dependent on ionic strength, the following values for Hmpp[183] are also at 0.6 M NaCl and are slightly different from the values at 0.15 M NaCl reported in Table 5.8.) Maltol has a hydroxyl log K_1 of 8.38 while that for Hmpp is 9.58. In both heterocyclic rings there is an

additional protonation constant with a log K_2 of -0.71 in maltol (μ = 0.5)[58] and 3.74 in Hmpp. The 4.5 log unit difference in K_2 is an effect of the ring nitrogen atom, which is better able to delocalize a positive charge than a ring oxygen. This would stabilize the dihydroxypyridinium cation in acidic solution and increase K_2 for Hmpp. The difference in K_1 is due to the greater ability of the ring oxygen to delocalize the negative charge of the deprotonated hydroxyl oxygen. This would stabilize the conjugate base and decrease K_1 for maltol. The net effect is an increase in the basicity of the chelating oxygen atoms in the 3-hydroxy-4-pyridinone ligands. This results in a large enhancement of the formation constant for the metal-ligand complexes: log β_3 for $Al(ma)_3$ is 22.48 compared to a value of 30.41 for $Al(mpp)_3$.

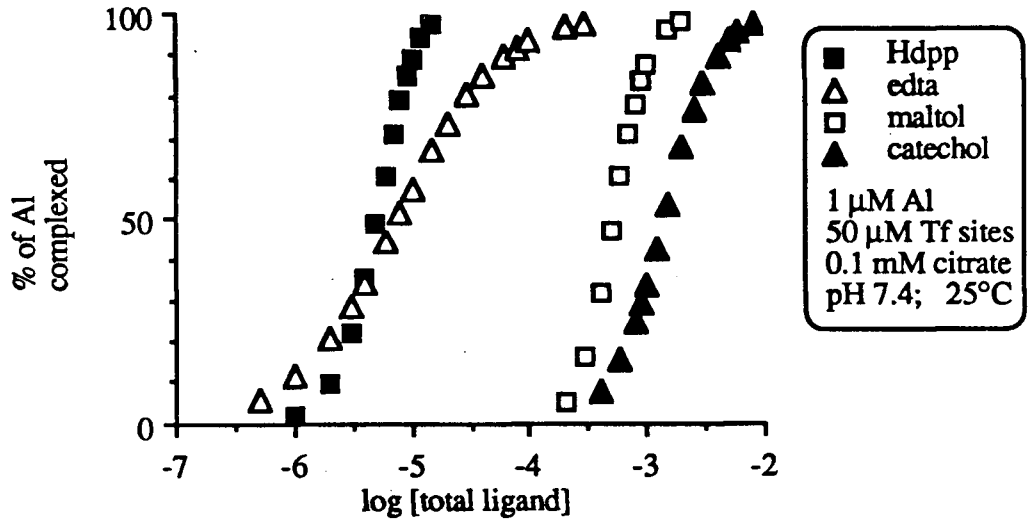

Figure 5.6. Plot of Al^{3+} complexation (%) vs. log of total ligand concentration (conditions and ligands are indicated in the legend).

Figure 5.6 is a plot that compares the metal binding affinities of several ligands regardless of denticities. Using formation constants taken from the literature for Al complexes with citrate[184] (100 μM) and transferrin[29] (50 μM vacant sites), a simple model of the metal binding capacity of human blood can be made (pH 7.4, 25 °C, 0.15 M NaCl).

For 1 μM Al, the plot shows that Hdpp is more efficient (lower ligand concentration required) at complexing 100% of the Al than is EDTA[185] (which is hexadentate and tetraprotic), pyrocatechol[186] (bidentate and diprotic), and maltol[59] (bidentate and monoprotic). It must be emphasized that this model is limited in an absolute sense, but it is valid in a comparative sense and it certainly illustrates the enhanced metal binding capacity of the 3-hydroxy-4-pyridinone ligands.

The solid state structures of Al-, Ga-, and $In(dpp)_3$ showed little variation in bonding parameters, although the M-O bond lengths did indicate the bonds were somewhat weaker in $Al(dpp)_3$ (see Section 3.4.1). However, the Ga and In complexes have significantly larger log β_n values than the Al analogues and this is illustrated by a plot of the log β_3 values for Hdpp, Hmpp, and Hmhpp (Figure 5.7). This graph shows that the order of stability for the tris-ligand metal complexes is the same as the order of the first dissociation constants for the hexxaquo ions; i.e., Ga > In > Al (see Section 2.5). Using the pK_a of the 3-hydroxyl proton (log K_1) as a measure of basicity, a plot of pK_a vs. ligand (Figure 5.8) correlates exactly with the relative stabilities of the metal complexes. Hdpp is the strongest base and it forms the most stable metal complexes. Taken together, these two graphs nicely illustrate that this ligand-metal system does comply to the HSAB principle paraphrased as: "the harder acid prefers the harder base."

The formation constants for the metal-ligand complexes show that the 3-hydroxy-4-pyridinones are very good bidentate chelators for the group 13 metals. These quantitative results are in complete agreement with our experimental observations and they also verify the hydrolytic stability of the tris-ligand complexes as established by ^{27}Al NMR. The predictive capability that these data affords is particularly useful in the context of our stated goal of using in vitro techniques to assess the suitability of a ligand for in vivo studies.

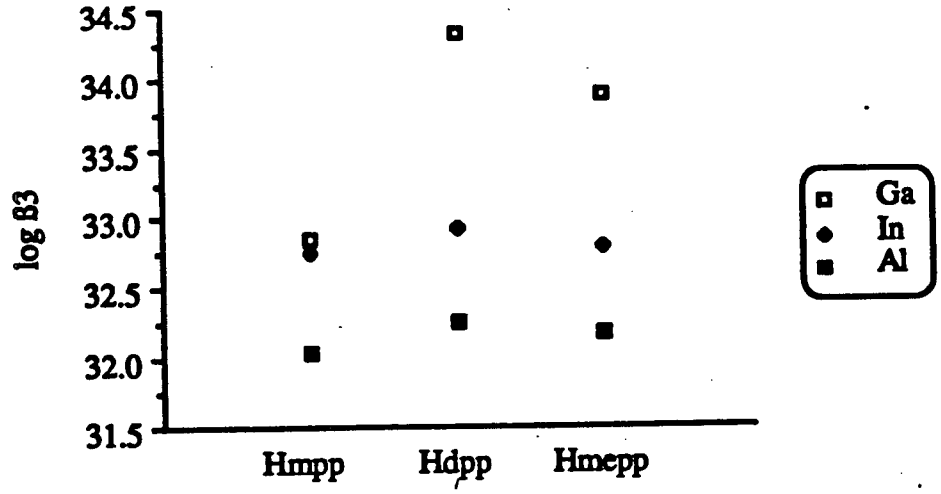

Figure 5.7. Plot of log β_3 for the Ga, In, and Al complexes (as indicated in the legend) vs. ligand.

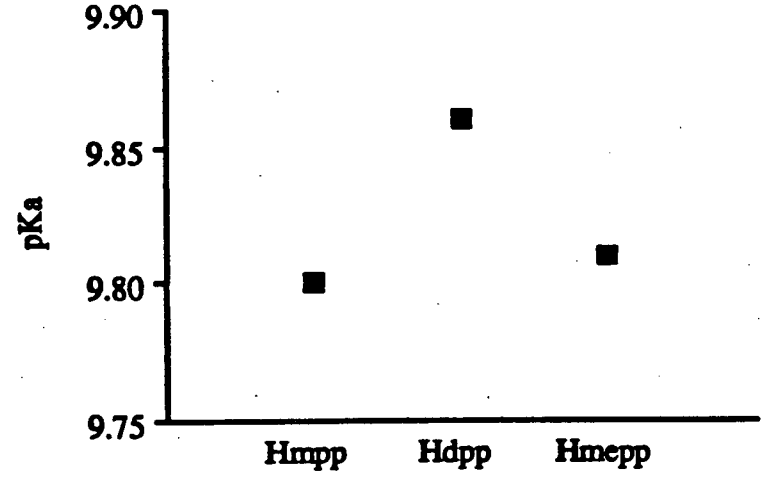

Figure 5.8. Plot of pKa of the hydroxyl proton vs. ligand (25 °C, 0.15 M NaCl).

Chapter VI Gallium-67 Biodistribution Study

6.1 Introduction

Our goal of developing radiopharmaceutical imaging agents and our interest in aluminum, which has no suitable isotopes for radiolabelling studies, explain why ^{67}Ga is the radionuclide that was chosen for these imaging experiments. The favorable nuclear decay properties and the relative paucity of work with this radionuclide (see Chapter I) were also factors that prompted our interest in ^{67}Ga. Despite the differences in electronic configuration and ionic radius, the aqueous coordination chemistry of Al and Ga is very similar. They are only found in the +3 oxidation state in water and their aqueous chemistry is dominated by their shared property of strong Lewis acidity. These ^{67}Ga biodistribution experiments with the 3-hydroxy-4-pyridinones can be considered first order approximations of the biological fate of the Al analogues. The similarity of in vitro aqueous behavior makes ^{67}Ga the best model available for Al.

The ligands--Hmpp, Hdpp, Hmhpp, and L-mimosine--form tris-ligand Ga complexes that are sufficiently water soluble for a biodistribution study; the solubilities range from 0.74 mM for $Ga(dpp)_3$ to 55 mM for the mimosine complex. $Ga(mhpp)_3$ has a log P of 1.4 and the other complexes have log P values near -1.6. None of these complexes has the the same combination of these properties seen in Ga-maltol (water solubility of 31 mM and log P of -0.22), but they do provide a range of lipophilicity that could result in variations in the biodistribution of ^{67}Ga. The formation constants for the Ga-ligand complexes are large enough to ensure hydrolytic stability in vivo.

Once the ligands and tris-ligand Ga complexes were completely characterized, a preliminary screening experiment with ^{67}Ga was performed to determine if the 3-hydroxy-4-pyridinones showed promise as imaging agents. It was at this point that the developmental work with maltol ceased as the image obtained for ^{67}Ga-maltol was identical to that of ^{67}Ga-citrate, that is to say, the same as ^{67}Ga-transferrin.[187] However, the results with Hdpp indicated that this ligand was affecting the ^{67}Ga biodistribution. Based on this screening and the in vitro studies, a biodistribution study using Hdpp, Hmpp, Hmhpp, and L-mimosine was initiated. This study is still in progress; therefore, only a brief description of the methodology and a summary of results to date will be presented herein. This work was done in collaboration with Dr. Donald Lyster and a complete report of the results is forthcoming.[188]

6.2 Materials and Methods

The biodistribution study was done in the Radiopharmacy at Vancouver General Hospital. The animal work-up and the data analysis were performed by Dr. D. Lyster, T. Rihela, and G. Webb. The ligands were synthesized and purified in our laboratory. Solutions at the proper concentrations were prepared in isotonic Trizma pH 7.4 buffer and delivered to the Radiopharmacy for radiolabelling and animal injection. The ^{67}Ga-citrate starting material was available by purchase.

For the preliminary screening experiment, anesthetized rabbits were injected with 0.43 mM Hdpp solution containing 0.5 mCi of ^{67}Ga-citrate (33 nM) and the imaging was done with a Siemans Large Field of View Gamma Camera. For a control, the same dosage

of ^{67}Ga-citrate without Hdpp was injected in a second rabbit and the images were compared at various time intervals over a period of hours.

The biodistribution experiments were performed in BALB/c mice which were sacrificed at varying time intervals up to 2 days post-injection. The percent injected dose per organ (i.d./organ) values were obtained for blood, liver, spleen, stomach, kidneys, lungs, heart, and brain. The organs were placed in vials and the radiation was measured in a well gamma counter. In all the experiments, the ligand to Ga molar ratio was kept constant (~10^4 to 1) and each mouse was given a 0.1 mL injection containing 1 μCi of ^{67}Ga. For example, the injection concentrations were 3.4 μM Hdpp and 0.25 nM ^{67}Ga. The study was then repeated using the same amount of ^{67}Ga and concentrated (near saturation) ligand solutions. Again using Hdpp as the example, the injection concentrations were 80 mM Hdpp and 0.25 nM ^{67}Ga for a molar ratio of 10^8 to 1. The injection concentrations of the other ligands were 1, 20, and 40 mM for Hmhpp, L-mimosine, and Hmpp respectively. As a control in both the dilute and concentrated ligand studies, ^{67}Ga-citrate solutions without added ligands were also administered to a separate test population.

6.3 Results and Discussion

The ^{67}Ga biodistribution experiments with dilute ligand solutions were done to assess the potential of these ligands as ^{67}Ga imaging agents. The injection concentration of ^{67}Ga necessary to produce the optimal radiation is on the nM level; therefore, formation of the tris-ligand ^{67}Ga complex is ensured by using μM ligand solutions. To assess the

efficacy of an imaging agent, it is desirable to keep the ligand concentration at a minimum because of the influence that a large excess of ligand can have on the biodistribution.

Metal ions are thought to cross membranes by one of two generalized processes: active transport requiring energy dependent ion pumps or passive transport; i.e., adsorption onto the cell membrane followed by diffusion into the cell.[189] The latter process may be facilitated by ligands that could aid the transport of the hydrophilic metal ion across the hydrophobic membrane. This can be envisaged as passage from the aqueous medium to the interior of the cell along a ligand cascade of increasing binding strength.[190] Therefore, the abundance and strength of extracellular metal-ligand binding affects metal uptake which is clearly demonstrated by the effect organic ligands can have on metal toxicity.[189] The objective of cellular accumulation could be adversely affected by a large excess of the imaging agent itself. This was of particular importance with these ligands since, with the exception of Hmhpp, the tris-ligand Ga complexes were significantly less lipophilic than was considered ideal. The preliminary screening had indicated that the ligands were affecting the ^{67}Ga biodistribution with μM ligand injection concentrations. To minimize potential interference with cellular uptake, the same ligand to metal ratio was maintained in the dilute ligand experiments.

The assessment of these ligands as chelating agents was done with concentrated ligand solutions. The objective of a chelating agent is the removal of a metal from the body and high concentrations of ligand in the blood can only facilitate this goal. In long term experiments, high levels can be maintained by repeatedly administering the ligand. We were conducting experiments of a shorter duration and were interested in determining if injection of saturated ligand solutions would be sufficient to produce a change in biodistribution. If this were to occur, it would be good evidence of the potential of these ligands as chelating agents.

The preliminary results of this study can be summarized be examining the uptake of ^{67}Ga (as percent of total ^{67}Ga) in the liver at 24 hours post-injection. The bar graph (Fig. 6.1) contains the data for the four ligands, both the dilute and concentrated experiments, and for the ^{67}Ga-citrate control. The liver is the principle organ where transferrin accumulates; therefore, any alteration from the biodistribution of ^{67}Ga-transferrin can be most readily observed in this organ. The uptake of ^{67}Ga-citrate (taken to be that of Ga-transferrin) is shown in the last column. It is obvious that these 3-hydroxy-4-pyridinones significantly reduce the uptake of ^{67}Ga in both the dilute and concentrated ligand experiments. This confirms in vivo what the in vitro experiments had shown--the 3-hydroxy-4-pyridinones are very good bidentate chelators of Ga..

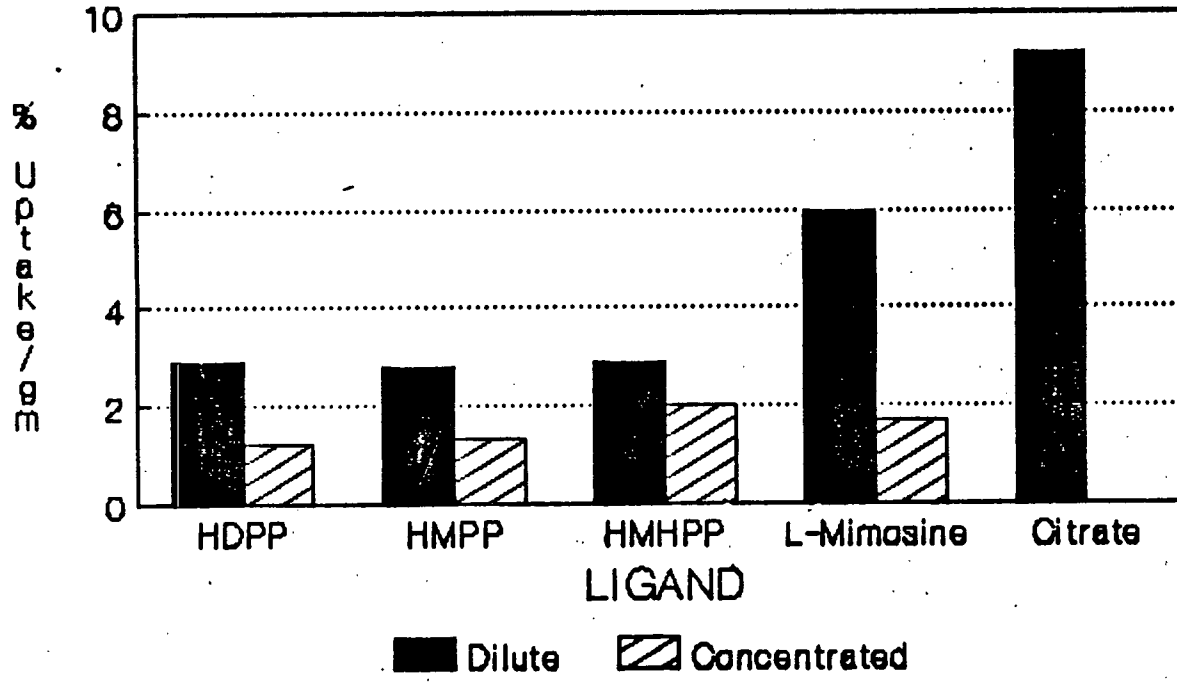

Figure 6.1. Liver biodistribution plotted as ^{67}Ga uptake vs. ligand for the dilute and concentrated ligand experiments.

These results indicate that these 3-hydroxy-4-pyridiones will not be useful as imaging agents; although they redirect ^{67}Ga from transferrin at concentrations that would

be viable for further development, they are not localizing the radionuclide in any particular organ. The ^{67}Ga uptake in the other organs examined is similar to that of the liver, and the levels of ^{67}Ga are uniformly reduced from that of ^{67}Ga-citrate. It appears that the ligands enhance the removal of the metal from the body, presumably via the urine; but this cannot be definitely proven until this study is completed. It was thought that the lipophilic Hmhpp complexes might have a different biodistribution. This did not occur, although it is possible that ^{67}Ga-Hmhpp may be removed through the hepatobiliary tract. This also has yet to be determined. We intend to exploit the ability of this class of ligands to redirect ^{67}Ga from transferrin. This will be done by synthesizing additional 3-hydroxy-4-pyridinone ligands with other substituents that could alter their biodistribution.

The further decrease in ^{67}Ga uptake seen for the concentrated ligand experiments is especially encouraging when viewed in concert with the positive results from the extensive studies of Hdpp as an iron chelating agent.[39] The fact that the two trivalent metal ions closest in size to Al can both be mobilized by Hdpp definitely indicates the potential of the 3-hydroxy-4-pyridinones as Al chelators. The results are even more impressive when the differences in transferrin binding constants are considered since the affinity of transferrin for Al is ca. eight and ten orders of magnitude less than for Ga and Fe, respectively.

This in vivo study also allows us to assess the relative merits of the methodology that we have been employing in our laboratory. The log P values for these ligands were significantly lower than ideal and this is undoubtedly a factor in the rapid elimination of the metal-ligand complexes from the body. Knowledge of the difference in log P values between the ligand and the metal complexes is very useful since the biodistribution results further indicate their potential as chelating agents. The aqueous solubility data were used in the design of this biodistribution experiment and this simple determination merits inclusion in future studies.

The formation constants can be employed in a manner complementary to experiments such as these biodistribution studies. Figure 6.2 is a plot that accounts for the dilution of the ligand and the ^{67}Ga in the circulatory system. It indicates what ligand injection concentration (in this case, Hdpp) is necessary to compete effectively with transferrin, using the transferrin binding constants and concentrations of human blood serum. This graph demonstrates both the utility of this model and the difficulties encountered in applying any simple model to the complex interactions in vivo. The model predicts that 80 mM Hdpp used in the concentrated ligand experiment is sufficient to complex almost all of the ^{67}Ga and this is supported by the results of the liver uptake of ^{67}Ga. The model also predicts that μM Hdpp should not alter the biodistribution, but the animal study indicates some redirection from transferrin. It is necessary to improve the model by including other factors such as Fe concentrations and concentrations of metal binding proteins such as albumin. This is not an easy task but the predictive capacity shown by the simple model definitely indicates this is a goal worth pursuing.

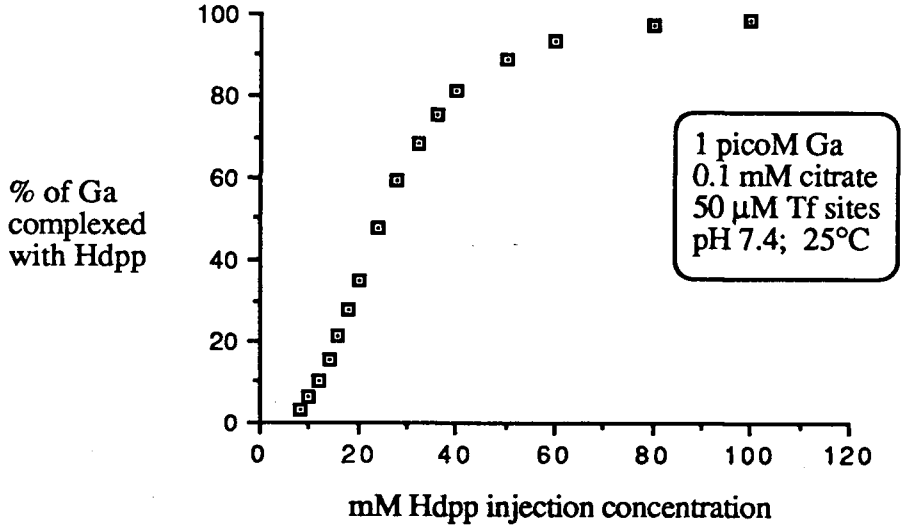

Figure 6.2. Graph of %Ga complexed as a function of Hdpp injection concentration (conditions as indicated in legend).

Chapter VII Conclusion and Suggestions for Future Work

The primary objective of our research is the investigation of the aqueous coordination chemistry of Al and Ga. We are also interested in biological applications of this chemistry with the dual goals of developing ^{67}Ga radiopharmaceuticals and using ^{67}Ga as a model for the biodistribution of Al. The preceding chapter addresses the biological aspects of our work and it serves as both the conclusion for that part of our research and as an indicator of the direction our future research in that area will take.

The core of my research was the synthesis and characterization of several 3-hydroxy-4-pyridinone ligands and their Al and Ga complexes. The ligand synthesis initially involved the use of a benzyl blocking group, but because of the length of the procedure, a preparation was developed using buffered solutions to control the ionic state of the starting materials, maltol and the primary amines. The buffered preparations pointed us towards the next logical step in this synthesis and this work is now being carried out in our laboratory. The formation of $Al(ma)_3$ enhances the reactivity of the complexed maltol ligands to nucleophilic attack. The electropositive metal acts to remove electron density from the 4-pyrone ring and it is well established that electron-withdrawing groups facilitate the conversion of 4-pyrones to 4-pyridinones. By the reaction of $Al(ma)_3$ with an excess of methylamine, $Al(dpp)_3$ can be produced almost quantitatively. This metal template reaction is now being used in the synthesis of other 3-hydroxy-4-pyridinone ligands.

We attempted the synthesis of multidentate ligands and the bispyridinone H_2exn was the initial product of this work. However the solubility properties of this compound restricted its use as a ligand. Multidentate ligands with the α-hydroxyketone moiety could

be made by joining two 4-pyridinone rings via an amide linkage and this should afford increased aqueous solubility. 3-Hydroxy-2-methyl-1-(β-ethylamino)-4-pyridinone, formed by the conversion of maltol with ethylenediamine, was prepared and isolated in our laboratory. Using a dicarboxylic acid (such as butanedioic or pentanedioic acids), it would be possible to link two of these ligands together via their N-ethylamine substituents. The coupling agent dicyclohexylcarbodiimide (DCC) could be used to form the peptide bonds and the length of the bridge between the rings could easily be varied as aliphatic dicarboxylic acids and DCC are readily available commercially.

One of the most interesting aspects of our work was the unusual solid state structures that were determined for the $M(dpp)_3 \cdot 12H_20$ complexes. Because of the extensive water network in these structures, attempts were made to grow crystals from water of the other metal complexes. This culminated in the determination of the $M(mepp)_3 \cdot 12H_20$ structures. The stability of the water network was somewhat unexpected and a close analysis of the structures suggests that a slightly larger N-alkyl group would disrupt its formation. The synthesis of 3-hydroxy-2-methyl-1-propyl-4-pyridinone is now being carried out; if the metal complexes of this ligand are sufficiently water soluble, attempts will be made to grow crystals to determine whether the water networks can still be formed with this larger N-substituent. Also, variable temperature potentiometric titrations will be performed to establish the enthalpic and entropic contributions of this water network to the overall thermodynamic stability of the $M(dpp)_3$ complexes.

The variable-temperature NMR experiments with Al- and $Ga(dpp)_3$ established that these metal complexes undergo *fac-mer* isomerization. Ligand exchange experiments with $Al(dpp)_3$ and $Al(ma)_3$ indicated that the ligand rearrangement process likely involved a dissociative mechanism. Further ligand exchange studies are planned to determine the lability of several of the tris-ligand metal complexes in aqueous solution. If the exchange

rates permit NMR detection, the ligand exchange between the tris(3-hydroxy-4-pyridinato) Al complexes and Al-transferrin is the ultimate goal of this research.

The affinity of the 3-hydroxy-4-pyridinone ligands for Al and Ga made the synthesis of the metal complexes relatively straightforward. The stability of the metal complexes is due to the basicity of both the oxygen atoms of the bidentate ligand. The ring nitrogen is primarily responsible for this base strength because of the stability of the pyridinium resonance hybrid and pyridinium cation. The hydrolytic stability of the Al complexes was established by variable-pH ^{27}Al NMR experiments, and potentiometric equilibrium measurements showed the thermodynamic stability of the tris ligand Al and Ga complexes. The favorable properties of these ligands reported in this thesis ensure this ligand system will be the basis of further research in our group.

References

1. Driscoll, C. T. *Environ. Health Perspect.* **1985**, *63*, 93.

2. *Aluminum in the Canadian Environment;* Havas, M., Jaworski, J. F., Eds.; National Research Council of Canada, Assoc. Committee Sci. Criteria Environ. Quality, Rep. No. NRCC 24759, 1986; p 331.

3. Cronan, C.S.; Schofield, C. L. *Science* **1979**, *204*, 304.

4. Alfrey, A. C. *Adv. Clinc. Chem.* **1983**, *23*, 69.

5. Krishnan, S. *Can. Res.* **1988**, 32.

6. Sorenson, J. R. J.; Campbell, I. R.; Tepper, L. B.; Lingg, L. B. *Environ. Health Perspect.* **1974**, *8*, 3.

7. Macdonald, T. L.; Martin, R. B. *TIBS* **1988**, *13*, 15.

8. Krueger, G. L.; Morris, T. K.; Suskind, R. R.; Widnek, E. M. *CRC Crit. Rev. Toxicol.* **1984**, *13*, 1.

9. Alfrey, A. C.; Legendre, G. R.; Kaehny, W. D. *N. Eng. J. Med.* **1976**, *294*, 184.

10. Perl, D. P.; Gajdusek, D. C.; Garutto, R. M.; Yanagihara, R. T.; Gibbs, C. J. *Science* **1982**, *217*, 1053.

11. Crapper, D. R.; Krishnan, S. S.; Quittkat, S. *Brain* **1976**, *99*, 67.

12. Crapper, D. R.; Krishnan, S. S.; Dalton, A. J. *Science* **1973**, *180*, 511.

13. Crapper, D. R.; DeBoni, U. in *Aluminum Neurotoxicity*; Liss, L., Ed.; Pathotox Publishers: Illinois, 1980; pp 3-15.

14. Dölken, A. *Arch. Exp. Pathol. Pharmakol.* **1897**, *40*, 58.

15. Llobet, J. M.; Domingo, J. L.; Gómez, M.; Tomás, J. M.; Corbella, *Pharmacol. Toxicol.* **1987**, *60*, 280.

16. Edwards, C. L.; Hayes, R. L. *J. Nucl Med.* **1969**, *10*, 103.

17. Hoffer, P. *J. Nucl. Med.* **1980**, *21*, 394.

18. Hayes, R. L.; Huber, K. F. *Metal Ions Biol. Syst.* **1983**, *16*, 279.

19. Tsan, M. F.; Scheffel, U. *J. Nucl. Med.* **1986**, *27*, 1215.

20. Hoffer, P. *J. Nucl. Med.* **1980**, *21*, 484; *Int. J. Nucl. Med. Biol.* **1981**, *8*, 243.

21. Tsan, M. B. *J. Nucl. Med.* **1985**, *26*, 88.

22. Green, M. A.; Welch, M. J.; Mathias, C. J.; Fox, K. A. A.; Knabb, R. M.; Huffman, J. C. *J. Nucl. Med.* **1985**, *26*, 170.

23. Taliaferro, C. H.; Martell, A.E. *Inorg. Chem.* **1985**, *24*, 2408 and references therein.

24. Taliaferro, C. H.; Martell, A.E. *Inorg. Chim. Acta* **1985**, *85*, 9 and references therein.

25. Baes, C. F.; Mesmer, R. E. *The Hydrolysis of Cations*; Wiley: New York, 1976; pp 112-123, 313-327.

26. Levin, V. A. *J. Med. Chem.* **1980**, *23*, 682.

27. Hansch, C.; Björkroth, J. P.; Leo, A. *J. Pharm. Sci.* **1987**, *76*, 663.

28. Kulprathipanja, S.; Hnatowich, D. J.; Beh, R.; Elmaleh, D. *Int. J. Nucl. Med. Biol.* **1979**, *6*, 138.

29. Martin, R. B.; Savory, J.; Brown, S; Bertholf, R.L.; Wills, M. R. *Clin. Chem.* **1987**, *33*, 405.

30. Shannon, R.D. *Acta. Crystallogr.* **1976**, *A32*, 75.

31. Harris, W. R.; Pecoraro, V. L. *Biochemistry* **1983**, *22*, 292.

32. Pierpont, C. G.; Buchanan, R. M. *Coord. Chem. Rev.* **1981**, *38*, 45.

33. Hancock, R. A.; Orszulik, S. T. *Polyhedron* **1982**, *1*, 313.

34. Borgias, B. A.; Barclay, S. J.; Raymond, K. N. *J. Coord. Chem* . **1986**, *15*, 109.

35. Veca, A.; Dreisbach, J. H. *J. Chem. Ed.* **1988**, *65*, 108.

36. Rajan, K. S.; Mainer, S.; Davis, J. M. *Bioinorg. Chem.* **1978**, *9*, 187.

37. Finnegan, M. M.; Lutz, T. G.; Nelson, W. O.; Smith, A.; Orvig, C. *Inorg. Chem.* **1987**, *26*, 2171.

38. McLachlan, D. R. *Neurobiol. Aging* **1986**, *7*, 525.

39. Kontoghiorghes, G. J.; Aldouri, M. A.; Hoffbrand, A. V.; Barr, J.; Wonke, B.; Kourouclaris, T.; Sheppard, L. *Br. Med. J.* **1987**, *295*, 1509.

40. Albert, A. *Selective Toxicity*, 7th. ed.; Chapman and Hall: New York, 1985; pp 430-489.

41. Lerch, J. U. *Monatshefte* **1884**, *5*, 407.

42. Boulton, A.J.; McKillop, A. in *Comprehensive Heterocyclic Chemistry Volume 2*; Katritzky, A. R., Rees, C.W., Eds.; Pergamon Press: New York, 1984; pp 1-27.

43. Brody, F.; Ruby, P. R. in *The Chemistry of Heterocyclic Compounds Volume 14: Pyridine and its Derivatives Part One*; Klingsberg, E.,Ed.; Interscience: New York, 1960; pp 99-589.

44. Meislich, H. in *The Chemistry of Heterocyclic Compounds Volume 14: Pyridine and its Derivatives Part Three*; Klingsberg, E., Ed.; Interscience: New York, 1962; pp 509-890.

45. Elkaschef, M. A-F.; Nosseir, M. H. *J. Am. Soc. Chem.* **1960**, *82*, 4344.

46. Brown, R. D. *J. Chem. Soc.* 1951, 2670.

47. Peratoner, A.; Tamburello, A. *Gazz. Chim. Ital.* **1906**, *36*, 33.

48. Yabuta, J. *J. Chem. Soc.* **924**, 575.

49. Bickel, A. F. *J. Am. Chem. Soc.* **1947**, *69*, 1801.

50. Adams, R.; Jones, V. V. *J. Am. Chem Soc.* **1947**, *69*, 1803.

51. Campbell, K. N.; Ackerman, J. F.; Campbell, B. K. *J. Org. Chem.* **1950**, *15*, 337.

52. Adams, R.; Johnson, J. L. *J. Am. Chem. Soc.* **1949**, *71*, 705.

53. Kleipool, R. J. C.; Wibaut, J. P. *Rec. Trav. Chim. Pays Bas* **1950**, *69*, 1041.

54. Heyns, K.; Vogelsang, G. *Chem. Ber.* **1954**, *87*, 1377.

55. Spenser, I. D.; Notation, A. D. *Can. J. Chem.* **1962**, *40*, 1374.

56. Harris, R. L. N. *Aust. J. Chem.* **1976**, *29*, 1329.

57. March, J. *Advanced Organic Chemistry*; McGraw Hill: New York , 1977; p 258.

58. Chous, G.; Benoit, R. L. *J. Org. Chem.* **1967**, *32*, 3974.

59. Hedlund, T.; Öhman, L.-O. *Acta Chem. Scand.* in press.

60. Nelson, W. O.; Karpishin, T. B.; Rettig, S. J.; Orvig, C. *Can. J. Chem.* **1988**, *66*, 123.

61. *Chem. Abstr.* **1985**, *102*, 113315Z. (patent)

62. Severin, Th.; Loidl, A. *Z. Lebensm. Unter.-Forsch*, **1976**, *161*, 119.

63. Kontoghiorghes, G.J. Ph.D. Thesis, University of Essex, U. K. , 1982.

64. Yasue, M.; Kawamura, N.; Sakakibara, J. *Yakugaku Zasshi*, **1970**, *90*, 1222.

65. Jakopcic, K.; Tamhina, B.; Zorko, F.; Herak, M.J. *J. Inorg. Nucl. Chem.* **1977**, *39*, 1201.

66. Looker, J. H.; Cliffton, M. D. *J. Heterocycl. Chem.* **1986**, *23*, 5.

67. Kontoghiorghes, G. J.; Sheppard, L. *Inorg. Chim. Acta* **1987**, *136*, L11.

68. Cavalier, L. F. *Chem Rev.* **1947**, *41*, 525.

69. Katritzky, A. R.; Jones, R. A. *J. Chem Soc.* **1960**, 2947.

70. Cook, D. *Can. J. Chem.* **1963**, *41*, 515,.2575.

71. Batts, B. D.; Spinner, E. *Aust J. Chem.* **1969**, *22*, 2581.

72. Bellamy, L. J. *The Infrared Spectra of Complex Molecules Volume 1*, 3rd. ed.; Chapman and Hall: New York, 1975; p 433.

73. Odinokov, S. E.; Nabiullin, A. A.; Mashkovsky, A. A.; Glazunov, V. P. *Spectrochim. Acta* **1983**, *39A*, 1055.

74. Bellamy, L. J. *The Infrared Spectra of Complex Molecules Volume 2*, 2nd. ed.; Chapman and Hall: New York, 1980; pp 240-280.

75. Bellamy, L. J.; Rogasch, P. E. *Proc. Roy. Soc. (A)* **1960**, *257*, 98.

76. Katritzkky, A. R.; Taylor, P. J. in *Physical Methods in Heterocyclic Chemistry Volume IV*; Katritzky, A. R., Ed.; Academic Press: New York, 1971; pp 266-432.

77. Hadzi, D.; Sheppard, N. *Proc. Roy. Soc. (A)* **1953**, *216*, 247.

78. White, R. F. M.; Williams, H. in *Physical Methods in Heterocyclic Chemistry Volume IV*; Katritzky, A. R., Ed.; Academic Press: New York, 1971; pp 177-216.

79. Cox, R. H.; Bothner-By, A. A. *J. Phys. Chem.* **1969**, *73*, 2465.

80. Penfold, B. R. *Acta Crystallogra.* **1953**, *6*, 591.

81. Porter, Q. N. *Mass Spectrometry of Heterocyclic Compounds*, 2nd ed.; Wiley: New York, 1985; pp 603-663..

82. Undheim, K.; Hurum, T. *Acta Chem.Scand.* **1972**, *26*, 2075.

83. Maquestiau, A.; van Haverbeke, Y.; de Meyer, C.; Katritzky, A. R.; Cook, M. J.; Page, A. D. *Can. J. Chem.* **1975**, *53*, 490.

84. Scarrow, R. C.; White, D. L.; Raymond, K. N. *J. Am. Chem. Soc.* **1985**, *107*, 6540.

85. Pearson, R. G. *J. Am. Chem. Soc.* **1963**, *85*, 3533.

86. Pearson, R. G. *J. Chem. Ed.* **1987**, *7*, 561.; Pearson, R. G. *Inorg. Chem.* **1988**, *27*, 734.

87. Cotton, F. A.; Wilkinson, G. *Advanced Inorganic Chemistry*, 5th ed.; Wiley: New York, 1988; pp 209.

88. Greenwood, N. N.; Earnshaw, A. *Chemistry of the Elements*; Pergamon Press: Oxford, 1984; pp 250-256.

89. Martin, R. B. *Clin. Chem.* **1986**, *32*, 1797.

90. Secco, F.; Venturini, M. *Inorg. Chem.* **1975**, *14*, 1978.

91. Motekaitis, R. J.; Martell, A. E. *Inorg. Chem.* **1984**, *23*, 18.

92. Letkeman, P.; Martell, A. E.; Motekaitis, R. J. *J. Coord. Chem.* **1980**, *10*, 47.

93. Martin, R. B. *J. Inorg. Biochem.* **1986**, *28*, 181.

94. Gregor, J. E.; Powell, H. K. J. *Aust. J. Chem.* **1986**, *39*, 1851.

95. Scarrow, R. C.; Riley, P. E.; Abu-Dari, K.; White, D.L.; Raymond, K. N. *Inorg. Chem.* **1985**, *24*, 954.

96. Tamhina, B.; Herak, M. J.; Jakopcic, K. *J. Less-Common Met.* **1973**, *33*, 289.; Herak, M. J.; Tamhina, B.; Jakopcic, K. *J. Inorg. Nucl. Chem.* **1973**, *35*, 1665.

97. Stünzi, H.; Perrin, D. D.; Teitei, T.; Harris, R. L. N. *Aust. J. Chem.* **1979**, *32*, 21.

98. Stünzi, H.; Harris, R. L. N.; Perrin, D. D.; Teitei, T. *Aust. J. Chem.* **1980**, *33*, 2207.

99. Tsai, W. C.; Ling, K.-H. *J. Chin. Biochem. Soc.* **1973**, *2*, 70.

100. Kontoghiorghes, G. J. *Inorg. Chim. Acta* **1987**, *135*, 145 and references contained therein.

101. Nelson, W. O.; Karpishin, T. B.; Rettig, S. J.; Orvig, C. *Inorg. Chem.* **1988**, *27*, 1045.

102. Nakamoto, K. *Infrared and Raman Spectra of Inorganic and Coordination Compounds*, 3rd. ed.; Wiley-Interscience: New York , 1978; pp 249-311.

103. Kido, H.; Saito, K. *J. Am. Chem. Soc.* **1988**, *110*, 3187.

104. Albert, A. *Heterocyclic Chemistry an Introduction*; Athlone Press: London,1959; p 424.

105. Klopman, G. *Chemical Reactivity and Reaction Paths*; Klopman, G., Ed.; Wiley: New York, 1974; pp 55-166.

106. Pauling, L. *The Nature of the Chemical Bond*, 3rd ed.; Cornell University Press: Ithaca, N.Y., 1960; pp 221-264.

107. Scarrow, R. C.; Raymond, K. N. Manuscript submitted to *Inorg. Chem.*

108. Novak, A. *Struct. Bond. (Berlin)* **1974**, *18*, 177.

109. Jeffrey, G. A.; Takagi, S. *Acc. Chem. Res.* **1978**, *11*, 264.

110. Evans, R. C. *An Introduction to Crystal Chemistry*, 2nd ed.; Cambridge Univ. Press: Cambridge, 1964; pp 283-301.

111. Nelson, W. O.; Rettig, S. J.; Orvig, C. *J. Am. Chem. Soc.* **1987**, *109*, 4121.

112. Matsuba, C. A.; Nelson, W. O.; Rettig, S. J.; Orvig, C. *Inorg. Chem.* **1987**, *27*, 3935.

113.. Nelson, W. O.; Orvig, C.; Rettig, S. J.; Trotter, J. *Can. J. Chem.* **1988**, *66*, 132.

114. Falk, M.; Knop, O. in *Water: A Comprehensive Treatise Volume 2*; Franks, F., Ed.; Plenum Press: New York - London, 1973; pp 55-113.

115. Peterson, D. W.; Levy, H. A. *Acta Crystallogr.* **1957**, *10*, 70.

116. Kamb, B. in *Structural Chemistry and Molecular Biology*; Rich, A., Davidson, N., Eds.; W. H. Freeman: San Francisco, 1968; pp 507-542.

117. Saenger, W. *Nature (London)* **1979**, *279*, 343.

118. Saenger, W. *Nature (London)* **1979**, *280*, 848.

119. Saenger, W.; Lindner, K. *Angew. Chem. Int. Ed. Engl.* **1980**, *19*, 398.

120. Neidle, S.; Berman, H. M.; Shieh, H. S. *Nature (London)* **1980**, *288*, 129.

121. Betzel, C.; Saenger, W.; Hingerty, B.; Brown, G. M. *J. Am. Chem. Soc.* **1984**, *106*, 7545.

122. Zabel, V.; Saenger, W.; Mason, S.A. *J. Am. Chem. Soc.* **1986**, *108*, 3664.

123. Del Bene, J.; Pople, J. A. *J. Chem. Phys.* **1970**, *52*, 4858; **1973**, *58*, 3605.

124. Jeffrey, G. A.; McMullan, R. K. *Prog. Inorg. Chem.* **1967**, *8*, 43.

125. Jeffrey, G. A. *Acc. Chem. Res.* **1969**, *2*, 344.

126. Wells, A. F. *Structural Inorganic Chemistry*, 5th ed.; Clarendon Press: Oxford, 1984; p 660.

127. Mak, T. C. W. *J. Chem. Phys.* **1965**, *43*, 2799.

128. Akitt, J. W. *Ann. Rep. NMR Spectrosc.* **1972**, *5A*, 465.

129. Harris, R. K. *Nuclear Magnetic Resonance Spectroscopy;* Pitman: London , 1983; pp 66-94, 118-142, Appendix 2.

130. Hinton, J. F.; Briggs, R. W. in *NMR and the Periodic Table*; Harris, R. K., Mann, B.E., Eds.; Academic Press: London,1978; pp 279-308.

131. Delpuech, J. J. in *NMR of Newly Accessible Nuclei Volume 2;* Laszlo, P., Ed.; Academic Press: London, 1983; pp 153-195.

132. Karlik, S. J.; Elgavish, G. A. ; Pillai, R. P.; Eichhorn, G. L. *J. Magn. Reson.* **1982**, *49*, 164.

133. Karlik, S. J.; Elgavish, G. A.; Eichhorn, G. L. *J. Am. Chem. Soc.* **1983**, *105*, 602.

134. Greenaway, F. T. *Inorg. Chim. Acta* **1986**, 116, L21.

135. Bertsch, P. M.; Barnhisel, R. I.; Thomas, G.W.; Layton, W. J.; Smith, S. L. *Anal. Chem.* **1986**, *58*, 2583.

136. Akitt, J. W.; Milic, N. B. *J. Chem. Soc., Dalton Trans.* **1984**, 981 and references therein.

137. Llinás, M.; De Marco, A. *J. Am. Chem. Soc.* **1980**, *102*, 2226.

138. Jaber, M.; Bertin, F.; Thomas-David, G. *Can. J. Chem.* **1977**, *55*, 3689.

139. Karlik, S. J.; Elgavish, G. A.; Eichhorn, G. L. *Inorg. Chem.* **1983**, *22*, 525.

140. Akitt, J. W.; Mann, B. E. *J. Magn. Reson.* **1981**, *44*, 584.

141. Benn, R.; Ruflinska, A.; Janssen, E.; Lehmkuhl, H. *Organometallics* **1986**, *5*, 825.

142. Girgis, A. Y.; Fay, R. C. *J. Am. Chem. Soc.* **1979**, *92*, 7061.

143. Gordon, J. G.; Holm, R. H. *J. Am. Chem. Soc.* **1970**, *92*, 5319.

144. Pignolet, L. H. *Top. Curr. Chem.* **1975**, *56*, 91.

145. Henderson, D. E.; Saltzman, J. J.; Uden, P. C.; Cheng, Z. *Polyhedron* **1988**, *7*, 369.

146. Fay, R. C.; Piper, T. S. *J. Am. Chem. Soc.* **1963**, *85*, 500.

147. Hatakeyama, Y.; Kido, H.; Harada, M.; Tomiyasu, H.; Fukutomi, H. *Inorg. Chem.* **1988**, *27*, 992.

148. Gennaro, M. C.; Mirti, P.; Casalino, C. *Polyhedron* **1983**, *2*, 13.

149. Eaton, S. S.; Hutchinson, J. R.; Holm, R. H.; Muetterties, E. L. *J. Am. Chem. Soc.* **1972**, *94*, 6411.

150. Eaton, S. S.; Eaton, G. R.; Holm, R. H.; Muetterties, E. L. *J. Am. Chem. Soc.* **1973**, *95*, 1116.

151. Binsch, B. G.; Kleier, D. A., Quantum Chemistry Program Exchange QPCE, Program No. 165; DNMR3, Chemistry Department, Indiana University.

152. Gutowsky, H. S.; Holm, C. H. *J. Chem Phys.* **1956**, *25*, 1228.

153. Fay, R. C.; Piper, T. S. *Inorg. Chem.* **1964**, *3*, 348.

154. Glasstone, S.; Laidler, K.; Eyring, H. *The Theory of Rate Processes*; McGraw-Hill: New York, 1941; p 190.

155. Allerhand, A.; Gutowsky, H. S.; Jonas, J.; Meinzer, R. A. *J. Am. Chem. Soc.* **1966**, *88*, 3185.

156. Pinnavaia, T. J.; Sebeson, J. M.; Case, D. A. *Inorg. Chem.* **1969**, *8*, 644.

157. Grossman, D. L.; Haworth, D. T. *Inorg. Chim. Acta* **1984**, *84*, L17.

158. Basolo, F.; Pearson, R. G. *Mechanisms of Inorganic Reactions*, 2nd ed.; Wiley: New York, 1967; pp 300-334.

159. Fay, R. C.; Piper, T. S. *J. Am. Chem.Soc.* **1962**, *84*, 2303.

160. Hutchinson, J. R.; Gordon, J. G.; Holm, R. H. *Inorg. Chem.* **1971**, *10*, 1004.

161. Imafuku, K.; Takahashi, K.; Matsumura, H. *Bull. Chem. Soc. Jpn.* **1979**, *52*, 111.

162. Silverstein, R. M.; Bassler, G. C.; Morrill, T. C. *Spectrometric Identification of Organic Compounds,* 4th ed.; Wiley: New York, 1981; pp 305-331.

163. Mason, S. F. in *Physical Methods in Heterocyclic Chemistry, Volume II;* Katritsky, A. R.; Ed., Academic Press: New York & London, 1963; pp 1-84.

164. Geiger, A.; Mausbach, P.; Schnitker, J. in *Water and Aqueous Solutions*; Neilson, G.W., Enderby, J. E.; Eds.; Adam Hilger: Bristol, 1986; pp 15-30.

165. Leo, A.; Hansch, C.; Elkins, D. *Chem. Rev.* **1971**, *71*, 525.

166. Meyer, H. *Arch. Exptl. Pathol. Pharmakol.* **1899**, *42*, 110.

167. Helmer, F.; Hansch, C.; Kiehs, K. *Biochemistry* **1968**, *7*, 2858.

168. Yokel, R. A.; Kostenbauder, H. B. *Toxicol. Appl. Pharmacol.* **1987**, *91*, 281.

169. Leo, A. J. *J. Pharm. Sci.* **1987**, *76*, 166.

170. *Partition Coefficient Determination and Estimation*; Dunn IV, W. J., Block, J. H., Pearlman, R.S., Eds.; Pergamon Press: Oxford, 1986; p 154.

171. Dunn III, W. J.; Koehler, M. G.; Grigoras, S. *J. Med. Chem.* **1987**, *30*, 1121.

172. Clarke, F. H.; Cahoon, N. M.; *J. Pharm. Sci.* **1987**, *76*, 611.

173. Gobas, F. A. P. C.; Lahittete, J. M.; Garofalo, G.; Shiu, W. Y.; Mackay, D. *J. Pharm. Sci.* **1988**, *77*, 265.

174. De Kock, A. C.; Lord, D. A. *Chemosphere* **1987**, *16*, 133.

175. Herz, W. "Der Verteilungssatz", Ferdinand Enke, Stuttgart 1909, p 5.

176. Purcell, W. P.; Bass, G. G.; Clayton, J. M.*Strategy of Drug Design: a guide to biological activity*; Wiley: New York; Appendix I pp 126-143.

177. Arnold, A. P.; Canty, A. J.; Moors, D. W.; Deacon, G. B. *J. Inorg. Biochem.* **1983**, *19*, 319.

178. McLachlan, D. R. Personal communication.

179. Bassett, J.; Denney, R. C.; Jeffery, G. H.; Mendham, J. *Vogel's Textbook of Quantitative Inorganic Analysis,* 4th ed.; Longman: London and New York, 1985; pp 834-835.

180. Kontoghiorghes, G. *Inorg. Chim. Acta* **1988**, *151*, 101.

181. Hansch, C. Personal communication.

182. Lutz, T. G.; Clevette, D. J.; Rettig, S. J.; Orvig, C. Submitted for publication.

183. Clevette, D. J.; Nelson, W. O.; Nordin, A.; Orvig, C.; Sjöberg, S. Submitted for publication.

184. Öhman, L. -O. *Inorg. Chem.* **1988**, *27*, 2565.

185. Martell, A. E.; Smith, R. M. *Critical Stability Constants*; Plenum: New York, 1974-1982; Vols. 1-5.

186. Öhman, L. -O.; Sjöberg, S. *Polyhedron* **1983**, *2*, 1329.

187. Larson, S. M. *Seminars in Nuclear Medicine* **1978**, *8*, 193.

188. Lyster, D. M.; Clevette, D. J.; Nelson, W. O.; Rihela, T.; Webb, G. A.; Orvig, C. Manuscript in preparation.

189. Langston, W. J.; Bryan, G. W. in *Complexation of Trace Metals in Natural Waters;* Kramer, C. J. M., Duinker, J. C., Eds.; Martinus Nijhoff/Dr W. Junk: The Hague, 1984; pp 375-392.

190. Williams, R. J. P. *Proc. R. Soc. (B)* **1981**, *213*, 361.

191. Gran, G. *The Analyst* **1952**, *77*, 661; *Anal. Chim. Acta* **1988**, *206*, 111.

192. Motekaitis, R. J.; Martell, A. E. *Can. J. Chem.* **1982**, *60*, 168.

193. Motekaitis, R. J.; Martell, A. E. *Can. J. Chem.* **1982**, *60*, 2403.

Appendix

Table A.1. Molecular weights (MW) of the 3-hydroxy-4-pyridinone ligands and their tris-ligand metal complexes. (The entries in italics are for the 3-hydroxy-4-pyrone ligands)

		MW of Tris-Ligand Metal Complexes		
Ligand	MW	AlL_3	GaL_3	InL_3
Hmpp	125.1	399.4	442.1	487.2
Hdpp	139.1	441.2	484.0	529.1
Hmepp	153.1	483.2	526.0	571.1
Mimosine	198.2	618.6	661.3	706.4
Hmhpp	209.3	651.8	694.6	739.7
H_2exn*	332.4	1048	1134	1224
Maltol	*126.2*	*402.3*	*445.0*	*490.1*
Kojic acid	*142.1*	*450.2*	*493.0*	*538.1*

*Molecular weights are for the M_2L_3 dimer.

Table A.2. Crystallographic data for the 3-hydroxy-4-pyridinone ligands.

compound	Hmpp	Hdpp	Hmepp
formula	$C_6H_7NO_2$	$C_7H_9NO_2$	$C_8H_{11}NO_2$
formula weight	125.1	139.2	153.2
crystal system	monoclinic	orthorhombic	othorhombic
space group	$P2_1/n$	*Pbca*	*Pbca*
a (Å)	6.8351 (4)	7.3036 (4)	12.5907 (8)
b (Å)	10.2249 (4)	13.0490 (6)	11.7477 (6)
c (Å)	8.6525 (4)	13.7681 (7)	11.0040 (6)
β (deg)	105.215 (4)		
V (Å^3)	583.51 (6)	1312.2 (1)	1627.6 (3)
Z	4	8	8
D_c (g/cm^3)	1.424	1.409	1.14
F(000)	264	592	592
diffractometer	Enraf-Nonius CAD4-F	Enraf-Nonius	Rigaku AFC6
μ (Cu-K$_\alpha$) (cm^{-1})	8.65	8.21	6.62
radiation	Cu-K$_\alpha$	Cu-K$_\alpha$	Cu-K$_\alpha$
$\lambda_{K\alpha}$ (Å)	1.540562	1.540562	1.54178
	1.544390	1.544390	
	Ni filter	Ni filter	graphite-monochromated
temperature	23°C	23°C	23°C
$2\theta_{max}$ (deg)	150	150	150.1
reflections with I ≥ 3σ (I)	914	857	1228
number of variables	111	128	145
R; Rw	0.037; 0.046	0.044; 0.046	0.053; 0.085
max Δ/σ (final cycle)	0.05	0.05	0.02
goodness of fit indicator	2.349	1.014	3.50
residual density (e/Å^3)	0.20	0.32	0.45

Table A.3. Crystallographic data for the $M(dpp)_3$ complexes (recorded with a Enraf-Nonius CAD4-F diffractometer).

compound	$Al(dpp)_3 \cdot 12\ H_2O$	$Ga(dpp)_3 \cdot 12\ H_2O$	$In(dpp)_3 \cdot 12\ H_2O$
formula	$C_{21}H_{48}AlN_3O_{18}$	$C_{21}H_{48}GaN_3O_{18}$	$C_{21}H_{48}InN_3O_{18}$
formula weight	657.6	700.3	745.44
crystal system	Trigonal	Trigonal	Trigonal
space group	$P\bar{3}$	$P\bar{3}$	$P\bar{3}$
a (Å)	16.600 (2)	16.6549 (6)	16.842 (1)
c (Å)	6.877 (1)	6.8691 (4)	6.8078 (7)
V ($Å^3$)	1641.3 (3)	1650.1 (1)	1672.3 (2)
Z	2	2	2
D_c (g/cm^3)	1.331	1.470	1.480
F(000)	704	740	776
radiation	Cu-K_α	Cu-K_α	Mo-K_α
$\lambda_{K\alpha}$ (Å)	1.540562 1.54439	1.540562 1.54439	0.70930 0.71359
	nickel filter	nickel filter	graphite monochromator
μ (cm^{-1})	11.97	17.89	7.67
temperature	22°C	22°C	21°C
$2\theta_{max}$ (deg)	150	150	60
reflections with $I \geq 3\sigma$ (I)	1662	1653	2496
number of variables	202	195	190
R; Rw	0.045; 0.051	0.047; 0.055	0.033; 0.037
max Δ/σ (final cycle)	0.17	0.023	0.027
goodness of fit indicator	1.020	1.023	1.492
residual density ($e/Å^3$)	0.23	0.48	-0.55 to +0.75 (near In)

Table A.4. Crystallographic data for the M(mepp)$_3$ complexes (recorded with a Rigaku AFC6).

compound	Al(mepp)$_3$·12 H_2O	Ga(mepp)$_3$·12 H_2O
formula	$C_{24}H_{54}AlN_3O_{18}$	$C_{24}H_{54}GaN_3O_{18}$
formula weight	699.7	742.4
crystal system	Trigonal	Trigonal
space group	$P\bar{3}$	$P\bar{3}$
a (Å)	17.1734 (8)	17.247 (1)
c (Å)	6.827 (1)	6.830 (2)
V (Å^3)	1743.7 (3)	1759.4 (1)
Z	2	2
D_c (g/cm^3)	1.33	1.40
F(000)	752	788
radiation	Cu-K_α	Mo-K_α
$\lambda_{K\alpha}$ (Å)	1.54178 graphite-monochromated	0.71069 graphite-monochromated
μ (cm^{-1})	11.56	8.50
temperature	21°C	21°C
$2\theta_{max}$ (deg)	150.3	55.0
reflections with $I \geq 3\sigma(I)$	1157	1918
number of variables	207	215
R; Rw	0.032; 0.038	0.029; 0.036
max Δ/σ (final cycle)	0.23	0.02
goodness of fit indicator	1.63	1.46
residual density (e/Å^3)	0.10	0.28

Table A.5. Hydrogen bond distances (Å) and angles for $In(dpp)_3 \cdot 12H_2O$.

Atoms	Interaction			
	O-H (Å)	H···O (Å)	O···O (Å)	O-H···O (deg)
O(3)-H(O3a)···O(1)	1.00	1.92	2.900(3)	165
O(3)-H(O3b)···O(2)	0.87(3)	1.99(3)	2.839(3)	168(3)
O(4)-H(O4a)···O(6)	0.70(4)	2.07(5)	2.744(4)	160(5)
O(4)-H(O4b)···O(4)	0.87(9)	1.90(9)	2.755(3)	169(6)
O(4)-H(O4c)···O(4)	0.72(8)	2.04(8)	2.755(3)	170(6)
O(5)-H(O5a)···O(4)	0.82	1.99	2.789(3)	166
O(5)-H(O5b)···O(5)	0.77(5)	2.01(5)	2.782(3)	179(5)
O(6)-H(O6a)···O(3)	0.66(4)	2.10(4)	2.759(4)	177(5)
O(6)-H(O6b)···O(5)	0.74(4)	2.06(4)	2.780(4)	164(4)

Table A.6. Hydrogen bond distances (Å) and angles for the $M(mepp)_3 \cdot 12\ H_2O$ complexes.

Interaction	O-H		H···O		O·····O		O-H····O (deg)	
	Al	Ga	Al	Ga	Al	Ga	Al	Ga
O(3)-H(1)···O(1)	0.81(5)	0.75(4)	2.10(5)	2.14(4)	2.877(2)	2.883(3)	161(4)	173(4)
O(3)-H(2)···O(2)	0.92(7)	0.77(3)	1.95(7)	2.08(3)	2.838(2)	2.834(3)	163(5)	168(3)
O(4)-H(3)···O(6)	0.83(7)	0.85(4)	1.99(7)	1.95(7)	2.795(3)	2.784(3)	166(4)	167(4)
O(4)-H(4)···O(4)	0.85(8)	0.71(7)	1.97(7)	2.11(7)	2.811(2)	2.810(3)	170(6)	172(5)
O(5)-H(6)···O(4)	0.89(1)	0.81(3)	2.04(6)	2.03(4)	2.828(3)	2.821(3)	145.83	164(3)
O(5)-H(5)···O(5)	0.82(6)	0.76(3)	2.02(6)	2.08(4)	2.833(2)	2.835(3)	171(4)	175(4)
O(6)-H(7)···O(3)	0.91(6)	0.79(4)	1.86(6)	2.00(4)	2.771(3)	2.763(3)	173(4)	165(4)
O(6)-H(8)···O(5)	0.76(8)	0.77(4)	2.11(8)	2.12(4)	2.859(3)	2.849(4)	168(5)	159(4)

Appendix Procedure A.1 Potentiometric Equilibrium Measurements

Potentiometric measurements of the ligands in the absence, and presence, of metal ions were performed with an Orion Research EA 920 pH meter equipped with Orion Ross research grade glass and reference electrodes. A Metrohm automatic buret (Dosimat 665) was used to add the standard NaOH. The temperature was maintained at 25.0 ± 0.1 °C throughout with water-jacketed beakers and a Julabo circulating bath, and the ionic strength was adjusted to 0.15 M (isotonic) by the addition of NaCl. All solutions were continuously degassed with prepurified Ar during the course of a titration.

The ligands were twice recrystallized or sublimed; concentrations were obtained by weighing. All metal-containing solutions were obtained from appropriate dilution of atomic absorption standard solutions of Al and Ga (Sigma or Aldrich). The exact amount of excess acid present in the metal ion solutions was determined by a Gran's plot[191] of $(V_o + V_t) \times 10^{-pH}$ vs. V_t, where V_o = the initial volume of 1:1 metal-Na_2EDTA solution, and V_t is the volume of added standard NaOH. The base consumed is equal to the excess acid plus the Na_2EDTA protons. The metal-ligand titrations were performed at a total ligand (C) to total metal ion (B) concentration ratio of just greater than three. NaOH solutions (0.1 M) were prepared from dilutions of 50% NaOH (less than 0.1% Na_2CO_3) with freshly boiled, distilled, deionized water and standardized potentiometrically against potassium hydrogen phthalate (KHP).

The electrodes were calibrated with standard aqueous HCl and NaOH solutions to read $-\log[H^+]$ directly. The range of $-\log[H^+]$ available was limited from 1.5 to 12 in which the electrode behavior was reversible and linear. Protonation and deprotonation reactions of the ligands were studied within the range $2 \leq -\log[H^+] \leq 10$ and the metal-ligand titrations were studied within the range $1.5 \leq -\log[H^+] \leq 4$. All titrations were performed in sets of 3 or 4 runs.

The proton dissociation constant of the ligands were determined by using the Fortran computer program PKAS.[192] In the M(III) systems, the computations allowed for the presence of $M(OH)^{2+}$, $M(OH)_2^{+}$, $M(OH)_3$ and $M(OH)_4^{-}$. In addition, $Al_2(OH)_2^{4+}$ and $Al_3(OH)_4^{5+}$ were included. Formation constants for these various metal species were taken from ref. 25. The stability constants for the main species ML^{2+}, ML_2^{+}, and ML_3 were determined by using the Fortran computer program BEST.[193] This program sets up simultaneous mass-balance equations for all the components present at each addition of base, and calculates the pH at each data point according to the current set of stability constants and total concentrations of each component. Stability constants judiciously chosen by the user are automatically adjusted in order to minimize the sum of squares of differences between the calculated and observed values of $-\log[H^+]$. Adjustment is continued until there is no further improvement in the fit. The constants are reported to the second decimal place, which is representative of the reproducibility of the potentiometric equipment employed.